

BONE TISSUE ENGINEERING USING MACROPOROUS
PHA-PLA AND PHBV SCAFFOLDS PRODUCED BY ADDITIVE
MANUFACTURING AND WET SPINNING

A THESIS SUBMITTED TO
THE GRADUATE SCHOOL OF NATURAL AND APPLIED SCIENCES
OF
MIDDLE EAST TECHNICAL UNIVERSITY

BY
AYŞE SELCEN ALAGÖZ

IN PARTIAL FULFILLMENT OF THE REQUIREMENTS
FOR
THE DEGREE OF DOCTOR OF PHILOSOPHY
IN
BIOLOGY

SEPTEMBER 2016

Approval of the thesis:

BONE TISSUE ENGINEERING USING MACROPOROUS
PHA-PLA AND PHBV SCAFFOLDS PRODUCED BY ADDITIVE
MANUFACTURING AND WET SPINNING

submitted by **AYŞE SELCEN ALAGÖZ** in partial fulfillment of the requirements for
the degree of **Doctor of Philosophy in Biological Sciences Department, Middle East
Technical University** by,

Prof. Dr. Gülbin Dural Ünver _____
Dean, Graduate School of **Natural and Applied Sciences**

Prof. Dr. Orhan Adalı _____
Head of Department, **Department of Biological Sciences, METU**

Prof. Dr. Vasıf Hasırcı _____
Supervisor, **Department of Biological Sciences, METU**

Examining Committee Members:

Prof. Dr. Orhan Adalı _____
Biological Sciences Dept., METU

Prof. Dr. Vasıf Hasırcı _____
Biological Sciences, METU

Prof. Dr. Alpaslan Şenköylü _____
Department of Orthopaedics and Traumatology, Gazi University

Doç. Dr. Ergin Tönük _____
Mechanical Engineering, METU

Doç. Dr. Halime Kenar _____
Arslanbey Vocational School, Kocaeli University

Date: 09.09.2016

I hereby declare that all information in this document has been obtained and presented in accordance with academic rules and ethical conduct. I also declare that, as required by these rules and conduct, I have fully cited and referenced all material and results that are not original to this work.

Name, Last Name: Ayşe Selcen Alagöz
Signature:

ABSTRACT

BONE TISSUE ENGINEERING USING MACROPOROUS PHA-PLA AND PHBV SCAFFOLDS PRODUCED BY ADDITIVE MANUFACTURING AND WET SPINNING

Alagöz, Ayşe Selcen

Ph.D., Department of Biological Sciences

Supervisor: Prof. Dr. Vasıf Hasırcı

September 2016, 107 pages

Bone supports and protects organs of body, stores minerals, produces blood cells and enables the movement of body. In addition, bone regulates homeostasis by controlling the concentration of key electrolytes in the blood and in the storage of Ca^{+2} and PO_4^{3-} ions. Trauma, tumor, nonunion fractures and diseases like osteoporosis lead to bone loss that affects millions of people. Current clinical treatments such as application of autograft and allograft for treatment of these problems are limited due to donor scarcity, donor site morbidity, disease transmission and rejection. Bone tissue engineering uses life science and engineering principles and presents a promising approach to treat bone defects. Scaffolds, signaling molecules, and cells are essential components of any tissue engineering application.

The aim of this study was to develop three dimensional structures which have suitable architecture for the treatment of bone defects. For this purpose, two different polymers, PHBV and PHA-PLA, were used to produce scaffolds by using two different techniques, rapid prototyping (fused deposition modelling, FDM) and wet spinning. With FDM the pore size, pore distribution within the 3D structure of scaffolds can be controlled. Wet spinning produces scaffolds with pores that are random and nonhomogeneous in size and distribution. Thus, the properties of the FDM products are predetermined. PHA-PLA was used to make scaffolds using both methods while PHBV

was only wet spun. Results showed that wet spun PHA-PLA and PHBV scaffolds had similar porosity (77% and 75%), and pore size (300 μm and 250 μm). On the other hand, FDM PHA-PLA scaffolds have higher compressive property than wet spun scaffolds because fibers in a layer contact with fibers at the subsequent layer.

Oxygen plasma treatment is known to improve the hydrophilicity of polymers and also increase surface reactivity to coat ELP-REDV on the surface of the polymer to promote endothelial cell attachment and increase proliferation of cells around the defect site. Optimum oxygen plasma treatment times and powers were determined as 4 min for PHBV scaffolds and 2 min for PHA-PLA scaffolds at 50W. The effect of oxygen plasma treatment and surface coating with ELP-REDV were shown by goniometer for contact angle, atomic force microscope for surface topography, FTIR-ATR, and Toluidine Blue staining for binding. It was seen that hydrophilicity of all scaffolds increased and moderately hydrophilic surfaces were obtained. FTIR-ATR analysis showed that surfaces of scaffolds were coated with ELP-REDV resulting in formation of amide I and amide II bands. Besides, oxygen plasma treatment and ELP-REDV attachment resulted in the increase of roughness (formation of valley and peaks) on the surfaces of samples and changed the surface roughness.

Isolated rabbit bone marrow stem cells were seeded on scaffolds and cell behavior (attachment, proliferation and differentiation) were studied. High cell proliferation on FDM scaffolds was observed compared with wet spun scaffolds. This shows that FDM scaffolds can provide surfaces suitable for cell proliferation. Presence of ELP-REDV sequences enhanced cell attachment and proliferation on the scaffolds. Alkaline phosphatase activity on FDM scaffolds was higher than on wet spun scaffolds because of more cell proliferation on FDM scaffolds. Osteopontin staining showed that after culturing for 3 weeks in the differentiation medium, cells secreted osteopontin which show osteogenic differentiation because this protein is secreted by mature osteoblasts at the later stages of osteoblastic differentiation. SEM images showed that cells cultured on the scaffolds proliferated and penetrated into the scaffolds and deposited calcium containing minerals. Ca^{+2} deposition was observed on all types of scaffolds by Alizarin Red staining.

It was concluded that FDM PHA-PLA and wet spun PHBV and PHA-PLA scaffolds have a significant potential for using bone tissue engineering.

Keywords: Bone Tissue Engineering, 3D construct, Rapid Prototyping, Wet Spinning, Elastin Like Polymers.

ÖZ

ISLAK EĞİRME VE EKLEMELİ ÜRETİM TEKNİĞİ İLE ÜRETİLMİŞ MAKRO GÖZENEKLİ PHA-PLA VE PHBV HÜCRE TAŞIYICILARIYLA KEMİK DOKU MÜHENDİSLİĞİ

Alagöz, Ayşe Selcen

Doktora, Biyolojik Bilimler Bölümü

Tez Yöneticisi: Prof. Dr. Vasıf Hasırcı

Eylül 2016, 107 sayfa

Kemik doku mineral depolama, kan hücresi üretmek, vücuttaki organları koruma ve desteklemek ve vücut hareketlerini sürdürme gibi önemli rollere sahiptir. Buna ek olarak, kemik doku kalsiyum ve fosfat iyonlarının depolayarak ve kanın içerisinde bulunan önemli elektrotların konsantrasyonunu kontrol ederek homeostazı düzenler. Travma, tümör, kaynamayan kemik kırıkları ve osteoporoz gibi hastalıklar her yıl milyonlarca insanı etkileyen kemik kayıplarına neden olmaktadır. Ototograft ve allograft gibi uygulamaların güncel klinik tedavilerde donörde bırakılan bölgesel hasar, immünolojik red, hastalık buluşması (enfeksiyon) açısından sınırlamalara sahiptir. Kemik doku mühendisliği yaşam bilimi ve mühendislik prensiplerini kullanarak kemik hasarlarının iyileşmesinde umut verici yaklaşımlar sunmaktadır. Hasarlı kemik dokunun yenilenmesi ve onarılması için kemik doku mühendisliğinin temel bileşenleri hücre iskeleleri, sinyal molekülleri ve hücrelerdir.

Bu çalışmanın amacı, kemik hasarlarının tedavisi için uygun bir mimariye sahip üç boyutlu bir yapı geliştirmektir. Bu amaç için, PHBV ve PHA-PLA polimerleri ıslak eğirme ve erimiş biriktirilmiş modelleme tekniği (FDM) ile hücre iskeleleri üretilmesi için kullanılmıştır. Erimiş biriktirilmiş modelleme tekniği gözenek boyutu, gözeneklerin dağılımını ve iskelelerinin üç boyutlu yapısını kontrol edebilme yeteneğine sahiptir. Bu

nedenle FDM ürünlerinin özellikleri önceden belirlenmiştir. PHBV polimeri sadece ıslak eğirme tekniği ile üretim için kullanılırken, PHA-PLA karışımı hem ıslak eğirme hem de erimiş biriktirme modelleme tekniği ile üretim için kullanılmıştır. Sonuçlar ıslak eğirme tekniği ile üretilen PHBV ve PHA-PLA hücre iskelelerinin FDM ile üretilmiş PHA-PLA hücre iskelelerine göre rastgele dağılmış liflerden dolayı daha yüksek gözenekliliğe ve gözenek büyüklüğüne sahip olduğunu göstermiştir. Diğer taraftan, FDM ile üretilmiş hücre iskelele liflerinin belirli noktalarda temas etmesi ve düzenli gözenekli yapısından dolayı ıslak eğirme tekniği ile üretilmiş iskelelere göre daha yüksek sıkışma özelliğine sahip olduğu gözlemlenmiştir.

Oksijen plazma uygulaması iskelelerin hidrofiliğini iyileştirirken, aynı zamanda hasarlı bölgede bulunan endotel hücrelerin yapışma ve çoğalmasını artırıcı etkiye sahip ELP-REDV sekansları ile iskelelerin yüzeylerini kaplamak için kullanılmıştır. Optimum oksijen plazma uygulama zamanı ve gücü PHBV iskeleler için 4 dakika 50 W ve PHA-PLA iskeleler için 2 dakika 50 W olarak belirlenmiştir. Oksijen plazma uygulamasının etkisi ve yüzeyin ELP-REDV sekansları ile kaplanması gonyometre, atomik kuvvet mikroskobu, Fourier dönüşüm Infrared (Kızılötesi) spektroskopisi (FTIR-ATR) ve Toluidini mavi boyaması ile karakterize edildi. Temas açısı ölçümü ile hücre iskelelerinin hidrofiliğinin arttığı ve oksijen plazma uygulamasından sonra orta derecede su sever yüzeyler elde edildiği gözlemlenmiştir. FTIR-ATR analizi sonucuna göre yüzeyde amid I ve amid II bağlarının oluşmuş ve yüzey ELP-REDV sekansı ile kaplanmıştır. Ayrıca, oksijen plazma uygulaması ve yüzeyin ELP-REDV sekansı ile kaplanması yüzeyde vadi ve tepelerin oluşmasına ve yüzey pürüzlülüğünün değişmesine neden olmuştur.

İzole edilmiş tavşan kemik iliği kök hücreleri, hücre iskelelerine ekilerek hücre yapışması, çoğalması ve farklılaşması gibi hücre davranışları *in vitro* ortamda kemik dokusu için incelendi. Erimiş modelleme yöntemi ile üretilmiş iskelelerde hücre yayılmasını sağlayacak geniş lif kalınlıklarından dolayı, ıslak eğirme ile üretilmiş iskelelere oranla daha yüksek hücre çoğalması gözlemlenmiştir. Bu da erimiş modelleme ile üretilmiş iskelelerin hücre çoğalması için daha uygun yüzeyler sağladığını

göstermektedir. Ayrıca, iskelelerinin yüzeyinde bulunan ELP-REDV dizilerinin varlığı hücre yapışması ve çoğalmasını arttırıcı etkiye sahiptir.

Hücrelerin alkalın fosfat aktivitesi erimiş modelleme tekniği ile üretilmiş iskelelerde ıslak eđirme ile üretilmiş iskelelere göre daha yüksek orandadır. Bunun nedeni hücrelerin erimiş modelleme ile üretilmiş iskelelerde daha çok çoğalmasıdır. Ayrıca, üç hafta farklılaşma faktörü içeren kültür ortamında kalan hücrelerin osteopontin sentezlediği gözlemlenmiştir. Bu protein osteoblastik farklılaşmanın geç evresinde olgun osteoblastlar tarafından sentezlendiği için osteojenik farklılaşma gözlemlenmiştir. Hızlı tarama mikroskop görüntüleri hücrelerin çoğalıp, iskelelerin içirisine doğru göç ettiğini ve mineral biriktirdiğini gösterdi. Ayrıca, iskeleler üzerinde kalsiyum birikimi gözlemlenmiştir.

FDM ile üretilmiş PHA-PLA ve ıslak eđirme ile üretilmiş PHBV ve PHA-PLA iskeleleri kemik doku mühendisliği alanında kullanmak için önemli bir potansiyele sahip olduğu sonucuna varılmıştır.

Anahtar Kelimeler: Kemik Doku Mühendisliği, Üç Boyutlu Yapı, Hızlı Prototipleme, Islak Eđirme, Elastin Benzeri Polimer.

Dedicated to my lovely father and mother...

ACKNOWLEDGEMENTS

I would like to express my special endless thanks and gratitude to my supervisor, Prof. Dr. Vasıf Hasırcı for his continues support, advice, guidance and encouragement during all the stages of my research. I feel very lucky to have had opportunity to do my thesis research under his guidance.

I also thank to contribution to this study at University of Valladolid, Spain to be able produce ELR.

I would also like to thank to Prof. Dr. Cemil Yıldız from GATA-OGEK Project.

I would also like to thank to my best labmate Esen Sayın and Cemile Bektaş for their encouragement, support and motivation especially for her great friendship.

I would like to thank to all friends in BIOMATEN especially Aylin Kömez, Ezgi Antmen, Arda Büyüksungur, Senem Büyüksungur, Gözde Eke, Menekşe Ermiş, Büşra Günay, Dr. Türker Baran, Deniz Sezlev, and our technician Zeynel Akın.

Finally, I would like to express my deepest gratitude to my perfect, lovely family Sedat Alagöz, Gülsen Alagöz, Selim Alagöz and Sinan Alagöz for their understanding, friendship, patience, love and trust in me.

This study was supported by DPT2011K120350 Ministry of Development grant, and TUBITAK 2211C PhD scholarship.

TABLE OF CONTENTS

ABSTRACT.....	v
ÖZ.....	viii
ACKNOWLEDGEMENTS	xii
CHAPTERS	
1. INTRODUCTION	1
1.1 Bone.....	1
1.1.1 Structure, Organization and Function of Bone	1
1.1.2 Bone Defect Treatment Methods	2
1.1.2.1 Biological Grafts.....	4
1.1.2.1.1 Autograft.....	4
1.1.2.1.2 Allograft.....	4
1.1.2.1.3 Xenografts.....	5
1.1.2.2 Synthetic Grafts	5
1.1.2.2.1 Metallic Grafts	6
1.1.2.2.2 Ceramic Grafts	6
1.1.2.2.3 Polymeric Grafts	7
1.1.2.2.4 Composites.....	7
1.1.2.3 Tissue Engineering	8
1.1.2.3.1 Bone Tissue Engineering	9
1.1.3 Materials Used as Scaffolds (Cell Carriers) in Bone Tissue Engineering .	12
1.1.3.1 Natural Materials	12
1.1.3.1.1 Collagen	13
1.1.3.1.2 Silk Fibroin	13
1.1.3.1.3 Chitosan	13
1.1.3.1.4 Alginate.....	14
1.1.3.1.5 Polyhydroxyalkanoates	14
1.1.3.2 Synthetic Materials	15

1.1.4	Scaffold Production Techniques for Bone Tissue Engineering	17
1.1.4.1	Wet Spinning Technique.....	17
1.1.4.2	Rapid Prototyping Technique	19
1.1.4.2.1	SLA.....	20
1.1.4.2.2	SLS.....	20
1.1.4.2.3	3DP	21
1.1.4.2.4	FDM.....	21
1.1.5	Modification properties of scaffolds	22
1.1.5.1	Surface Modification with Oxygen Plasma	23
1.1.5.2	Coating with cell adhesive molecules.....	24
1.1.5.2.1	Elastin-like Polymers (ELPs).....	24
1.1.6	Cell Sources for Bone Tissue Engineering	25
1.2	Aim of This Study	26
1.3	Novelty of This Study.....	27
2.	MATERIALS and METHODS.....	29
2.1	Materials	29
2.2	Methods	30
2.2.1	Scaffold Production.....	30
2.2.1.1	Production of PHBV scaffolds by wet spinning	30
2.2.1.2	Production of PHA-PLA scaffolds by wet spinning.....	31
2.2.1.3	Production of PHA-PLA scaffolds by rapid prototyping	31
2.2.2	Surface Modification of Scaffolds with Oxygen Plasma	32
2.2.3	Immobilization of ELP-REDV on all scaffolds	32
2.2.4	Characterization of scaffolds.....	32
2.2.4.1	Morphology of all scaffolds.....	33
2.2.4.2	Mechanical Testing.....	33
2.2.5	Characterization of PHBV and PHA-PLA films.....	33
2.2.5.1	Surface wettability measurement of PHBV and PHA-PLA films	33
2.2.5.2	FTIR-ATR analysis of PHBV and PHA-PLA films.....	34

2.2.5.3	Toluidine Blue Staining of PHBV and PHA-PLA films	34
2.2.5.4	Atomic force microscopy (AFM) of PHBV and PHA-PLA films	34
2.2.6	In vitro studies.....	34
2.2.6.1	Bone Marrow Mesenchymal Stem Cells Isolation	34
2.2.6.2	Characterization of isolated rabbit bone marrow mesenchymal stem	35
2.2.6.3	Sterilization and BMSC seeding on all types of scaffolds.....	36
2.2.6.4	Rabbit Bone Marrow Mesenchymal Stem Cell Culture	36
2.2.6.5	Determination of cell proliferation	36
2.2.6.6	Alkaline phosphatase (ALP) Assay for the Assessment of BMSC Differentiation	37
2.2.6.7	Microscopic evaluation of cell morphology	37
2.2.6.7.1	Scanning electron microscopy	37
2.2.6.7.2	Confocal laser scanning microscopy	38
2.2.6.7.3	Alizarin Red Staining for Determining of Mineral Deposition	38
3.	RESULTS AND DISCUSSION	39
3.1	Preparation and characterization of the scaffolds.....	39
3.1.1	Wet spun PHBV scaffolds	39
3.1.2	Wet spun PHA-PLA scaffolds	39
3.1.3	FDM PHA-PLA scaffolds.....	40
3.1.4	Mechanical characterization.....	42
3.1.5	Contact angle measurement	44
3.1.5.1	Surface wettability of PHBV and PHA-PLA films	44
3.1.6	Surface roughness of films.....	47
3.1.6.1	Surface roughness of PHBV film	47
3.1.6.2	Surface roughness of PHA-PLA film	48
3.1.7	ELP-REDV attachment of PHBV and PHA-PLA films.....	50
3.1.7.1	Toluidine Blue staining of PHBV films	50
3.1.7.2	Toluidine Blue staining of PHA-PLA films	51
3.1.8	FTIR-ATR Analysis.....	51

3.1.8.1	FTIR-ATR Analysis of PHBV films	52
3.1.8.2	FTIR-ATR Analysis of PHA-PLA films	53
3.2	In vitro studies	55
3.2.1	Cell proliferation	55
3.2.2	ALP analysis	59
3.2.2.1	ALP analysis of scaffolds	59
3.2.3	Microscopy.....	61
3.2.3.1	SEM analysis	61
	SEM analysis of PHBV wet spun scaffolds	61
3.2.3.1.1	SEM analysis of PHA-PLA wet spun scaffolds	61
3.2.3.1.2	SEM analysis of FDM PHA-PLA scaffolds	67
3.2.4	Evaluation of Mineralization by Surface Analysis Using EDX Analysis..	68
3.2.4.1	Energy dispersive X-ray (EDX) analysis.....	68
3.2.4.1.1	Energy dispersive X-ray (EDX) analysis of scaffolds	68
3.2.5	Confocal microscopy.....	73
3.2.5.1	Confocal microscopy of wet spun PHBV scaffolds	73
3.2.5.2	Confocal microscopy of wet spun PHA-PLA scaffolds	74
3.2.5.3	Confocal microscopy of PHA-PLA FDM scaffolds	75
3.2.6	Alizarin Red Staining	76
3.2.6.1	Alizarin Red Staining of PHBV wet spun scaffolds	77
3.2.6.2	Alizarin Red Staining of PHA-PLA wet spun scaffolds.....	78
3.2.6.3	Alizarin Red Staining of PHA-PLA FDM scaffolds	78
4.	CONCLUSION	81
	REFERENCES.....	85
	APPENDICES.....	105
A.	APPENDIX	105
B.	APPENDIX	106
	CURRICULUM VITAE	107

LIST OF FIGURES

FIGURES

Figure 1.1: The Structure of Cortical and Trabecular bone (Bose et al., 2013).....	3
Figure 1.2: Strategy of tissue engineering.....	9
Figure 1.3: Schematic representation of various 3D printing techniques. a) stereolithography (SLA), b) selective laser sintering (SLS), c) three-dimensional printing (3-DP), d) first fused deposition modelling (FDM) (Peltola et al., 2008).	19
Figure 1.4: Differentiation process of BMSC (Kaplan, 2007).....	26
Figure 2.1: Wet spinning process.....	30
Figure 2.2: Scaffold designed to produce a cylindrical 3D scaffold for bone tissue engineering with SketchUp Software, (a) top, (b) side view.	31
Figure 3.1: Microscopic images of wet spun PHBV, wet spun PHA-PLA and FDM PHA-PLA scaffolds; (a, d, g) top view of μ -CT images, (b, e, h) SEM micrographs, and (c, f, i) stereomicrographs of scaffolds.....	41
Figure 3.2: Representative compressive stress-strain curves of: a) wet spun PHBV scaffold, b) wet spun PHA-PLA scaffold, and c) FDM PHA-PLA scaffold.	43
Figure 3.3: Contact angle measurement of PHA-PLA films (a) Untreated PHBV film, (b) PHBV film treated with oxygen plasma.....	46
Figure 3.4: AFM results of oxygen plasma treated PHBV films; (a) Untreated PHBV, (b) PHBV film treated with oxygen plasma and (c) PHBV film treated with oxygen plasma and coated with ELP-REDV.	48
Figure 3.5: AFM results of PHA-PLA films; (a) Untreated PHA-PLA, (b) PHA-PLA film treated with oxygen plasma and (c) PHA-PLA film treated with oxygen plasma and coated with ELP-REDV.....	49
Figure 3.6: Stereomicroscope image of PHBV film. (a) PHBV film, (b) PHBV-O ₂ , and (c) PHBV-O ₂ -ELP-REDV.	51

Figure 3.7: Stereomicroscope image of PHA-PLA film; (a) PHA-PLA film, (b) PHA-PLA-O₂, and (c) PHA-PLA-O₂-ELP-REDV.52

Figure 3.8: FTIR–ATR spectra of PHBV films treated with oxygen plasma and REDV.53

Figure 3.9: FTIR–ATR spectra of PHA-PLA films treated with O₂ plasma for 1 min at 50W and REDV.54

Figure 3.10: FTIR–ATR spectra of PHA-PLA films treated with O₂ plasma for 2 min at 50W and REDV.54

Figure 3.11: Rabbit BMSC proliferation on TCPS, wet spun scaffolds. Statistical differences were determined between TCPS seeded and other groups by one way Anova (*p<0.05, **p<0.01, ***p<0.001).56

Figure 3.12: Rabbit BMSC proliferation on TCPS, wet spun PHA-PLA scaffolds. Statistical differences were determined between TCPS seeded and other groups by one way Anova (*p<0.05, **p<0.01, ***p<0.001).57

Figure 3.13: Rabbit BMSC proliferation on TCPS, FDM PHA-PLA scaffolds. Statistical differences were determined between TCPS seeded and other groups by one way Anova (*p<0.05, **p<0.01, ***p<0.001).58

Figure 3.14: Alkaline phosphatase activity of RBMSC proliferation on wet spun PHBV scaffolds.62

Figure 3.15: Alkaline phosphatase activity on wet spun PHBV is normalized to cell number.....62

Figure 3.16: Alkaline phosphatase activity of RBMSC proliferation on wet spun PHA-PLA scaffolds.....63

Figure 3. 17: Alkaline phosphatase activity on wet spun PHA-PLA scaffolds is normalized to cell number.....63

Figure 3.18: Alkaline phosphatase activity of RBMSC proliferation FDM PHA-PLA scaffolds.64

Figure 3. 19: Alkaline phosphatase activity on FDM PHA-PLA scaffolds is normalized to cell number.....64

Figure 3.20: SEM micrographs of unseeded PHBV wet spun scaffolds and rabbit BMSCS on PHBV wet spun scaffolds (Arrow shows cells).	65
Figure 3.21: SEM micrographs of unseeded PHA-PLA wet spun scaffolds and rabbit BMSCS on wet spun PHA-PLA scaffolds (Arrow shows cells).	66
Figure 3.22: SEM micrographs of unseeded PHA-PLA FDM scaffolds and rabbit BMSCS on untreated FDM PHA-PLA scaffolds (Arrow shows cells).	67
Figure 3.23: Elemental analysis of wet spun PHBV scaffold surfaces on Day 28. (A) SEM micrographs, and (B) EDX analysis.	70
Figure 3.24: Elemental wet spun PHA-PLA scaffold surfaces on Day 28. (A) SEM micrographs, and (B) EDAX analysis.....	71
Figure 3.25: Elemental analysis of FDM PHA-PLA scaffold surfaces on Day 28. (A) SEM micrographs, and (B) EDAX analysis.	72
Figure 3.26: Osteopontin immunofluorescence of control (unseeded) and seeded wet spun PHBV scaffolds on Day 28. Stains: osteopontin: blue; DRUQ5: nuclei,green; FTIC: actin, red. Scale bars: 100 μ m. Arrows show osteopontin.	74
Figure 3.27: Osteopontin immunofluorescence of control (unseeded) and seeded wet spun PHA-PLA scaffolds on Day 28. Stains: osteopontin: blue; DRUQ5: nuclei,green; FTIC: actin, red. Scale bars: 100 μ m. Arrows show osteopontin.	75
Figure 3.28: Osteopontin immunofluorescence of control (unseeded) and seeded FDM PHA-PLA scaffolds on Day 28. Stains: osteopontin: blue; DRUQ5: nuclei,green; FTIC: actin, red. Scale bars: 100 μ m. Arrows show osteopontin.....	76
Figure 3.29: Alizarin Red staining of unseeded and seeded PHBV wet spun scaffolds on Day 28. Scale bars: 200 μ m.	77
Figure 3.30: Alizarin Red staining of unseeded and seeded wet spun PHA-PLA scaffolds on Day 28. Scale bars: 200 μ m.	79
Figure 3.31: Alizarin Red staining of unseeded and seeded FDM PHA-PLA scaffolds on Day 28.	79

LIST OF TABLES

TABLES

Table 1.1: Synthetic Commercial Grafts Used in Repair.....	10
Table 1.2: Natural materials for bone tissue engineering.....	16
Table 3.1: Characterization of scaffolds.	41
Table 3.2: Young’s Modulus of the three scaffolds.....	43
Table 3.3: Young’s Modulus of Typical Bone Tissues in Human Body	43
Table 3.4: Contact angle of PHBV and PHA-PLA films.....	46
Table 3.5: Surface characteristics of PHBV film.....	48
Table 3.6: Surface characteristics of PHA-PLA film.....	50
Table 3.7: Ca/P ratio on PHBV and PHA-PLA scaffolds at 4 week.	69

LIST OF ABBREVIATIONS

μ -CT	Micro Computed Tomography
3D	Three Dimensional
3-DP	Three Dimensional Printing
AFM	Atomic Force Microscope
ALP	Alkaline Phosphatase
AM	Additive Manufacturing
BMMSC	Bone Derived Mesenchymal Stem Cell
BMP	Bone Morphogenetic Protein
BSA	Bovine Serum Albumin
CAD	Computer Aided Design
CLSM	Confocal Laser Scanning Microscopy
DAPI	4',6-diamine-2-phenylindole drochloride
DBM	Demineralized Bone Matrix
DMEM	Dulbecco's Modified Eagle Medium
ECM	Extracellular Matrix
ELP	Elastin Like Polymer
ELR	Elastin Like Recombinamer
FDM	Fused Deposition Modeling
FTIR-ATR	Fourier Transform Infrared-Attenuated Total Reflectance
TGF- β	Transforming Growth Factor Beta
HA	Hydroxyapatite
IGF	Insulin-like Growth Factors
FGF	Fibroblast Growth Factors
ITT	Inverse Temperature Transition
MSC	Mesenchymal Stem Cell
OPN	Osteopontin
PFA	Paraformaldehyde
PGA	Polyglycolic Acid
PHA	Polyhydroxyalkanoate
PHBV	Poly(3-hydroxybutyrate-co-3 hydroxyvalerate)

PIPES	Piperazine-N, N'-Bis(ethanesulfonic acid)
PLA	Poly(lactic acid)
PLGA	Poly(lactic acid-co-glycolic acid)
PMMA	Polymethylmethacrylate
PVA	Polyvinyl Alcohol
REDV	Valine-Proline-Glycine-X-Glycine
RGD	Arginine, Glycine, Aspartic Acid
RP	Rapid Prototyping
SEM	Scanning Electron Microscope
SFF	Solid Free Form Fabrication
SLA	Stereolithography
SLS	Selective Laser Sintering
TCPS	Tissue Culture Polystyrene
v/v	volume/volume
VEGF	Vascular Endothelial Growth Factor
w	weight
w/v	weight/volume

CHAPTER 1

1. INTRODUCTION

The aim of this study was to develop 3D scaffolds for bone tissue engineering and compare the effect of predetermined architecture of the FDM scaffold with those of the less organized, wet spun scaffolds in terms of the quality of the tissue engineered product. In order to improve cell adhesion and proliferation, surfaces were modified by treatment with oxygen plasma and containing with synthetic biological cues such as elastin like polypeptides (ELP) to make the surfaces more attractive for cells.

1.1 Bone

1.1.1 Structure, Organization and Function of Bone

Bone is a connective tissue. It plays crucial roles in the performance of our body such as supporting and protecting organs, storing minerals, producing blood cells and in the movement of the body. In addition, bone regulates homeostasis by controlling the concentration of key electrolytes in the blood and stores Ca^{+2} and PO_4^{-3} ions.

Bone is a composite tissue composed of organic matrix (20–30w/w.%), inorganic bone mineral (60–70w/w.%), and water (10 w/w.%) (Chen et al., 2006). The organic matrix mainly consists of type I collagen (over 90%) (Hing, 2004). The inorganic part is composed of hydroxyapatite ($\text{Ca}_6(\text{PO})_4.2\text{H}_2\text{O}$). The collagen matrix contributes to the toughness of the tissue, while the mineral phase provides stiffness to tissues (Wang et al., 2004).

Osteoblasts (bone forming cells) and osteoclasts (bone resorbing cells) are the two main types of cells which play an important role in bone formation (Nguyen et al., 2013). Osteoblasts synthesize the organic component of matrix including type I collagen and

different non-collagenous matrix components including matrix proteins (osteopontin, osteocalcin, bone sialoprotein) during the ossification process. Calcium phosphate secreted by osteoblast may initially be amorphous and noncrystalline, but also it gradually turns into more crystalline forms. Mineralization process is also promoted by osteoblasts. Bone matrix is surrounded by some osteocytes (Ferreira et al., 2012). Osteoclasts dissolve and resorb some bone mineral during osteolysis. Osteoclasts break down bone tissue via removing its mineralized matrix and breaking up the organic bone (Bohner, 2010).

Bone tissue is composed of two main structures: cortical and trabecular bone (Fig. 1.1). Cortical bone, also known as compact bone, is a highly organized structure with low porosity (10%) and a dense outer shell. Its compressive strength is in the range 167–215 MPa while its tensile strength is in the range 107–140 MPa (Bose et al., 2013). Histologically, cortical bone includes tightly packed units, called osteons which are surrounded by interstitial lamellae and connected by Haversian or Volkmann's Canals containing vessels and nerves (Jayakumar et al., 2010). Trabecular spongy bone is usually surrounded with cortical bone. It has high porosity because of the interconnected network of pores. It has a lower Young's modulus (E) (10 – 900 MPa) and higher elasticity than cortical bone (Andric et al., 2011).

1.1.2 Bone Defect Treatment Methods

Bone fractures or defects related with aging, diseases, tumors, nonunion fractures, congenital defects increasingly create health problems in the world (Venkatesan et al., 2015). Approximately 10 million bone fractures are treated every year in the United States alone. An estimated 2.2 million people per year need bone tissue transplant worldwide (Walmsley et al., 2016). Although bone tissue has self regeneration capability, this ability is limited to a few millimeters in healthy bone. Thus, the regeneration process of bone is inadequate for large bone defects created by bone tumor resection or comminuted fractures. Porous fillers allowing ingrowth of blood vessels are

required to fill the defective site to heal bone defects (Butscher et al., 2011). The ideal bone substitute should mechanically support the structure, be biocompatible, osteoinductive, osteoconductive, bioresorbable, and inexpensive (Duan et al., 2010). Biological bone graft substitutes are clinically used in the treatment of bone defects. However, these grafts have limitations like immunogenicity, disease transfer, insufficient supply and cost (Pina et al., 2015).

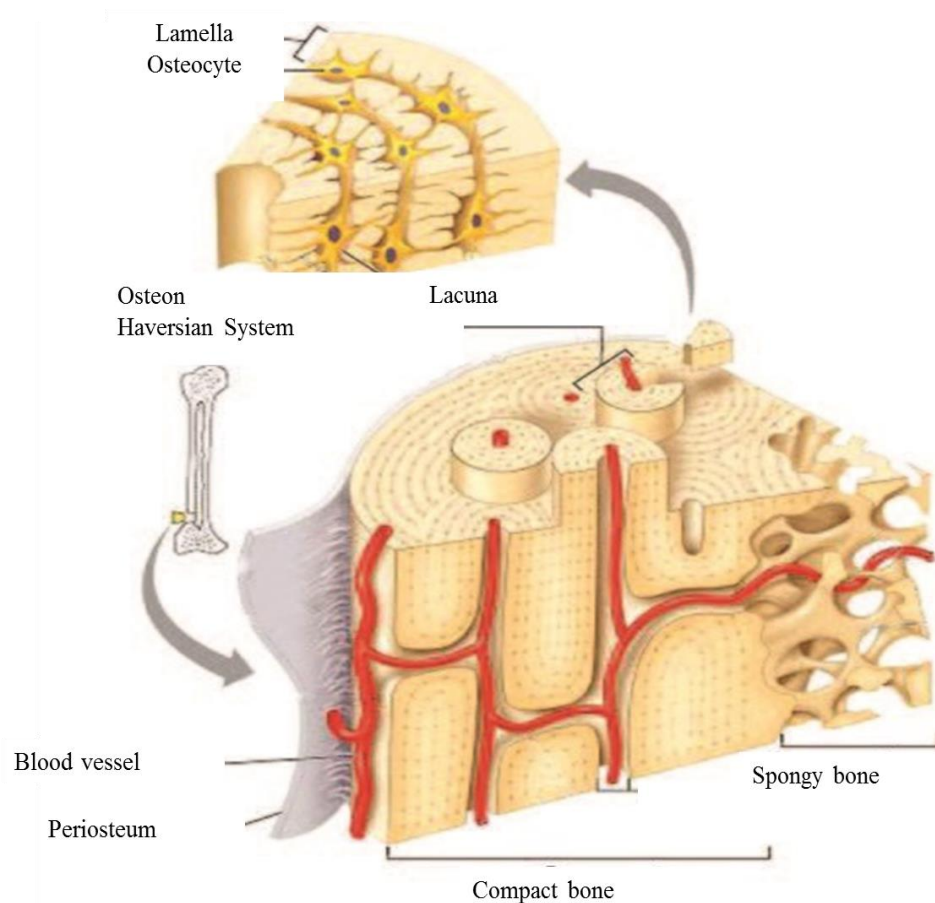


Figure 1.1: The Structure of Cortical and Trabecular bone (Bose et al., 2013).

Bone tissue engineering offers a promising new approach to bone repair and eliminates these problems. Tissue engineering requires a number of components such as cells (primary adult osteoblasts (bone cells), bone marrow mesenchymal stem cell), 3D cell

carriers called scaffolds, and adhesion, growth and differentiation regulating compounds (growth factors, adhesive proteins) (Motamedian et al, 2015).

1.1.2.1 Biological Grafts

Bone grafts are widely used as treatment materials especially for skeletal fractures that have failed to heal and for the regeneration of bone defects caused by aging, infections, diseases, tumors and nonunion fractures. The bone substitutes commonly used in the treatment of bone defects are biological autografts, allografts and xenografts. Also, cadaver bone and demineralized bone matrix are used as biological grafts in the treatments (Kolk et al., 2012).

1.1.2.1.1 Autograft

The donor for the autograft bone is the patient and the tissue is implanted back into the same individual. The iliac crest, proximal tibia, greater trochanter and distal radius are the most often used donor sites (Griffin et al., 2015). The main advantages are that they are nonimmunogenic, have a low risk of disease transmission and have osteoinductive and osteoconductive properties (Cheng et al., 2014). Although autografts are considered as the gold standard in bone treatment, they have some limitations (Viateau et al., 2014) such as that they are in short supply due to donor site morbidity which is liable to cause infection and further pain. Also, the additional surgeries increase the healing time for the patients (Reichert et al., 2012).

1.1.2.1.2 Allograft

Allografts harvested usually from other humans including cadaver bones and living donors harvested hip arthroplasty. Allografts do not have the limitation of donors and require less surgery on the patient (Cheng et al., 2014). However, allografts have some drawbacks such as immune response and transmission of diseases like HIV and hepatitis

B. Also, they lack the osteogenic properties due to the absence of viable cells (Kolk et al., 2012).

Demineralized bone matrix (DBM) is an allograft bone which is produced through decalcification of the in cortical bone with chemical and radiation treatments (Gardin et al., 2012). This process removes the mineral content leaving behind the collagen and noncollagenous proteins, including growth factors (Dinopoulos et al., 2012). Demineralized bone matrix has osteoconductive and osteoinductive properties but their level depends on storage, processing, and sterilization methods and change from donor to donor. One of the disadvantages of DBM is that it has a risk to transmitting human immunodeficiency virus (HIV). Another drawback is the variation because of donors (Nandi et al., 2010).

1.1.2.1.3 Xenografts

Xenografts are biological grafts derived from nonhuman species (pigs) (Bohner, 2010). Pigs are widely used because they are economical and have considerable compatibility with human tissue (Du et al., 2011). Xenografts exhibit osseointegration and osteoconduction, and perhaps osteoinduction (Oryan et al., 2014). Nevertheless, the main problems of xenografts are immunogenicity and disease transmission from species to species (Zheng et al., 2010).

1.1.2.2 Synthetic Grafts

Synthetic bone grafts consist of metals, ceramics, polymers and composites with or without growth factors and cells (Table 1.1). A synthetic bone graft substitute should be biocompatible, bioresorbable, and cost effective in addition to osteoconductive, osteoinductive and osteogenic properties. Besides, they should possess proper mechanical properties to support defective site during healing process (Duan et al., 2010).

1.1.2.2.1 Metallic Grafts

Metallic bone substitutes like stainless steel, titanium and cobalt-chromium, alloys are widely used in the treatment of bone defects. The main advantages of metal implants are their excellent mechanical properties, biocompatibility and relatively low cost (Nguyen et al., 2012). They are especially used at load bearing areas like joint implants (Rengier et al., 2010). Their limitations are that they are not biodegradable and they lack cell adhesion (Park et al., 2011). In addition, metals possess much higher moduli than natural bone and cause stress shielding (weakening of the bone due to load being carried by the metal and not the bone). Moreover, sometimes second surgery is required for metal implants to remove from patient (Nguyen et al., 2012).

1.1.2.2.2 Ceramic Grafts

Bioceramics such as hydroxyapatite (HA), calcium phosphates, and bioactive glasses are commonly used as synthetic substitute for bone tissue engineering (Gerhardt et al., 2010). Ceramics are biocompatible and osteoconductive materials. They have properties similar to that of the natural inorganic component of bone. They increase the mineralization of osteoblast and bone tissue formation because of calcium ions release from ceramics (Seol et al., 2013). However, ceramic implants have some limitations such as being brittle and having low tensile strengths and toughness. Thus, they cannot appropriately match the mechanical properties of bone. Furthermore, processability of ceramics is difficult because high temperature is required (Gloria et al., 2010). Bioceramics are also used in various applications including dental implants (Jayaswal et al., 2010), and cranio-maxillofacial reconstruction (Dorozhkin, 2010). For example, Neobone is synthetic bone graft which are composed of hydroxyapatite and used as bone filler in knee tissue operation (Deie et al., 2008).

1.1.2.2.3 Polymeric Grafts

Polymeric materials are also used as bone grafts. Polymers can be studied in two groups: natural and synthetic polymers. Natural polymers such as collagen and silk fibroin are biodegradable, have low production costs and biocompatible. However, they rapidly degrade and might carry the risk of disease transmission and immune problems (Puppi et al., 2010). Synthetic polymers such as Polylactic acid (PLA), polycaprolactone (PCL), and polyglycolic acid (PGA) have longer degradation time and higher mechanical properties when compared to natural polymers. Besides, they are highly reproducible (Dhandayuthapani et al., 2011). Polymer based bone graft substitutes are the following: Cortoss is an injectable resin-based product for load-bearing site applications such as vertebral augmentation (Laurencin et al., 2006). Porous poly(lactic acid-co-glycolic acid) foam was developed by using particulate leaching technique and clinically used for oro-maxillo-facial surgery (Davies et al., 2010).

1.1.2.2.4 Composites

Composites are formed by two or more than two materials such as ceramic and polymer (Bose et al., 2012). Composite materials are usually classified into: fibrous composite materials composed of fibers embedded in a matrix, laminated composite materials that consist of layers of composite materials, particulate composite materials that are made up of particles embedded in a matrix, and combinations of these (Gloria et al., 2011). Composites are promising biomaterials for bone tissue engineering applications because they have an exceptional strength to weight property compared to monolithic materials. Polymer-ceramic composed of collagen and hydroxyapatite composites mimic the natural bone. Fiber reinforced composite materials are widely used for hard tissue applications including skull reconstruction, hip and other joint replacements, ankle, total knee, and bone fracture repairs, and in the dental applications. Besides, upper and lower limb prostheses are commonly produced from composite material with underlying matrix because of strength to weight properties (Scholz et al., 2011). For example,

Collagraft is a commercial composite bone graft materials which is composed of collagen and calcium phosphate and used for long bone fracture (Cornell et al., 1991). Healos (DePuy Orthopaedics, Inc, Warsaw, Ind) is a polymer based bone graft substitute composed of collagen fibers coated with hydroxyapatite and used for spinal fusions (Boughton et al., 2008). Tricos is another commercial composite material which is combining of fibrin matrix and hydroxyapatite coated beta calcium phosphate. Tricos is used in periprosthetic bone operations (Goyenvalle et al., 2010).

1.1.2.3 Tissue Engineering

The term of tissue engineering was firstly used in a review paper by Langer and Vacanti in 1993 as “ Tissue engineering is an interdisciplinary area that combines life sciences and engineering principles and mainly aims regeneration and/or repair of organ loss and tissue damage caused by diseases, injuries, aging and trauma” (Langer et al., 1993). Three main components of tissue engineering strategy are scaffolds, undifferentiated or differentiated cells, and biological signaling molecules like growth factors (GFs) (Fig. 1.2) (Asghari et al., 2016). Scaffolds are three dimensional structures that act as temporary extracellular matrix (ECM) and provide surface for cell attachment, differentiation and growth and accelerate regeneration of damaged tissue (Smith et al., 2010). Growth factors are the other key substances in this area and they guide adhesion, proliferation, migration, and differentiation of cells and vascularization (Santos et al., 2010).

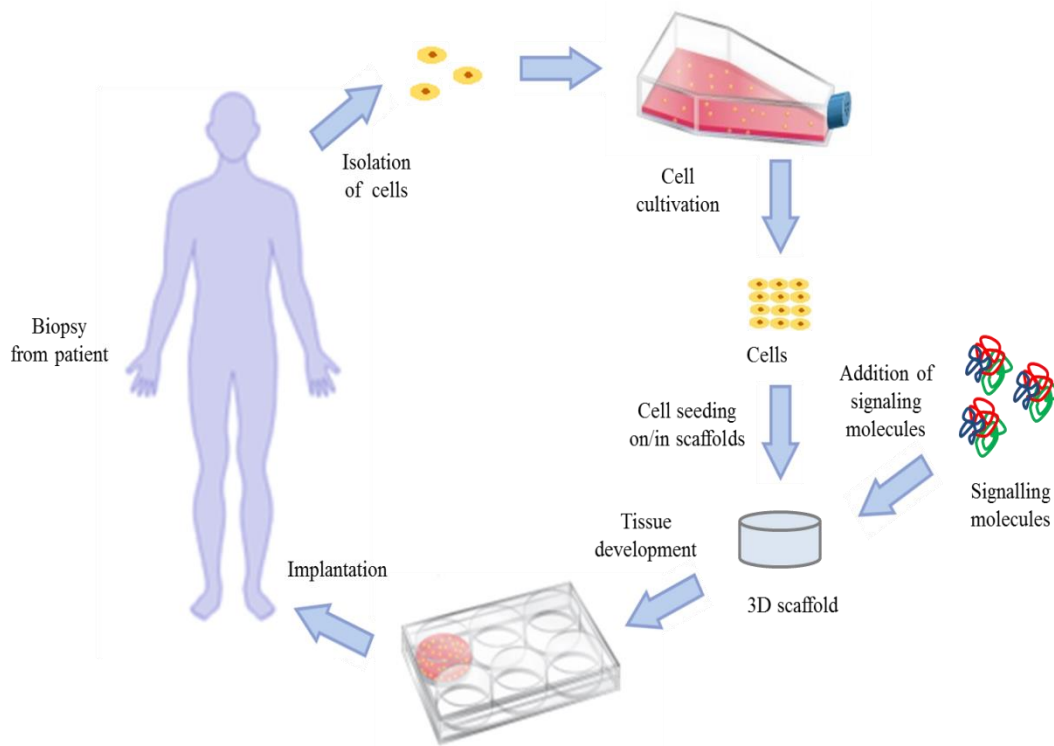


Figure 1.2: Strategy of tissue engineering.

1.1.2.3.1 Bone Tissue Engineering

Bone defects and nonunion fractures caused by aging, diseases, and tumors increasingly create health problems in the world. Each year, over 6.2 million bone fractures are recorded in the U. S. A. and 10% of them do not properly heal because of delayed union or non-union. Also, osteoporosis currently affects 10 million people and it is estimated to increase to 14 million by 2020 (Fu et al., 2011). In the treatment of bone defects, autologous bone of the patient and allograft bone from other individuals, usually from cadaver, are used (Kretlow et al., 2007).

Table 1.1: Synthetic Commercial Grafts Used in Repair

Product Name	Materials	Applications	Company Name	References
Neobone	Hydroxyapatite (HA)	Knee tissue	Toshiba Ceramics Co., Tokyo	(Deie et al., 2008)
Cortoss	PMMA	Vertebral augmentation	Stryker, USA	(Laurencin et al., 2006)
OsteoScaf	PLGA	Oro-maxillo-facial surgery	DENTSPLY Friadent CeraMed, Sweden	(Davies et al., 2010)
Collagraft	Collagen and calcium phosphate	Long bone fracture	Zimmer Corp, Warsaw	(Cornell et al., 1991)
Healos	Collagen fibers and hydroxyapatite	Spinal fusions	DePuy Orthopaedics, Inc, Warsaw, Ind	(Boughton et al., 2008)
Tricos	Fibrin matrix and hydroxyapatite coated beta calcium phosphate	Periprosthetic bone surgery	Baxter Bio Science, Singapore	(Goyenvalle et al., 2010)

However, autograft and allograft treatments have some drawbacks such as donor scarcity, limited supply, pathogen transfer and immune rejection (Liu et al., 2004).

Bone tissue engineering is a promising approach for bone repair and eliminates the problems mentioned above. It involves a number of components which are cells ranging from primary adult osteoblasts (bone cells) to bone marrow mesenchymal stem cells, three dimensional scaffolds, and bioactive agents such as growth factors for vascularization, differentiation, etc. (Stevens, 2008).

Cell source should be non-tumorigenic, non-immunogenic, and potent proliferative and should have osteogenic potential to be able to use in bone tissue engineering application. The various primary cell types from autogenic, allogenic, and xenogenic cell sources and stem cells can be used (Zhang et al., 2012).

Scaffolds act as an artificial extracellular matrix, provide structural support for cell attachment and proliferation and have high porosity, high pore interconnectivity and uniform pore distribution to allow cell growth, migration and nutrient flow (Mouriño et al., 2010). They are produced by various processing techniques including solvent casting, particulate leaching (Thadavirul et al., 2014), electrospinning (Prabhakaran et al., 2009), freeze drying (Sultana et al., 2012), gas foaming (Dehghani et al., 2011), wet spinning (Tuzlakoglu et al., 2010) and rapid prototyping (Yilgor et al., 2009). Wet spinning is a nonsolvent induced precipitation technique and produces continuous fibers using both natural polymers and synthetic polymers (Puppi et al., 2012). Conventional techniques have some limitations in pore size, pore interconnectivity, pore shape, porosity and form. However, rapid prototyping overcomes these limitations by using three dimensional computed tomography (3D CT) data to design the desired shape and produce the product with controlled pore size, pore interconnectivity and porosity (Liu et al., 2010).

Growth factors are cytokines secreted by various types of cells and act as signaling molecules. A wide range of activities including survival, adhesion, proliferation, migration and differentiation are stimulated or inhibited by growth factors. Growth factors are also involved in a complex cascade of events for tissue formation and skeletal

repair (Lee et al., 2011). Many growth factors are key components of osteogenesis and angiogenesis for bone tissue. Bone morphogenetic proteins (BMP-2 and BMP-7) (Yilgor et al., 2009), transforming growth factor beta (TGF- β) (Chen et al., 2012), insulin-like growth factors I (Meinel et al., 2003), platelet-derived growth factor (PDGF) (Kaigler et al., 2011), fibroblast growth factors (FGF) (Qu et al., 2011) and vascular endothelial growth factor (VEGF) (Luo et al., 2012) have been used to induce bone formation in bone tissue engineering applications.

1.1.3 Materials Used as Scaffolds (Cell Carriers) in Bone Tissue Engineering

A number of materials are used in bone tissue engineering. These are generally polymeric molecules from natural and synthetic origin because in most applications biodegradability is needed and ceramics and metals are not suitable.

1.1.3.1 Natural Materials

Various natural materials, biopolymers, have been used to produce scaffolds for bone tissue engineering because of their low or non-toxicity, biodegradability, renewability, low manufacture and disposal costs (Puppi et al., 2010). Natural polymers are derived from natural animal and plant sources. They have a wide range of advantages for tissue engineering such as providing biological signaling, appropriate cell adhesion, and cell responsive degradation. However, there are some limitations for their use in bone tissue engineering including their poor mechanical properties, rapid degradability, batch-to-batch variability, disease transmission risk and immunogenic problems (Ko et al., 2010). Various natural polymers like collagen, silk fibroin, chitosan, and alginate have been used for bone tissue application (Table 1.2).

1.1.3.1.1 Collagen

Collagen is found abundantly in the extracellular matrix (ECM) of many tissues such as bone, cartilage, skin, tendons, and blood vessels and provides mechanical and structural support to tissues (Puppi et al., 2010). Collagen serves as a structural support in the ECM and adheres to cells via interaction of its domains with integrin receptors in the cell membrane (Sell et al., 2010). Although it is a suitable scaffold material, collagen has an important limitation such as low mechanical properties. Collagen can be crosslinked or combined with other natural or synthetic polymers to overcome these problems (Ferreira et al., 2012). Collagen scaffolds have been reported to support and promote human osteogenesis for bone tissue engineering because of its biological nature (Aravamudhan et al., 2013; Keogh et al., 2010; Murphy et al., 2010).

1.1.3.1.2 Silk Fibroin

Silk fibroin is another fibrous protein, and it is composed of fibroin and sericin (Kasoju et al., 2012). It is obtained from the cocoon and nets of various insects such as spiders and silkworms. Although silk fibers are widely used as suture materials, they are also very attractive materials for bone tissue engineering because of their slow degradability, high mechanical strength and flexibility (Correia et al., 2012). The main problem of silk is that it may cause immune response at the implantation site if sericin is not properly removed (Kasoju et al., 2012).

1.1.3.1.3 Chitosan

Chitosan is the second most abundant natural material after cellulose. It is composed of β -(1 \rightarrow 4)-2-acetamido-d-glucose and β -(1 \rightarrow 4)-2-amino-D-glucose units. This polysaccharide is derived from the deacetylation of chitin found in the exoskeleton of crabs and shrimps, insects and the cell walls of fungi (Venkatesan et al., 2010). It is biodegradable, biocompatible and has blood coagulation properties. Moreover, it can be easily processed into different forms like films, sponges, beads, fibers, and microspheres

(Costa-Pinto et al., 2011). However, it is not a mechanically suitable material for load bearing implants (Venkatesan et al., 2012).

1.1.3.1.4 Alginate

Alginate is also a linear polysaccharide composed of (1,4)-linked β -D-mannuronic acid (M) and α -L-guluronic acid (G) monomers that change in composition and sequence along the polymer chain. It is extracted from brown algae, certain seaweeds or bacteria (Ko et al., 2010). Reversible hydrogels of alginate can be produced in the presence of divalent ions such as Ca^{2+} and Ba^{2+} via ionic cross-linking. Main advantages of alginate are its non-immunogenicity and biocompatibility. Also, it has gently gelling ability which permits encapsulation of various materials including cells (Augst, et al., 2006). Poor mechanical properties of alginate due to its extensive hydrophilicity is the main problem for bone tissue engineering (Valente et al., 2012).

1.1.3.1.5 Polyhydroxyalkanoates

Polyhydroxyalkanoates (PHAs) are biopolyesters accumulated by a wide variety of microorganisms as an intracellular carbon and energy storage compound (Baek et al., 2012). Poly(3-hydroxybutyrate-co-3-hydroxyvalerate) (PHBV) is a natural polymer that belongs to the polyhydroxyalkanoate (PHA) family and it is synthesized by plants and various microorganisms via fermentation (Zhang et al., 2015). PHBV is very promising polymer in the biomedical field because of its biodegradability, biocompatibility, biological origin and thermoplasticity. It is biocompatible because the main degradation product of PHBV, 3-hydroxybutyrate, is a constituent of the human blood and it was reported that 3-hydroxybutyrate promotes proliferation of fibroblasts and keratinocytes by hindering apoptotic and necrotic cell death and by stimulating a rapid increase in cytosolic calcium ion influx (Zonari et al., 2014). However, it is more hydrophobic than most other natural polymers like collagen and silk fibroin. The wettability of the polymer is a very important issue in terms of cell attachment on scaffolds (Lei et al.,

2015; Yilgor et al., 2012; Kose et al., 2005; Tezcaner et al. 2003). Various methods have been used to increase the hydrophilicity of PHBV such as oxygen plasma surface treatment (Wang et al., 2013).

1.1.3.2 Synthetic Materials

Synthetic polymers are more preferable biomaterials than natural polymers in terms of their processability, good mechanical properties, batch-to-batch uniformity, and cost. Their major drawback is that their degradation products are usually not naturally found in body and may cause to problems if accumulated (Murphy et al., 2013).

Poly(lactic acid) (PLA), poly(glycolic acid) (PGA), and their copolymers poly(lactide-co-glycolide) (PLGA), poly-L-lactic acid (PLLA), polycaprolactone (PCL) are widely used in bone tissue engineering (Goonoo et al., 2013). Poly(lactic acid) (PLA) is an aliphatic polyester derived from agricultural products such as corn, potato, and wheat (Zhou et al., 2013). PLA has been used as fixation devices such as screws and plates in orthopedic applications because of their bioabsorbability. This feature prevents bone erosion when implanted in the human body unlike metallic implants such as titanium plates (Lasprilla et al., 2012). Polyglycolic acid (PGA) is a crystalline polymer and exhibits high stiffness (Gentile et al., 2014). However, acidic degradation product glycolic acid released from PGA may prevent the regeneration of tissue (Shrivats et al., 2014). Poly(lactic acid-co-glycolic acid) PLGA is FDA-approved polymer and displays different properties depending on the ratio of lactide to glycolide in the copolymer such as crystallinity, degradation rate and mechanical properties.

Cell attachment on PLGA surfaces is poor because of its hydrophobicity (Meng et al., 2010). Polycaprolactone (PCL) is a FDA-approved synthetic polyester which also displays biocompatibility. PCL is very flexible, has excellent processability and low melting (60 °C) and glass transition (−60 °C) temperature. However, it is hydrophobic and has a slow degradation rate which is not suitable to bone remodeling process (Thuaksuban et al., 2011).

Table 1.2: Natural materials for bone tissue engineering

Material	Advantage	Disadvantage	References
Collagen	<ul style="list-style-type: none"> • Biodegradability • Cell-binding properties • Low antigenicity 	<ul style="list-style-type: none"> • High degradation rate • Low mechanical properties 	(Ferreira et al., 2012)
Silk fibroin	<ul style="list-style-type: none"> • Slow degradability • High mechanical strength • Flexibility 	<ul style="list-style-type: none"> • Immune response 	(Correia et al., 2012; Kasoju et al., 2012)
Chitosan	<ul style="list-style-type: none"> • Antibacterial • Biodegradable • Biocompatible • Antibacterial • Blood coagulation properties 	<ul style="list-style-type: none"> • Low mechanical properties 	(Costa-Pinto et al., 2011; Venkatesan et al., 2012)
Alginate	<ul style="list-style-type: none"> • Non-immunogenicity • Biocompatibility • Gelling ability 	<ul style="list-style-type: none"> • Low mechanical properties • Nondegradable 	(Augst et al., 2006; Valente et al., 2012)
PHBV	<ul style="list-style-type: none"> • Biodegradability • Biocompatibility • Biological origin • Thermoplasticity 	<ul style="list-style-type: none"> • Hydrophobic • Low rate of degradation 	(Kose et al., 2003; Tezcaner et al., 2003; Pinar Yilgor et al., 2009; Zonari et al., 2014)

1.1.4 Scaffold Production Techniques for Bone Tissue Engineering

Scaffolds play a very important role in bone tissue engineering. They should have proper and interconnected porosity for diffusion of necessary nutrients and oxygen, and removal of waste product. They should provide sufficient mechanical support during regeneration and repair of damaged bone tissue. Moreover, the degradation rate should match the rate of bone formation in order to maintain structural strength (Bose et al., 2012).

In the recent years, fiber based polymeric scaffolds produced with electrospinning, melt spinning (extrusion), wet spinning have gained increasing attention in bone tissue engineering applications (Tamayol et al., 2013). In electrospinning, nano and microfibers are obtained from polymer solution using a high electric field between a positively charged syringe tip and a negatively charged collector. Main advantages of this technique are that it is easy to scale up, has low cost and synthetic and natural polymers can be processed using this approach (Di Martino et al., 2011). However, this technique has some difficulties in terms of obtaining thick 3D complex scaffolds with small size pores (Leong et al., 2010). In melt spinning, the polymer is heated until its melting point and then extruded through a nozzle to produce continuous fiber strands (Park et al., 2013). Various synthetic polymers like poly(3-hydroxybutyrate) (Hinüber et al., 2010) and PLA (Hufenus et al., 2012) have been used to form such fibers for bone tissue engineering. However, this method cannot use organic solvents and generally requires high temperature and expensive equipment (Tamayol et al., 2013).

1.1.4.1 Wet Spinning Technique

Wet-spinning is a non-solvent-induced phase inversion technique permitting the production of a continuous polymeric fiber and based on solution/precipitation event (Mota et al., 2013). This technique allows the production of wide range diameters from approximately 30 to 600 μm (Lee et al., 2011). Wet spinning is a simple method and a

form highly porous scaffolds (Tamayol et al., 2013). Wet spinning products are made up of fibers as in a ball of yarn (Mota et al., 2013). This process is based on simple solution and precipitation. Firstly, polymer is dissolved in a suitable solvent. After polymeric solution is loaded into syringe, it is extruded into a coagulation bath at a constant rate by a syringe pump to form randomly distributed polymeric fibers. Fiber properties depend on spinning rate, concentration of the polymer solution and coagulation bath (Yilgor et al., 2009). Among other fabrication techniques for bone tissue engineering, wet spinning has some advantages in terms of its ease of operation under physiological conditions and cost effectiveness (Barui et al., 2011). Also, it tends to produce higher porosity and larger pore size products because of their thick fibers (250–500 μm). Thus, these properties promote cell adhesion, proliferation and migration within the inner part of the scaffolds (Neves et al., 2011). Also, wet spinning has been widely preferred for processing natural polymers, such as chitin and chitosan, which cannot be produced by other spinning techniques (Puppi et al., 2012).

Characterization of poly(ϵ -caprolactone)/chitosan blend fibers produced by wet spinning from blend solutions showed that the surface roughness of the blend fibers could promote cell attachment and have potential for tissue engineering applications (Malheiro et al., 2010). Chitosan and chitosan/PEO blends were also used to fabricate fiber mesh scaffolds by wet spinning. Chitosan-based 3-D scaffolds were loaded with poly(lactic acid-co-glycolic acid) (PLGA) nanocapsules containing bone morphogenetic protein 2 (BMP-2) and poly(3-hydroxybutyrate-co-3-hydroxyvalerate) (PHBV) nanocapsules containing BMP-7 made the early release of BMP-2 and longer term release of BMP-7 possible (Yilgor et al., 2009). The sequential delivery system released from scaffolds achieved the production of tissue engineered bone. At another study, three dimensional chitosan scaffolds were prepared by wet spinning technique. In vitro studies confirmed that mesh structure of the chitosan scaffold was proper for cell ingrowth (Tuzlakoglu et al., 2004).

1.1.4.2 Rapid Prototyping Technique

Rapid prototyping (RP) which is also known as solid free form fabrication (SFF) or additive manufacturing (AM) is a promising fabrication method for bone tissue engineering. Rapid prototyping technology was introduced in the late 1980s with stereolithography system (STL). Then, different techniques of RP such as selective laser sintering, 3D printing, and fused deposition modelling have been developed over the past 20 years (Fig. 1.3) (Melchels et al., 2010). An RP system coupled with computer aided design (CAD) was used for the first time at the Massachusetts Institute of Technology (MIT) in 1993 as a biplotter and a fused deposition model for tissue engineering application (Park et al., 2012).

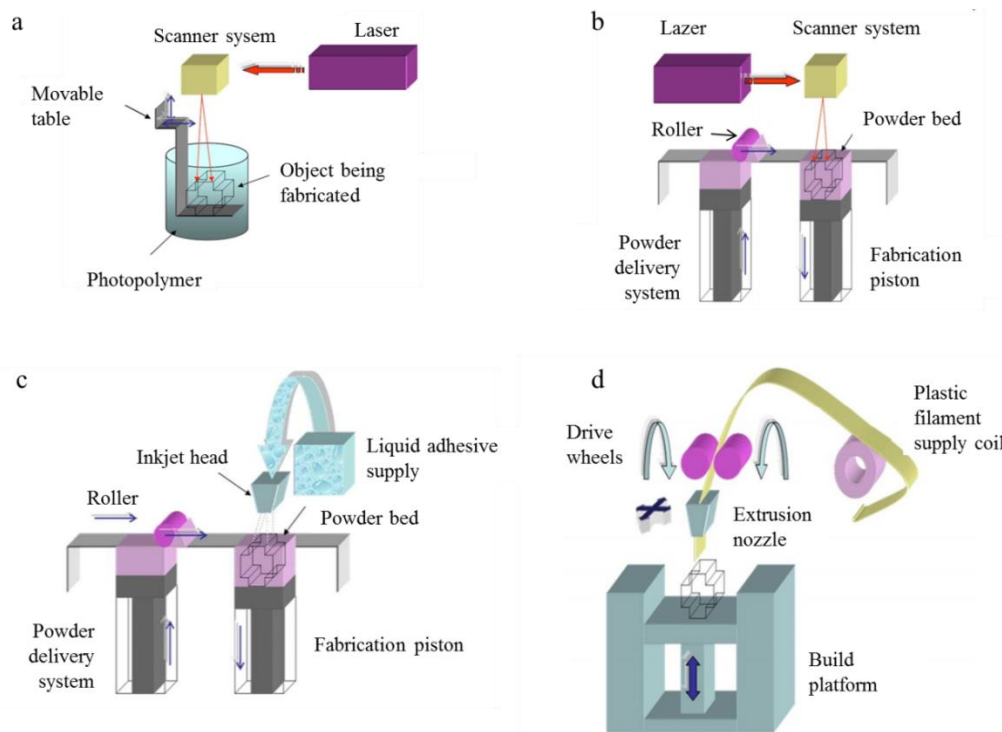


Figure 1.3: Schematic representation of various 3D printing techniques. a) stereolithography (SLA), b) selective laser sintering (SLS), c) three-dimensional printing (3-DP), d) first fused deposition modelling (FDM) (Peltola et al., 2008).

In contrast to conventional techniques which utilize top-down approaches for the production of scaffolds, rapid prototyping techniques use the bottom-up approach as the manufacturers desired complex shaped geometry is produced layer by layer guided by the computer program using cross sectional data obtained from slicing a computer aided model of the patient. RP technology can process various types of materials including wood, metal, ceramic and polymer to produce 3D structures (Hoque et al., 2011). RP techniques can control size, shape, interconnectivity, branching, and geometry of structure and offer production of patient specific scaffolds whereas conventional techniques cannot control the morphological properties of the scaffolds (Martínez-Vázquez et al., 2015).

1.1.4.2.1 SLA

Stereolithography (SLA) is technique useful in producing scaffolds with high accuracy and precision. It is based on photopolymerization using a photocrosslinkable liquid resin that is polymerized and crosslinked by exposure to ultraviolet laser according to a CAD model. After the first layer is photocrosslinked, platform recoated with fresh resin material to build second layer (Fig. 1.3a). This process is continued until 3D structure is formed (Melchels et al., 2010). Some of the materials used in stereolithography for tissue engineering are resins, thermoplastic elastomers, and poly(ethyleneglycol) (PEG)-based hydrogels (Lee et al., 2007).

1.1.4.2.2 SLS

The selective laser sintering (SLS) technique uses a laser beam, usually a CO₂ laser, in order to sinter thin layers of ceramic, metal or thermoplastic powders to obtain solid, 3D objects. When the laser beam interacts with powder, the temperature of the powder is increased and sintering occurs. Thus, material powders fuse together to form a solid structure (Hutmacher et al., 2004). Complex external and internal geometry of the product can be controlled (Fig. 1.3b). Various materials including polymers, ceramics

and composites are used to produce scaffolds via SLS technique for bone tissue engineering (Duan et al., 2011). Organic solvents cannot be used with this system; SLS is cost effective and a fast system (Williams et al., 2005).

1.1.4.2.3 3DP

Another most versatile RP technique is three-dimensional printing (3-DP). It was developed in early the 1990s at MIT (Sachs et al., 1993). In this method, powder layer is spread on the build piston and instead of using a laser to sinter the material, a liquid binder in the ink-jet printing head is printed onto the thin layer of powder to form the first layer by a controlled computer system. After a layer is built, the build platform is lowered and a new layer of powder added and the printing is repeated to obtain scaffold. Then, the unbound powder is removed after the completion of the structure (Butscher et al., 2011) (Fig. 1.3c). 3-DP can process various types of materials including ceramic, metallic, polymeric, and composite materials. Binders are selected according to properties of the materials (Bose et al., 2013).

1.1.4.2.4 FDM

The first fused deposition modelling (FDM) was developed by Crump in 1992 (Crump, 1992). This method extrudes molten polymer through a nozzle onto a platform with a layer by layer process which is controlled by a computer program (Xu et al., 2014) (Fig. 1.3d). Various thermoplastic materials have been processed with this approach for bone tissue engineering. These materials include polycaprolactone (PCL), polymethylmethacrylate (PMMA) (Espalin et al., 2010; Chen et al., 2011), and composite materials like polycaprolactone/hydroxyapatite (PCL/HA) blend (Park et al., 2010), polylactic acid/tricalcium phosphate (PLA/TCP) (Drummer et al., 2012), poly(lactide-co-glycolide)/ β -tricalciumphosphate/ hydroxyapatite (PLGA/ β -TCP/HA) (Kim et al., 2012).

1.1.5 Modification properties of scaffolds

Chemical and physical characteristics of the biomaterial surface affect cell behavior like adhesion, proliferation, migration and differentiation in bone tissue engineering. Cell attachment on biomaterial surface are more crucial biological events because surface of materials can directly affect cellular response and following regeneration of tissue (Liu et al., 2004). Cell attachment is related to the surface properties of materials like wettability, surface roughness, topography and charge (Jiao et al., 2007). Chemical, physical and biological modification techniques have been used to produce different surface properties of biomaterials (Wu et al., 2014). In the chemical treatment, there is a direct reaction between biomaterials and surrounding media such as chemical etching (Wei et al., 2008), electrochemical etching (Sun et al., 2007), hydrolysis (Neuhaus et al., 2010), oxidation techniques (Wu et al., 2007), anodization (Sjostrom et al., 2012), plasma modification (Declercq et al., 2013). In physical modification, properties of scaffold like surface roughness and topographies can be changed without altering the chemical composition. It can be carried out through a direct mechanical process to the substrate or depositing coatings, without chemical reactions (Wu et al., 2014). Physical modification techniques are mainly composed of plasma spraying (Zhang et al., 2013), porogen introduction (Liu et al., 2006), and physical vapor deposition (Liu et al., 2012). In the biological modification, biomolecules are immobilized on material surfaces with like RGD, fibronectin, heparin/heparin sulfate-bind peptides and growth factors by covalent attachment, simple physical coating and entrapment, electrostatic self-assembly to promote initial cell attachment and proliferation (Dhandayuthapani et al., 2011). Plasma treatment is a chemical modification technique where surface of scaffolds is exposed to reactive gases to form new functional groups on the polymer surfaces (Jiao et al., 2007). Plasma modification is a convenient and all-purpose technique that can change surface properties, mainly wettability, surface roughness, and the surface energy, without changing the bulk properties (Desmet et al., 2009; Jacobs et al., 2012). Plasma technique is solvent-free so hazardous solvents are not used (Morent et al., 2011).

Various gases like NH₃, O₂, N₂, CO₂ at low pressure can be used as the gas sources to create new functional groups and change the surface topography by creating micro and nano-motifs and improve its biocompatibility (Intranuovo et al., 2014). In addition, plasma treatment can also be used for immobilization of ECM proteins such as gelatin, to modify polymeric surfaces in order to promote cell attachment and proliferation (Chen et al., 2011).

1.1.5.1 Surface Modification with Oxygen Plasma

Oxygen plasma modification is achieved under nontoxic oxygen gas that can create hydroxyl and carboxyl groups on surfaces of polymer. This treatment increase hydrophilicity of the materials owing to incorporation of hydrophilic functional groups and promote cell adhesion and proliferation on the structure (Correia et al., 2016). Besides, oxygen plasma treatment can enhance the surface roughness of materials and can affect cell attachment, proliferation and differentiation (Kara et al., 2014; Jacobs et al., 2012; Hasirci et al., 2010).

In fact, various polymers such as PCL (Yildirim et al., 2011; Yilgor et al., 2012; Scislowska-Czarnecka et al., 2015), PLGA (Castillo-Dalí et al., 2014; Roh et al., 2016), PLA (Khorasani et al., 2008) and PHBV (Kose et al., 2003; Wang et al., 2006; Wang et al., 2013) have been exposed oxygen plasma to increase cell attachment and proliferation in bone tissue engineering applications. Moreover, oxygen plasma treatment has been used to coat surfaces with proteins like collagen (Polini et al., 2010), and gelatin (Chen et al., 2011). Ai et al. (2011) reported that after oxygen plasma treatment, PHBV films were immersed into collagen solution to coat the surface of films and the results showed that collagen coated film had higher hydrophilicity than the uncoated film. Cellular activity (cell viability, attachment and proliferation) on the treated film was better than the uncoated film. In another study, PHBV nanofiber mat was exposed oxygen plasma and then immediately dipped into laminin to coat the surface of the mat. Results showed that cell attachment and proliferation were better

with the laminin coated nanofiber mat than the untreated mat (Sahebalzamani et al., 2014).

1.1.5.2 Coating with cell adhesive molecules

1.1.5.2.1 Elastin-like Polymers (ELPs)

Elastin-like polypeptides (ELPs), also known as Elastin-like recombinamers (ELRs), are artificial polypeptides produced by recombinant DNA technology. They can be designed to have certain properties as a result of the repeating amino acid sequences introduced to the polypeptide structure (Rodríguez-Cabello et al., 2009). ELPs are promising polypeptides in the area of biomaterials because of their molecular versatility, biodegradability, biomimetic character and biocompatibility (Tejeda-Montes et al., 2014). The mechanical properties of ELP exhibit similarity to natural elastin (Gonzalez De Torre et al., 2014).

ELPs are composed of repeating pentapeptide sequences Val-Pro-Gly-X-Gly, where X represents any amino acid except proline and this motif is inspired from natural elastin (Tejeda-Montes et al., 2014). Up to now, a number of ELPs have been tested in tissue engineering of cartilage (Betre et al., 2006), oral mucosa (Kinikoglu et al., 2011), ocular application (Martínez-Osorio et al., 2009), liver (Janorkar et al., 2008), cell sheets (Mie et al., 2008), and bone (Amruthwar et al., 2013).

All functional ELPs display Inverse Temperature Transition (ITT) where free chains of polymer exhibit a disordered conformation and are fully hydrated below their transition temperature in aqueous solution, whereas above this temperature, polymer chains reorganize and get into more ordered structures and become insoluble. It is a completely reversible process (Gonzalez De Torre et al., 2014).

The ELP with the REDV sequence (R: Arginine, E: Glutamic acid, D: Aspartic acid and V: Valine) was firstly synthesized chemically by Urry and coworkers (Nicol et al.,

1992). However, more effort was required for their production due to the conventional synthesis technique. Advances in genetic engineering have overcome difficulties and allowed production of well defined and complex proteins like ELP-REDV (Girotti et al., 2004). The ELP with the REDV sequence is especially important in the adhesion and spreading of endothelial cells on fibronectin via its $\alpha_4\beta_1$ receptor over smooth muscle cells and platelets (Castellanos et al., 2015). This sequence was also reported to enhance proliferation of other cell types such as conjunctival epithelial cells line (Martínez-Osorio et al., 2009).

1.1.6 Cell Sources for Bone Tissue Engineering

Autologous cells isolated from patient periosteum and bone tissues of the patient can be used as osteogenic cell sources and this avoids the risks involved in allogenic and xenogenic transfers. However, it has some drawbacks including limited cell supply, donor site morbidity and limited proliferation capacity (Marolt et al., 2010). Other alternative cell sources are allogeneic cells that are obtained from another individual but there are some drawbacks like immune reactions, donor scarcity, and pathogen transmission from viruses (Badylak et al., 2010). Xenogeneic cells that are harvested from non-human donors can be utilized as another cell source. However, immunogenicity, risk of transmission of infection, and ethical and social problems are their main drawbacks (Salgado et al., 2004).

Mesenchymal stem cells (MSC) are promising cell sources for regeneration of mesenchymal tissue such as bone because they have the ability to differentiate into different cell types and turn into various mesenchymal tissues including muscle, tendon/ligament, cartilage, bone, dermis, fat and other connective tissues (Fig. 1.4) (Caplan, 2007). MSC were initially obtained from bone marrow stem cell niche. Then, various potential sources including adipose tissue and peripheral blood were characterized for MSCs (Hilfiker et al., 2011). After BMSC are isolated from marrow,

they are expanded in vitro and then following addition of certain exogenous factors, BMSC can be differentiated into osteogenic cells (Seong et al., 2010).

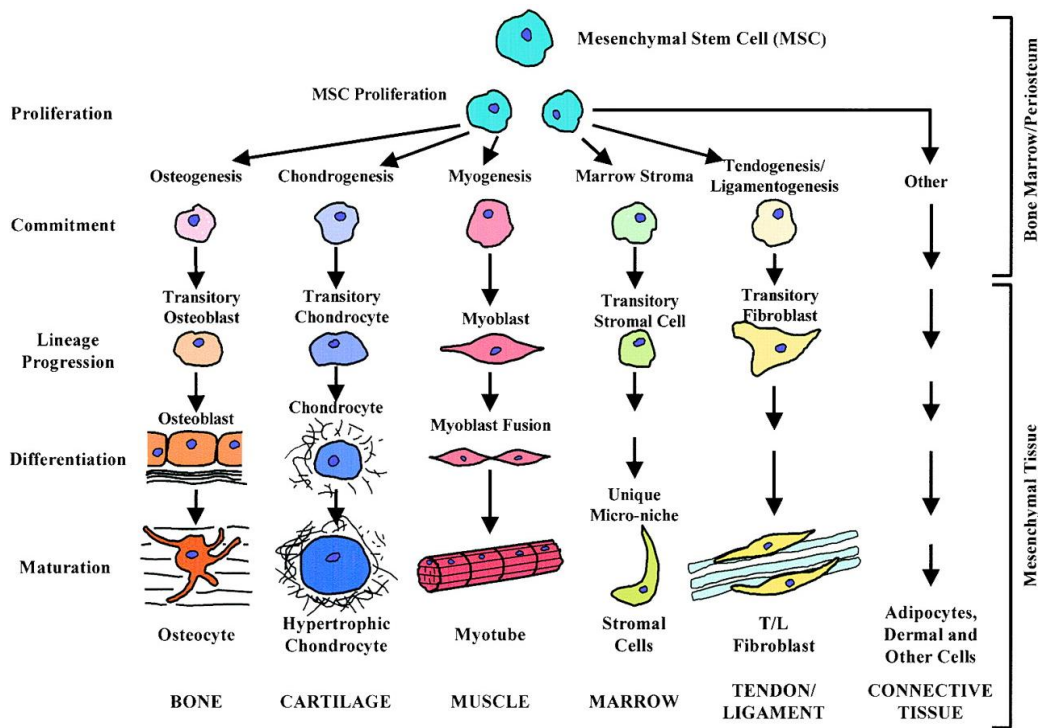


Figure 1.4: Differentiation process of BMSC (Kaplan, 2007).

1.2 Aim of This Study

The aim of this study was to develop suitable tissue engineered scaffolds to replace the damaged bone tissue. For this purpose, scaffolds of poly(3-hydroxyalkanoate)-poly(lactic acid) (PHA-PLA) blend with optimal pore size and homogenous pore distribution were produced with fused deposition modelling (FDM) and wet spinning and poly(3-hydroxybutyrate-co-3-hydroxyvalerate) (PHBV) scaffolds were produced with wet spinning and compared with PHA-PLA as a scaffold.

PHA-PLA and PHBV polymers have hydrophobic character. In order to increase hydrophilicity of polymers, oxygen plasma treatment was achieved to promote cell adhesion and proliferation on surface of scaffolds that was coated with ELP-REDV. Finally, stem cells that were isolated from rabbit bone marrow were seeded to scaffolds and cell behavior and vascularization for bone tissue were studied *in vitro* and *in vivo*.

1.3 Novelty of This Study

Fused deposition modelling is a recently introduced technique to the production of biomaterials and tissue engineering, where it can achieve controlled and homogenous pore size and distribution and can be tailored to make scaffolds with desired 3D forms. On the other hand, wet spinning produces products with pores that are randomly distributed and not uniform in size and distribution. In the present study, FDM and wet spinning methods were used to compare the influence of organized, predetermined architecture of a scaffold with that of a less organized, fibrous scaffold using two different polyesters: PHBV and PHA-PLA blends and tested them for bone tissue engineering.

To the best of our knowledge, elastin-like polymers, ELPs, consisting of amino acid sequences were used for the first time to coat the surface of scaffolds in order to attract endothelial cells which are located around defective site so that it can be vascularized as needed in a thick implant which otherwise cannot maintain the viability of the cells that have penetrated deep into the scaffold. All these together constitute a biodegradable scaffold suitable for bone tissue engineering.

CHAPTER 2

MATERIALS and METHODS

2.1 Materials

PHBV (HV content 8% w/v) was kindly provided by Profs T. Volova and E. Shishatskaya of Siberian Federal University (Russia). 2.85 mm PLA-PHA filament with a density of 1.24 gr/cc was purchased from Colorfabb Company (Netherlands). ELP-REDV sequences were produced at the Bioforge laboratories (Vallodolid, Spain) and were a kind gift of Prof. R. Cabello. Coomassie brilliant blue, bovine serum albumin (BSA), Amphotericin B, 4',6-diamine-2-phenylindole dihydrochloride (DAPI), FITC-conjugated Phalloidin, Toluidine Blue O, β -glycerophosphate, L-ascorbic acid, and dexamethasone were obtained from Sigma-Aldrich (USA). Dulbecco's Modified Eagle Medium High Glucose and Penicillin Streptomycin were purchased from Lonza (Switzerland). Fetal bovine serum was purchased from Biowest (USA). Alamar Blue was taken from Invitrogen Inc (USA). Alkaline phosphatase kit (ALP) was obtained from Anaspec (Belgium). Alizarin Red solution was purchased from Cyagen (Germany). Monoclonal mouse anti-rabbit osteopontin antibody conjugated with Alexa Fluor[®] 532 was taken from Origene (USA). CD13, CD146, CD14 and CD105 antibodies for flow cytometer were obtained from Genetex (USA). Nucleo Casette was purchased from ChemoMetec (Denmark). All other chemicals were analytical grade and used as received.

Female New Zealand White rabbits were kindly provided by Prof. Dr. Cemil Yildiz of Gulhane Military Medical Academy (Turkey).

2.2 Methods

2.2.1 Scaffold Production

2.2.1.1 Production of PHBV scaffolds by wet spinning

PHBV was dissolved in chloroform (8% w/w) to prepare proper solution. After PHBV solution was loaded into glass syringe and placed onto syringe pump (NE-300 New Era Pump System Inc. Wantagh, NY, USA), solution was extruded into a coagulation bath of methanol at a constant rate to obtain PHBV microfibers. Then, these fibers were kept in methanol at -4°C overnight. After that, they were placed into a teflon mold to give cylindrical shape and put in vacuum oven to dry at 50°C for 1h. Finally, three dimensional, interconnected and highly porous structure was formed (Fig. 2.1).

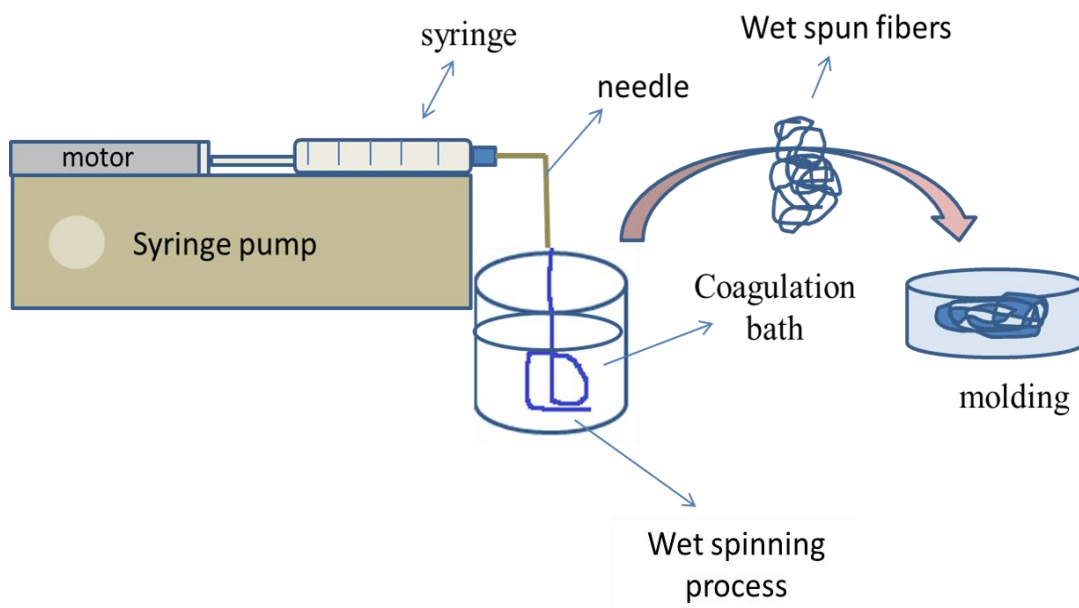


Figure 2.1: Wet spinning process.

2.2.1.2 Production of PHA-PLA scaffolds by wet spinning

PHA-PLA filament was cut into pieces by a blade and then dissolved in chloroform (13 % w/w) to obtain a polymer solution. After that, scaffolds were produced by same process mentioned above (Section 2.2.1.1).

2.2.1.3 Production of PHA-PLA scaffolds by rapid prototyping

Cylindrical porous scaffolds (10.0 mm in diameter, 5.0 mm in thickness) were designed as 5 layers that were arranged to have 45° between layer by using the Software SketchUp (Google, USA) (Fig. 2.2). The designed 3D model was converted from TXT to STL file and then Ultimaker 2 (Ultimaker, Netherlands) compatible G-Code file was obtained from this STL file since the machine requires G-Code (open source) for processing.

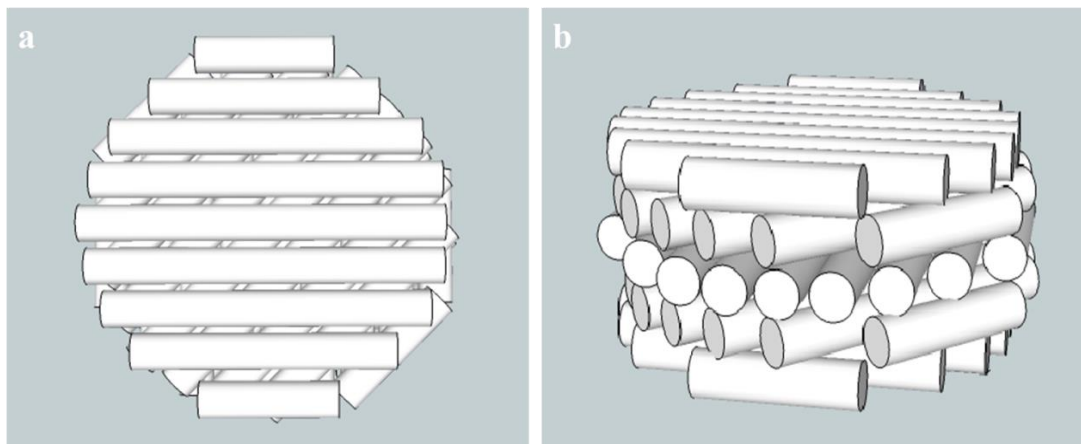


Figure 2.2: Scaffold designed to produce a cylindrical 3D scaffold for bone tissue engineering with SketchUp Software, (a) top, (b) side view.

After PHA-PLA filament was heated above the melting temperature, molten material extruded through nozzle (0.4 mm diameter) onto the table at a print rate 250 mm/s during production of scaffolds.

2.2.2 Surface Modification of Scaffolds with Oxygen Plasma

In order to increase the hydrophilicity of the scaffolds, to promote cell adhesion and also to activate the surface for ELP-REDV binding, oxygen plasma treatment was applied (Advanced Plasma Systems Inc. (USA)).

For this purpose, samples were placed in the RF plasma reactor chamber and oxygen gas was introduced (20 mTorr) and the discharge was applied to PHBV wet spun scaffolds at 50W for 4 min, and PHA-PLA wet spun and FDM scaffolds at 50W for 2 min.

Also, PHBV films (2% w/w in chloroform) and PHA-PLA films (5% w/w in chloroform) were prepared to study the chemical changes on the surface by solvent casting on petri plates. After the PHBV and PHA-PLA films were dried at -4°C temperature for 3 days, they were removed from petri plate and cut by a blade to obtain a film with 2x2 cm² dimensions. Later, PHBV films and PHA-PLA films were placed in the plasma reactor and oxygen gas was flushed in and system activated at 50 W for 4 min and 50 W for 2 min, respectively. Flow rate was controlled to keep the pressure at 20 mTorr.

2.2.3 Immobilization of ELP-REDV on all scaffolds

Immediately, after oxygen plasma treatment, all scaffolds were immersed into ELP-REDV solution (0.1% w/v in distilled water) for 2 h to coat ELP-REDV on the surface of scaffolds. Then, the samples were washed with distilled water to remove unattached REDV and dried at room temperature overnight. A similar modification was done on solvent cast PHBV and PHA-PLA films to study the chemical changes on the surface.

2.2.4 Characterization of scaffolds

These experiments were achieved by all types of scaffolds (PHBV wet spun, PHA-PLA wet spun and PHA-PLA FDM scaffolds).

2.2.4.1 Morphology of all scaffolds

Morphology of all samples was studied by using SEM and stereomicroscope. The mean fiber diameter and pore size of scaffolds were determined using NIH image J software on micrographs with x50 magnification from samples. The porosity of scaffolds was measured by micro CT (SkySkan Instruments Ltd., Belgium).

2.2.4.2 Mechanical Testing

Compressive strength of dry PHBV wet spun scaffolds with diameter 10 mm and thickness 5 mm was measured by Stable Micro Systems Testing Machines (UK) with a 5 kN load cell at velocity of 3 mm/min. Six specimens were used to determine Young's modulus of scaffolds.

Compressive stresses of dry PHA-PLA wet spun and FDM scaffolds were determined by AGS-X Universal Testing Machines (Shimadzu, USA). PHA-PLA wet spun samples with diameter 9 mm and thickness 5 mm and PHA-PLA FDM samples with diameter 10 mm and thickness 5 mm were placed between compression plates and they tested with 5 kN load cell at a velocity of 0.1 mm/min. Six replicates were to determine average values of stiffness of scaffolds and given as modulus of elasticity (E).

2.2.5 Characterization of PHBV and PHA-PLA films

2.2.5.1 Surface wettability measurement of PHBV and PHA-PLA films

The contact angles of the PHBV and PHA-PLA films with water were measured using sessile-drop method with deionized water by a contact angle goniometer (One Attension, Biolin Scientific, Sweden). Droplets of deionized water (7 μ L) were placed at 6 different locations on the film surface and water contact angle values were measured from cross sectional images captured by digital camera system.

2.2.5.2 FTIR-ATR analysis of PHBV and PHA-PLA films

In order to show that ELP-REDV is chemically attached on the PHBV and PHA-PLA films, the sample surfaces were analyzed with FTIR-ATR spectroscopy (Perkin Elmer Spectrum, Frontier, Massachusetts, USA). All PHBV and PHA-PLA films were scanned 4 times in the range $300\text{-}3250\text{ cm}^{-1}$ and $1000\text{-}3500\text{ cm}^{-1}$ with a resolution of 4 cm^{-1} , respectively.

2.2.5.3 Toluidine Blue Staining of PHBV and PHA-PLA films

Toluidine Blue staining was used to show ELP-REDV coating on the surface of PHBV and PHA-PLA films. For this purpose, Toluidine Blue O solution (10% w/w in ethanol pH 2) was dropped on the films and waiting for 2-3 min. After films were washed three times with distilled water, they were examined with stereomicroscope.

2.2.5.4 Atomic force microscopy (AFM) of PHBV and PHA-PLA films

Atomic force microscopy was used to study the influence of oxygen plasma exposure and coating of ELP-REDV on surface topography of PHBV and PHA-PLA films. For this purpose, PHBV films produced by solvent casting and rectangular PHA-PLA films produced with Ultimaker under the same condition as the scaffolds were used. Samples were examined with a Quesant Universal SPM instrument in noncontact mode by using silicon cantilevers (Ambios Technology Inc., USA) at room temperature.

2.2.6 In vitro studies

2.2.6.1 Bone Marrow Mesenchymal Stem Cells Isolation

Bone mesenchymal stem cells (BMSCs) were isolated from the tibia and femur of New Zealand white rabbits (female, weight, ca. 3 kg, 24 weeks) with the approval of Gulhane

Military Medical Academy Ethics Committee and kindly provided by Prof. Cemil Yıldız. For the isolation of BMSCs, first muscle and connective tissue were removed from femur and tibia and then the ends of bone were cut with lancet under sterile conditions. Bone marrow of the shaft was flushed out with DMEM (high glucose) including fetal bovine serum (10%), penicillin-streptomycin (1%) and amphotericin B (250 ng/mL) into centrifuge tube. Then, cell suspension was centrifuged at 400 g for 10 min. After supernatant were removed, pellet was resuspended in growth medium and transferred in T-75 flasks.

2.2.6.2 Characterization of isolated rabbit bone marrow mesenchymal stem

Cells at passages 1 and 3 were analyzed by flow cytometer (BD Accuri C6, USA) by using surface markers (CD13, CD14, CD105 and CD146) in order to characterize of isolated rabbit BMSc. After trypsinization and centrifugation of cells, supernatant was removed and pellet was washed with FACS buffer. After centrifugation, 4% (w/v) paraformaldehyde was added on the pellets for fixation of cells at room temperature for 15 min. Then, cells were centrifuged and washed with FACS buffer. Obtained pellets resuspended with FACS buffer were divided into 100 μ L for each eppendorfs. 1 μ L antibody solution was added into each tube and incubated at room temperature for 30 min. 1 μ L of PBS was put in the each eppendorfs and then centrifuged. Obtained pellet was resuspended with PBS (400 μ L) and then examined with flow cytometer through 4 channels (forward scatter channel (FSC), size scatter channel (SSC), fluorescence channel (FL1 filter, laser 488 nm), and fluorescence channel (FL4 filter, laser 647 nm)). Data was analyzed with CFlow[®]Plus software (BD Biosciences, USA). An isotype control was employed in each experiment to calculate specific staining.

2.2.6.3 Sterilization and BMSC seeding on all types of scaffolds

All scaffolds were placed into 24 well plates and submerged for 2h in 70% aqueous ethanol solution for sterilization, washed twice with phosphate buffered saline (PBS), and dried in a laminar flow hood.

Rabbit bone marrow mesenchymal stem cells (RBMSCs) were detached from the surface of the TCPS plate with 0.25% Trypsin-EDTA at 37°C for 5 min and the Trypsin activity was inhibited with the standard growth medium. Cell suspension was centrifuged (3000 g, 5 min) and the pellet was suspended in the growth medium, the cell number was determined with the Nucleocounter (ChemoMetec, Denmark). 5×10^4 cells were seeded onto the scaffolds in the 24 well tissue culture plates and placed in a CO₂ incubator at 37°C for 1 h to allow cell attachment. 2 mL growth medium was added into each well and medium was changed three times a week until cell number determination.

2.2.6.4 Rabbit Bone Marrow Mesenchymal Stem Cell Culture

Rabbit bone mesenchymal stem cells on all scaffolds were cultured in high glucose DMEM (Gibco, USA) containing fetal bovine serum (10%), penicillin-streptomycin (1%) and amphotericin B (250 ng/mL) for 7 days. After 7 days, osteogenic medium including DMEM supplemented with FBS (10%), penicillin-streptomycin (1%) and amphotericin B (250 ng/mL), β -glycerophosphate (10 mM), L-ascorbic acid (50 μ g/mL), dexamethasone (10 nM) was used to promote osteogenic differentiation for additional 21 days.

2.2.6.5 Determination of cell proliferation

Cell numbers on the scaffolds was determined with Alamar Blue assay (Invitrogen, Carlsbad, CA) on Days 1, 7, 14, 21, and 28. Samples were washed twice with DMEM High colorless medium (Lonza, Switzerland), placed in 1mL Alamar Blue solution (10% in DMEM High colorless medium including penicillin- streptomycin (100 μ g/mL)

and amphotericin B (100 UI/mL)) for 1 h at 37 °C and 5% CO₂. The reduced solution (200 µL) was transferred into 96 well plates and absorbances at 570 and 595 nm were measured with an Elisa plate reader (Molecular Devices, USA) at room temperature. Percent reduction values were calculated from Alamar Blue equation (Appendix A, Equation 1) and cell numbers were determined using a calibration curve (Appendix A).

2.2.6.6 Alkaline phosphatase (ALP) Assay for the Assessment of BMSC Differentiation

Alkaline phosphatase activity was measured colorimetrically by using SensoLyte pNPP Alkaline Phosphatase Assay Kit (AnaSpec Inc., USA) after 7, 14, 21 and 28 days of cell culture. Briefly, scaffolds were washed twice with PBS and component B (assay buffer) to remove nonadherent cells. Scaffolds were placed in 500 µL lysis buffer (kit component) and cells were lysed by 3 freeze - thaw cycles (-80 °C and 37 °C). After centrifugation (3000 rpm for 5 min) to remove residual material, 50 µL supernatant was added followed by 50 µL ALP dilution buffer and Component A to each well, and incubated for 1 h at 37 °C. Reaction was stopped with 50 µL stop solution and absorbance was measured by microplate reader at 405 nm. ALP concentration was determined from the ALP calibration curve. ALP levels for each cell were calculated by dividing the cell number which was measured by Alamar Blue assay.

2.2.6.7 Microscopic evaluation of cell morphology

2.2.6.7.1 Scanning electron microscopy

Cell morphology and mineral deposition on all type of scaffolds were determined by scanning electron microscopy. After 28 days cell in the culture, the cell seeded scaffolds were fixed with paraformaldehyde (PFA) (4% w/v in distilled water, pH 7 - 7.5) for 40 min at room temperature, and washed three times with piperazine-N,N'-bis(2-ethanesulfonic acid) (PIPES) buffer. Then, scaffolds were immersed into 4 % Osmium

Tetroxide solution and three times washed with PBS. After the scaffolds were dehydrated through a series of graded alcohol solutions, they were lyophilized. Scaffolds were coated with a thin layer of gold before examining with SEM (QUANTA 400F, Holland).

2.2.6.7.2 Confocal laser scanning microscopy

At the end of 28 days in the culture, cell seeded scaffolds were three times washed with PBS to remove nonadherent cells and then fixed in 4% (w/v) paraformaldehyde for 30 min. Samples were submerged into Triton-X 100 (1% v/v in PBS, pH 7.4) for permeabilization of cell membrane for 5 min. After washing with PBS, samples were incubated in BSA (1% w/v in PBS) at 37°C for 30 min to avoid non-specific binding. Cells were stained with Alexa Fluor 488 conjugated phalloidin (1:200 dilution of stock, in PBS) in order to stain the actin filaments. After washing steps, nucleus was stained with DRAQ 5 (1:1000 dilution of stock, in PBS with 1% BSA). After washing with PBS, osteopontin was stained with monoclonal antibody labelled with Alexa Fluor® 532 mouse against rabbit OPN (1:50 dilution of stock, in PBS). Samples were examined with confocal laser scanning microscopy (CLSM) (Leica TCS SPE, Germany).

2.2.6.7.3 Alizarin Red Staining for Determining of Mineral Deposition

In order to determination of mineralization on the scaffolds, Alizarin Red staining was done. After 4 weeks, all cell seeded scaffolds were fixed with PFA for 15 min at room temperature. After samples were washed twice with PBS, they were stained with Alizarin Red solution (Cyagen, Germany) for 10 min. Samples were left overnight into distilled water on stirrer to remove residue of dying. Then, samples were visualized with stereomicroscope for PHA-PLA FDM scaffolds and phase contrast microscope for PHBV and PHA-PLA wet spun scaffolds.

CHAPTER 3

RESULTS AND DISCUSSION

3.1 Preparation and characterization of the scaffolds

3.1.1 Wet spun PHBV scaffolds

After optimizing polymer concentration as (8% w/w in chloroform), PHBV microfibers were produced by wet spinning and placed in Teflon mold to obtain cylindrical PHBV scaffolds. Figures 3.1a show the μ CT of the wet spun PHBV scaffolds. μ CT images show interconnected 3D structure with a porosity of approximately 75 % (Table 3.1). The average fiber diameter and pore size were measured as 90 μ m and 250 μ m, respectively, using SEM images and NIH image J program (Fig 3.1b) (Table 3.1). Stereomicrographs present the overall appearance of the scaffold (Fig 3.1c).

3.1.2 Wet spun PHA-PLA scaffolds

A suitable fiber could not be obtained with 8 and 10 % w/w PHA-PLA in chloroform and when the concentration was raised to 13% fibers with smooth surfaces could be produced. Porosity of scaffolds was determined by μ -CT and found as 77% (Figure 3.1f) (Table 3.1). Highly interconnected structures were obtained as shown by the micrographs. The average fiber diameter and pore sizes were found as 100 μ m and 350 μ m, respectively, using μ CT and SEM (Figures 3.1d and e).

3.1.3 FDM PHA-PLA scaffolds

PHA-PLA FDM scaffolds were prepared by Ultimaker and fiber diameter, pore size and porosity were determined using the μ -CT, SEM, and stereomicrographs (Figure 3.1g, h, i). μ -CT images revealed that interconnected 3D structures with a porosity of approximately 50% were obtained (Table 3.1). Average fiber diameter and pore size of scaffolds were measured with NIH image J program and found as 1 mm and 125 μ m, respectively.

Table 3.1: Characterization of scaffolds.

Scaffolds	Porosity (%)	Pore size (μ m)	Fiber diameter (μ m)
PHBV wet spun	75	250	90
PHA-PLA wet spun	77	300	100
PHA-PLA FDM	50	125	1000

Porosity and pore interconnectivity of the scaffolds are very important properties for bone tissue engineering because they influence the space for new tissue growth, diffusion of essential nutrients, removal of waste products and vascularization (Liao et al., 2002). However, porosity also influences mechanical properties of scaffolds and highly porous structures have low mechanical properties. Thus, there should be a balance between them and is a big challenge for bone tissue engineering (Ramay et al., 2004). Pore size of the scaffolds should be at least 100 μ m for proper diffusion of nutrition and oxygen into the scaffolds for survival of cells (Bose et al., 2012).

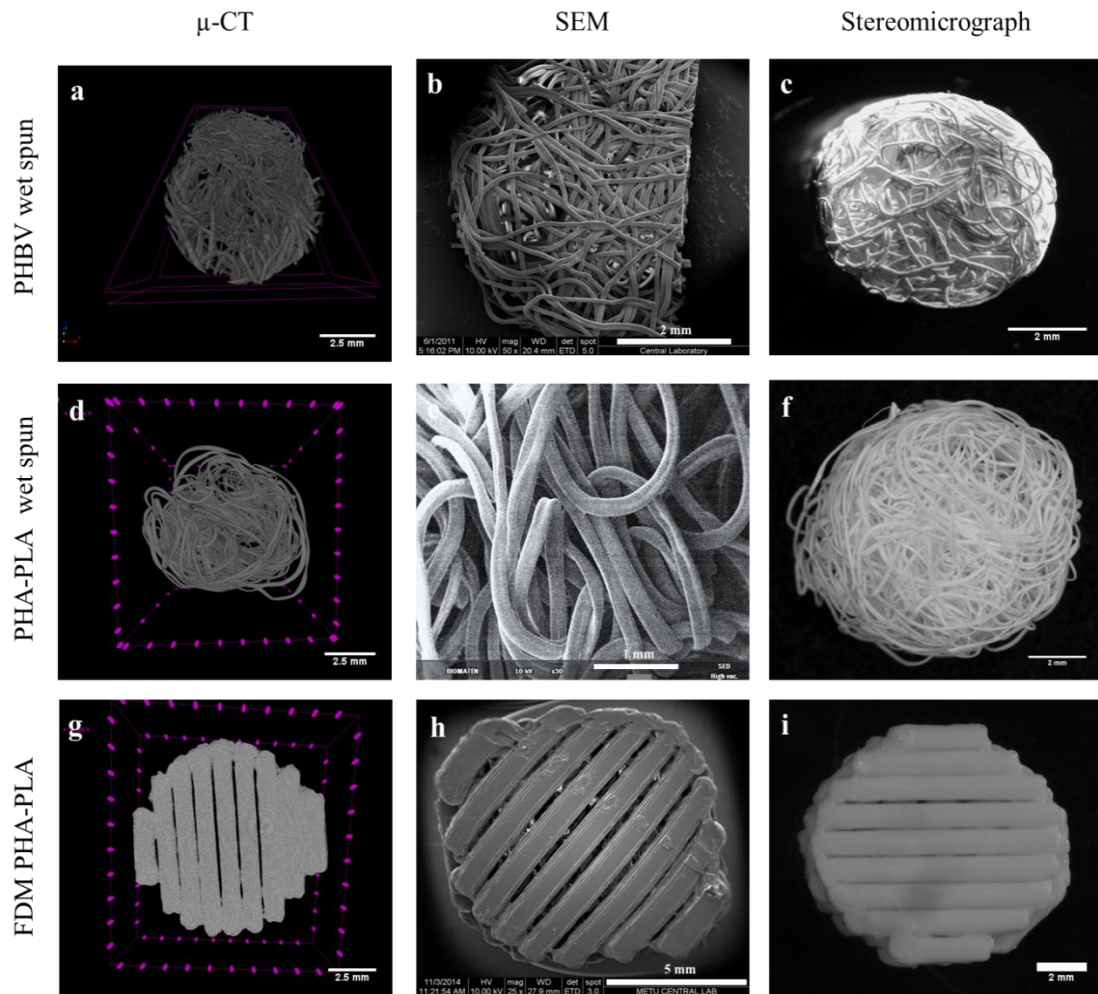


Figure 3.1: Microscopic images of wet spun PHBV, wet spun PHA-PLA and FDM PHA-PLA scaffolds; (a, d, g) top view of μ -CT images, (b, e, h) SEM micrographs, and (c, f, i) stereomicrographs of scaffolds.

The ideal pore size for bone ingrowth was reported to be in the range 200-350 μm since pore size smaller than 150 μm does not support the vascularization of the structure (Bose et al., 2012). In this study, the pore size of FDM PHA-PLA scaffold was slightly lower than the recommended while the pore sizes of wet spun PHA-PLA and PHBV scaffolds were in agreement with ideal pore size range in the literature. Besides, μ -CT analysis

revealed that wet spun PHA-PLA and PHBV scaffolds are highly porous and interconnected. However, FDM PHA-PLA scaffold had a lower porosity than the other two because of the larger fiber diameter and smaller pore sizes but this yields better mechanical properties than the other wet spun scaffolds. The main function of bone is load carrying and these scaffolds had better mechanical properties than others (Section 3.1.4).

3.1.4 Mechanical characterization

Mechanical properties of the all types of scaffolds were evaluated in dry state (n=6). Representative compressive stress-strain curves of the scaffolds are presented in Figure 3.2. Young's Moduli of scaffolds were calculated from the slope of the line that is drawn as a tangent to the compressive stress-strain curve. Since a value for Young's modulus is not representative for the entire of the stress-strain curve, it was calculated from this tangent. Mechanical test was stopped before excessive loading of the plates. For this reason, ultimate compressive strength and fracture were not calculated. The Young's modulus (E) of wet spun PHBV was 4.65 ± 0.69 MPa, whereas for wet spun PHA-PLA constructs it was 1.25 ± 0.10 MPa. E value for the wet spun PHBV was slightly higher than wet spun PHA-PLA (4.65 vs 1.25), however, for the FDM PHA-PLA, it was 363.00 ± 0.50 MPa, 100 to 300 times higher than the wet spun scaffolds (Table 3.2). The reason for this distinct difference is that wet spun scaffolds were distinctly more porous than the FDM scaffold (Section 3.1.2). Also, wet spun scaffolds have an irregular porous form composed of randomly distributed fibers. However, fibers of FDM scaffolds contact with each other that prevents deformation.

In Table 3.3 the Young's moduli of typical bone tissues in human body are presented. While enamel and dentin exhibit Young's modulus as high as 41 and 18.6 GPa, respectively, trabecular and cortical bone's values range from 0.1 to 2 GPa and from 15 to 20 GPa, respectively. The PHBV and PHA-PLA wet spun scaffolds prepared in this study are too soft compared to these tissues. On the other hand, PHA-PLA FDM

scaffolds possess mechanical properties similar to cortical bone. Thus, this scaffold can be a viable choice for *in vivo*.

Table 3.2: Young’s Modulus of the three scaffolds.

Samples	Young’s Modulus (MPa)
Wet spun PHBV scaffolds	4.65±0.69
Wet spun PHA-PLA scaffolds	1.25±0.10
FDM PHA-PLA scaffolds	363.00 ± 0.50

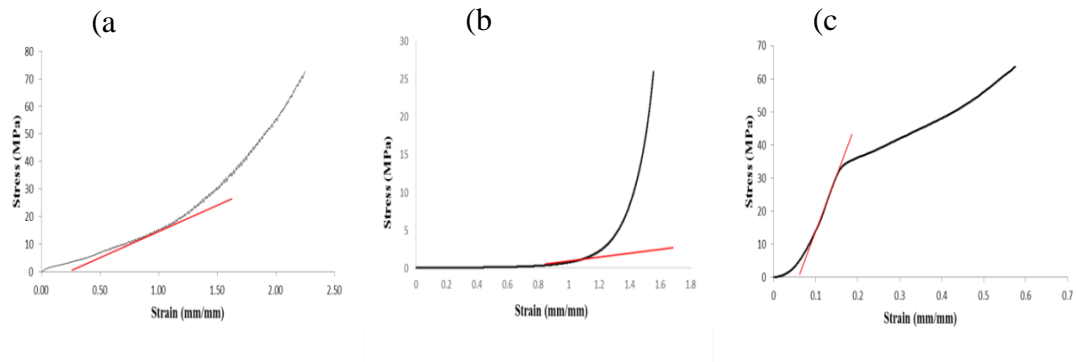


Figure 3.2: Representative compressive stress-strain curves of; a) wet spun PHBV scaffold, b) wet spun PHA-PLA scaffold, and c) FDM PHA-PLA scaffold.

Table 3.3: Young’s Modulus of Typical Bone Tissues in Human Body

Structure	Young’s Modulus (GPa)	Reference
Enamel	41	(Mijiritsky et al., 2004)
Dentin	18.6	(Singh et al., 2015)
Thigh bone (Femur)	10-15	(Antonialli et al., 2011)
Tibia	18.1	(Bose et al., 2015)
Cortical Bone	15 - 20	(Bose et al., 2012)
Trabecular Bone	0.1 -2	(Bose et al., 2012)

3.1.5 Contact angle measurement

The contact angles of the PHBV and PHA-PLA films with water were determined using a commercial contact angle goniometer before and after oxygen plasma treatment.

3.1.5.1 Surface wettability of PHBV and PHA-PLA films

Surface wettability of materials is very important in the interaction of materials with cells or proteins. Highly hydrophilic or highly hydrophobic surfaces are not suitable for protein adhesion, cell attachment and proliferation (Faucheux et al., 2004). Menzies et al. (2010) divided materials into three groups according to their contact angles: hydrophobic (contact angle above 80°), moderately wettable (contact angle in the range 48°- 62°) and hydrophilic ones (contact angle less than 35°). They reported that moderately wettable surfaces enhance cell attachment, growth and proliferation.

PHBV is a hydrophobic polyester. For this reason, oxygen plasma treatment was applied to improve the hydrophilicity of the scaffolds and their cell adhesiveness. Another reason for O₂ plasma treatment was to activate the surface of scaffolds to be able to coat with ELP-REDV and make it more cells attractive. PHBV films (representing 3D scaffolds) were prepared by solvent casting and treated at 50W according to section 2.2.2. After that, contact angles were immediately measured by sessile drop method. Results showed that the contact angle of the untreated PHBV films was decreased significantly from 83° ± 3.43 to 59° ± 2.45 after oxygen plasma treatment (p≤0.05) (Table 3.4). Results indicate that wettability of PHBV is improved. This surface is probably better for cell attachment and proliferation since cells generally prefer moderately wettable surfaces.

Oxygen plasma treatment to increase surface wettability of PHBV structures was extensively studied by others (Kose et al., 2005; Ferreira et al., 2009; Wang et al., 2013). Tezcaner et al. (2003) showed that oxygen plasma treatment parameters like power and time affected the changes in surface wettability of PHBV; hydrophilicity of PHBV

increased when these parameters (power and duration) were increased. In another study, Wang et al. (2006) showed that the contact angle of the PHBV films decreased from $75.2^\circ \pm 5.6^\circ$ to $52.4^\circ \pm 3.9^\circ$ after treatment with 100 W and 2 min. The differences between contact angles measured in our study and Wang group might be related with chain length or relation between chains.

PHA-PLA has hydrophobic character because of hydrophobic functional groups like the extra methyl group on the lactide. PHA-PLA films were exposed to oxygen plasma at 50 W for 4 min and contact angles of films were measured by sessile-drop method as before. Results showed that contact angle of the untreated PHA-PLA film decreased significantly, from $79^\circ \pm 0.5$ to $39^\circ \pm 0.60$, and a more hydrophilic surface was obtained which is not proper surface for cell attachment. Different treatment times were applied to obtain less hydrophilic surfaces. When oxygen plasma was applied for 1 min at 50 W, contact angle of film decreased to 63° which is moderately hydrophilic surface. However, FTIR-ATR results showed that surface of film was not coated with ELP-REDV after the film was exposed to oxygen plasma and dipped into ELP-REDV solution (Section 3.1.8.2). When the film was exposed to oxygen plasma for 2 min at 50 W, contact angle of film decreased to $56^\circ \pm 1.50$ ($p \leq 0.05$) (Figure 3.3) (Table 3.4). Thus, a less hydrophilic surface was obtained and also amide I and amide II bands were observed in the FTIR-ATR spectra (Section 3.1.8.2) indicating that the surface was significantly activated to bind the REDV.

Thus, these results were compared to another material because PHA-PLA blend has not been exposed to oxygen plasma in the literature. Yamaguchi et al. (2004) found that contact angle of untreated poly(L-lactic acid) film was 67° . However, this value was decreased to 51° after oxygen plasma treatment at 10W for 1 min. In other study, Armentano et al. (2009) prepared PLLA films and applied oxygen plasma for 5 min at 10W. It was observed that contact angle of PLLA films decreased from $89.2^\circ \pm 0.4^\circ$ to $51.5^\circ \pm 0.5^\circ$ and this change affected and improved to cell attachment on the structure. Their result is highly different from results found in this study. The reason may be related with materials where they used PLLA and PHA-PLA blend was used in our

study. Thus, they have different chemical properties like crystallinity, chemical composition, and polymer properties such as molecular weight.

Table 3.4: Contact angle of PHBV and PHA-PLA films.

Sample	O ₂ plasma applied (Power [Watt], Time [Min])	Contact angle (deg)
PHBV	0	83 ± 3.43
PHBV	50, 4	59 ± 2.45
PHA-PLA	0	79 ± 0.50
PHA-PLA	50, 1	63 ± 0.44
PHA-PLA	50, 2	56 ± 1.50
PHA-PLA	50, 4	39 ± 0.60

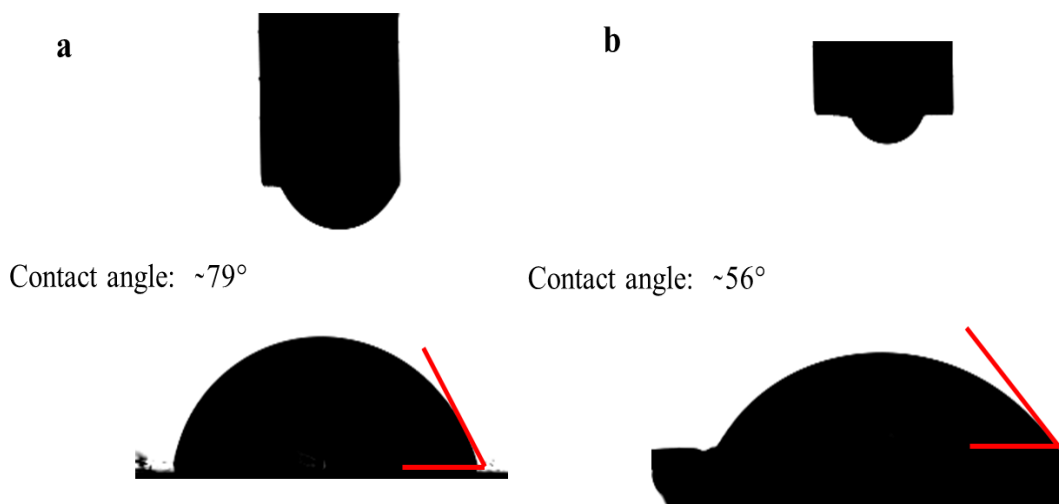


Figure 3.3: Contact angle measurement of PHA-PLA films (a) Untreated PHA-PLA film, (b) PHA-PLA film treated with oxygen plasma.

3.1.6 Surface roughness of films

Surface topography and chemistry influence the interaction between biological environment and biomaterial (Tezcaner et al., 2003). In this study, surface morphology and roughness were studied with atomic force microscopy (AFM) to determine whether the surface of the structure was coated with ELP-REDV or not. After the plasma treatment, it is difficult to determine exact surface roughness of three dimensional scaffolds directly because of its rough and porous architecture. For this reason, rectangle shape PHBV film was produced by solvent casting and PHA-PLA film was produced by Ultimaker under same condition of production of PHA-PLA scaffold and then, surface characterization of the films was analyzed by atomic force microscope (AFM).

3.1.6.1 Surface roughness of PHBV film

AFM images showed that the morphology of untreated PHBV film surface consisted of smooth, dome-like structures. After oxygen plasma treatment, the number of dome-like structures was reduced and more uniformity. However, the film exhibited more dome-like structures after the surface was exposed oxygen plasma and then coated with ELP-REDV (Figure 3.4). This result was also supported with Peak-Valley and RMS (Root Mean Square) deviation values of films (Table 3.5). Peak-Valley value indicates the distance between the highest peak and the lowest valley along the Z axis. Peak-Valley value of untreated PHBV film was 1.422 μm . This value was significantly decreased, to 668.9 μm , after the oxygen plasma treatment. However, it was significantly increased, to 2.509 μm , after the surface of films was coated with ELP-REDV. Also, RMS (Root Mean Square) deviation value of the surfaces showed that surface roughness of the untreated PHBV films was significantly higher than the films treated with oxygen plasma (303.4 nm vs 112.2 nm) but it was significantly increased due to ELP-REDV (391.5 nm). These results showed that surface topography of the film was changed after

the oxygen plasma treatment and also, coating with ELP-REDV. This result is an indicator of successful ELP-REDV coating on the surface of PHBV films.

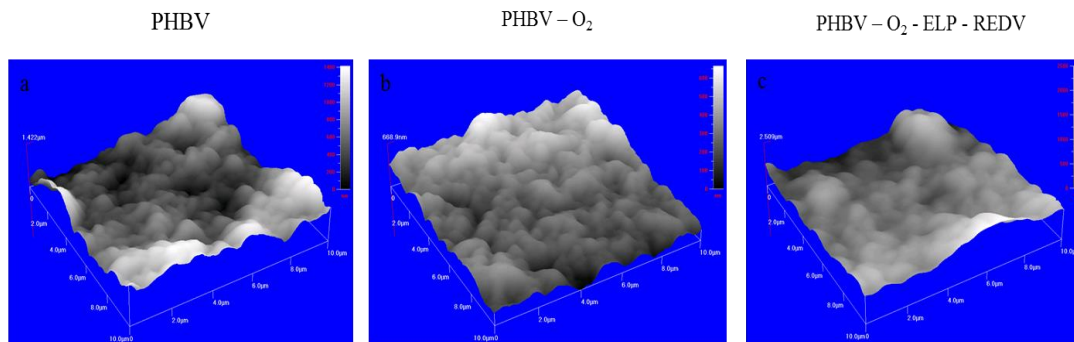


Figure 3.4: AFM results of oxygen plasma treated PHBV films; (a) Untreated PHBV, (b) PHBV film treated with oxygen plasma and (c) PHBV film treated with oxygen plasma and coated with ELP-REDV.

Table 3.5: Surface characteristics of PHBV film.

Property	PHBV (nm)	PHBV - O ₂ (nm)	PHBV - O ₂ - ELP (nm)
Average Height	615.2	312.4	1224
RMS deviation (Sq)	303.4	112.2	391.5
Max deviation	806.6	356.5	1285
Peak (Sp)	806.6	356.5	1285
Valley (Sv)	615.1	312.4	1224
Peak – Valley (St)	1422	668.9	2509

3.1.6.2 Surface roughness of PHA-PLA film

Fig 3.5 shows AFM results of untreated, oxygen plasma treated and oxygen plasma treated and ELP-REDV coated PHA-PLA films. As can be seen in the AFM images, surface of PHA-PLA film was almost smooth which contained some dome-like structures. After the oxygen plasma treatment, more dome-like structures were formed.

However, the number of these dome-like structures was reduced after oxygen plasma treatment and ELP-REDV coating. These observations were supported by the RMS (Root Mean Square) deviation and Peak-Valley values (Table 3.6). Unlike that observed with PHBV films, the RMS deviation values of the surfaces showed that surface roughness of the treated PHA-PLA films were significantly higher than the film not treated with oxygen plasma. Peak-Valley values of surface of films treated with oxygen plasma were also higher than the untreated film (1.797 μm vs 1.641 μm). These results showed that surface roughness of scaffolds was increased after oxygen plasma treatment. However, RMS and Peak-Valley values of film treated with oxygen plasma and coated with ELP-REDV decreased again (342.8 nm vs 153.5 nm and 1.797 μm vs 554.6 μm) when compared to oxygen plasma treated film. These results showed that surface topography of films increased after oxygen plasma treatment and then decreased upon oxygen plasma treatment and ELP-REDV coating.

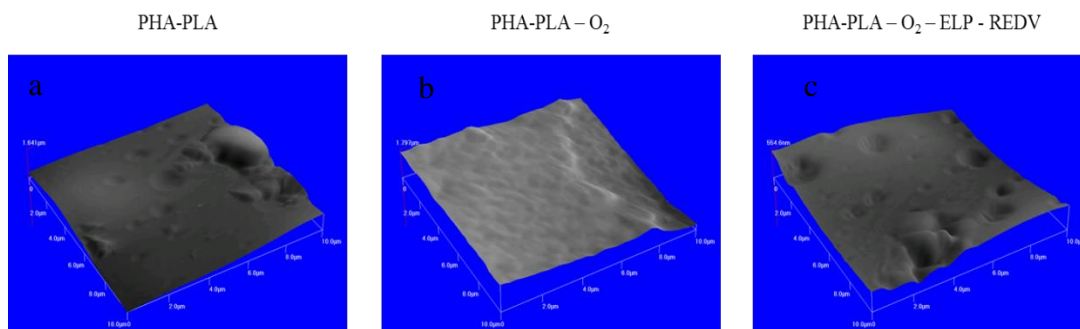


Figure 3.5: AFM results of PHA-PLA films; (a) Untreated PHA-PLA, (b) PHA-PLA film treated with oxygen plasma and (c) PHA-PLA film treated with oxygen plasma and coated with ELP-REDV.

Table 3.6: Surface characteristics of PHA-PLA film

Property	PHA-PLA	PHA-PLA - O ₂	PHA-PLA - O ₂ - ELP
Average Height (nm)	529.6	1.298	295.5
RMS deviation (Sq) (nm)	243.0	342.8	153.5
Max deviation (μm)	1.112	1.298	295.5
Peak (Sp) (μm)	1.112	499.6	259.0
Valley (Sv) (μm)	529.6	1.298	295.5
Peak – Valley (St) (μm)	1.641	1.797	554.6

3.1.7 ELP-REDV attachment of PHBV and PHA-PLA films

3.1.7.1 Toluidine Blue staining of PHBV films

After the oxygen plasma treatment at 50 W for 4 min, PHBV films were dipped into aqueous ELP-REDV solution (0.1% , w/w) for attachment of the ELP on the films. The surface of the PHBV films were dyed with Toluidine Blue (an acidophilic metachromatic dye) and examined by stereomicroscopy. Toluidine blue, specifically stains the acidic parts (or the negatively charged groups) of the surface such as sulfates (SO_4^{-2}), carboxylates ($-\text{COO}^-$), and phosphates ($-\text{PO}_4^{-3}$) (Sridharan et al., 2012). Stereomicrographs of untreated and oxygen plasma treated PHBV films showed that the intensities of blue dots on the surface were similar. However, after the coating of ELP-REDV, the intensity of the blue colors on the surface increased significantly due to the acidic amino acids of ELP-REDV such as aspartic acid and glutamic acid (Figure 3.6) showing that coating was uniform and successfully.

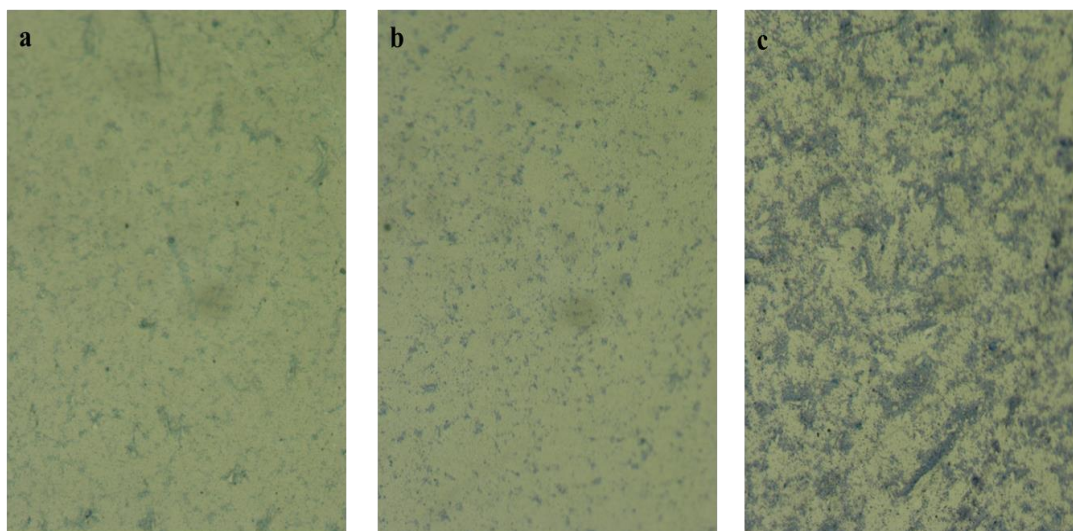


Figure 3.6: Stereomicroscope image of PHBV film stained with Toluidine Blue; (a) PHBV film, (b) PHBV-O₂, and (c) PHBV-O₂-ELP-REDV.

3.1.7.2 Toluidine Blue staining of PHA-PLA films

ELP-REDV attachment was performed as in section 3.1.7.1. Results showed again that protein coating on the surface of PHA-PLA films was achieved (Fig 3.7).

3.1.8 FTIR-ATR Analysis

FTIR-ATR analysis was done in order to show the attachment of ELP-REDV coating on the surfaces of PHBV and PHA-PLA films through a spectroscopic method.

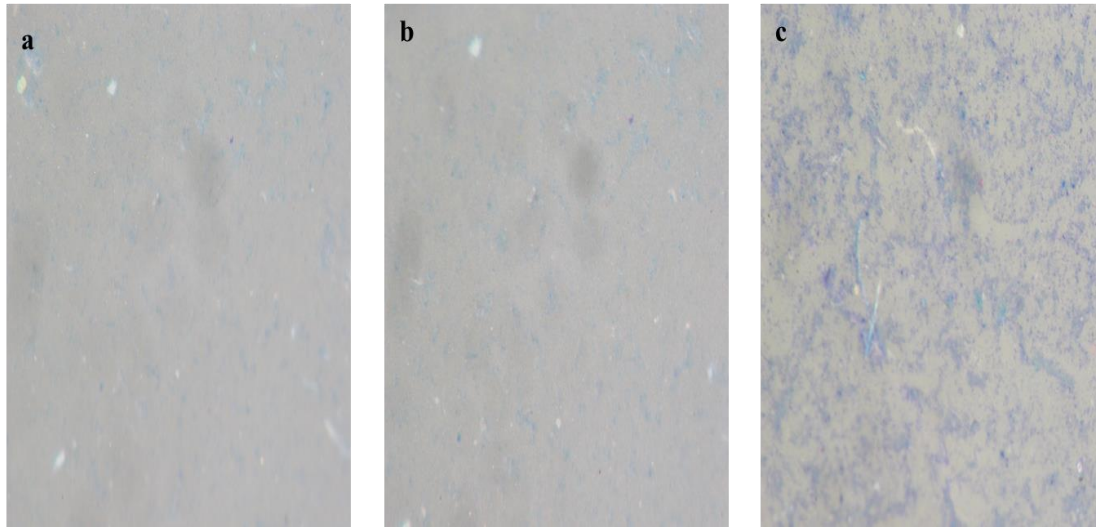


Figure 3.7: Stereomicroscope image of PHA-PLA film stained with Toluidine Blue; (a) PHA-PLA film, (b) PHA-PLA-O₂, and (c) PHA-PLA-O₂-ELP-REDV.

3.1.8.1 FTIR-ATR Analysis of PHBV films

FTIR analysis of PHBV films are shown in Fig 3.8. FTIR-ATR results showed that after oxygen plasma treatment stretching band in 1635 cm^{-1} (C=O) was formed because of oxidization (Meng et al., 2008). After the oxygen plasma treatment and ELP-REDV coating, two new bands amide I (1635) and amide II (1660 cm^{-1}) stretching bands (Wang et al., 2009) were formed. These new peaks are an evidence of ELP-REDV binding on the surface of films because PHBV does not have amino groups. Also, strong band in 1720 cm^{-1} from carbonyl group (Biazar et al., 2011), the stretching band in $2800\text{--}3000\text{ cm}^{-1}$ from methyl group (Biazar et al., 2011) and multiple bands in the range of 500 cm^{-1} to 1450 cm^{-1} were observed for untreated PHBV sample. After the oxygen plasma treatment and ELP-REDV attachment, same band patterns were observed on PHBV.

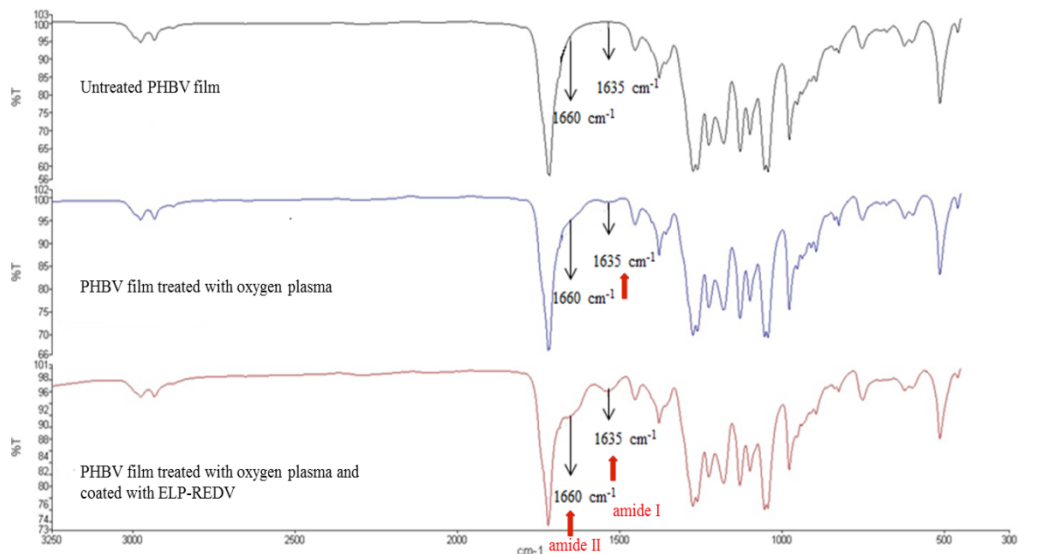


Figure 3.8: FTIR–ATR spectra of PHBV films treated with oxygen plasma and REDV.

3.1.8.2 FTIR-ATR Analysis of PHA-PLA films

PHA-PLA films were exposed to plasma treatment for 1 min at 50 W and then dipped into REDV solution. However, FTIR-ATR result showed that amide I and amide II bands indicating protein presence were not formed (Fig. 3.9). Different treatment durations were applied to coat surfaces with ELP-REDV as mentioned above (Section 3.1.5.1). FTIR-ATR results of films demonstrated that amide I (1545 cm^{-1}) and amide II (1652 cm^{-1}) bands were formed when films were exposed oxygen plasma for 2 min at 50W (Fig 3.10) (Serrano et al., 2007).

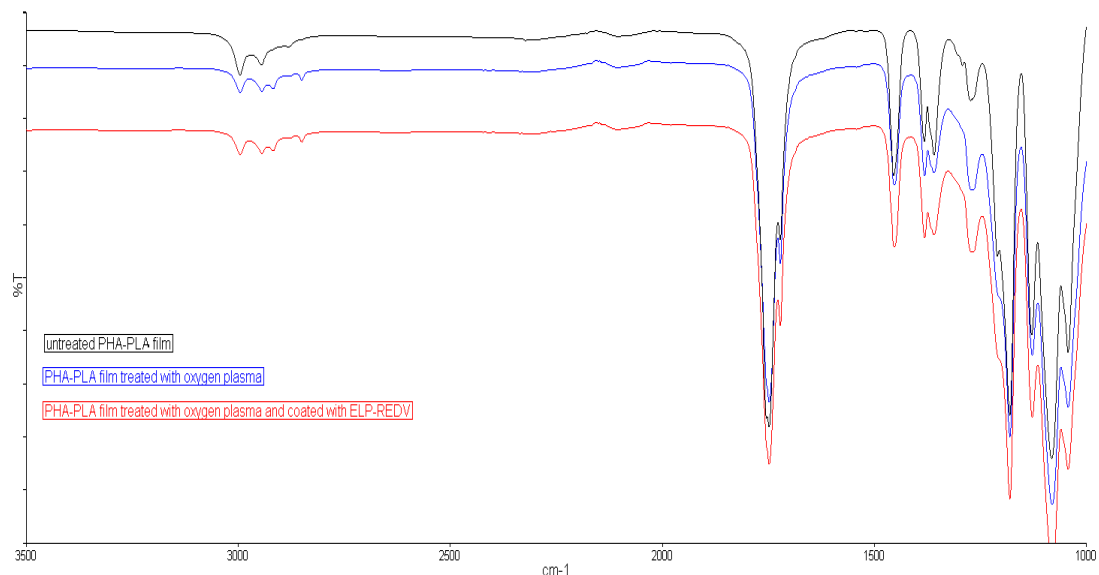


Figure 3.9: FTIR–ATR spectra of PHA-PLA films treated with O₂ plasma and coated REDV for 1 min at 50W.

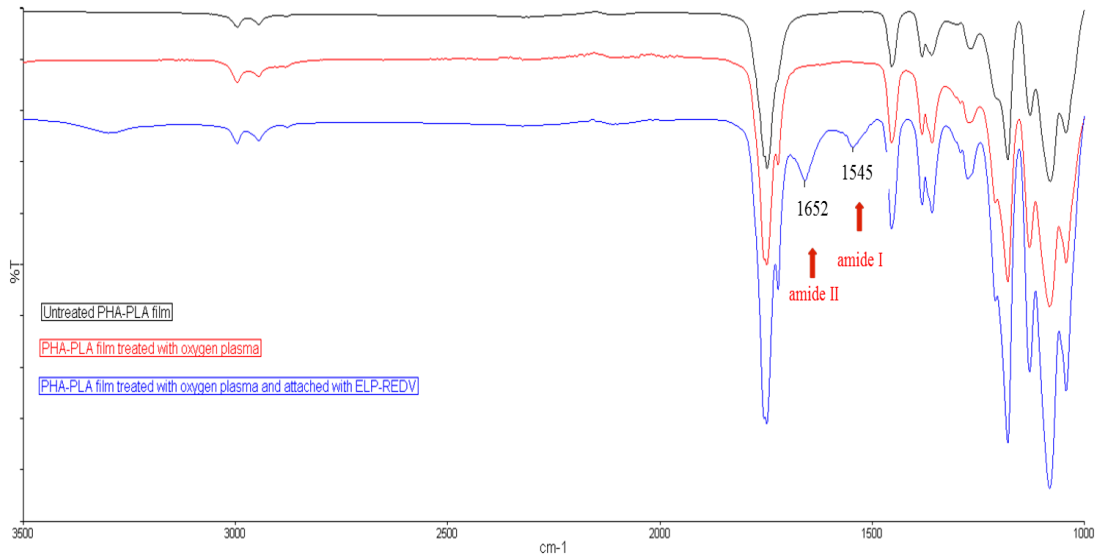


Figure 3.10: FTIR–ATR spectra of PHA-PLA films treated with O₂ plasma and coated with REDV for 2 min at 50W.

Different bands located around 1040 (-OH bending), 1080 (-C-O- stretching), 1120 (-C-O- stretching), 1180 (-C-O-C stretching), and 1760 cm⁻¹ (-C=O stretching) are

characteristic peaks of PLA (Gomes et al., 2008; Rocca-Smith et al., 2016). After the oxygen plasma treatment and ELP-REDV attachment, intensity of these peaks did not change.

3.2 In vitro studies

3.2.1 Cell proliferation

Attachment and proliferation of rabbit bone mesenchymal stem cells on wet spun PHBV, PHA-PLA scaffolds and FDM PHA-PLA scaffolds were determined by Alamar blue assay. 5×10^4 cells were seeded on all scaffolds for each type (untreated, O₂ plasma treated and, O₂ plasma treated and coated with ELP-REDV), and TCPS as the control group. Cell number was determined by using a calibration curve (Appendix A).

Figure 3.11 shows cell number of all types of PHBV wet spun scaffolds for each time point. Initial cell attachment on TCPS as a control group was good but it was significantly higher than the other groups showing that cell attachment was very low on the scaffolds. Cell number increased during the whole period (28 Days). Cell attachment on PHBV scaffolds treated with O₂ plasma and PHBV scaffolds coated with ELP-REDV were significantly higher than on untreated PHBV wet spun scaffolds. On day 7, osteogenic medium was introduced to the cell culture to induce differentiation of the cells towards osteoblasts. Results showed that cell numbers on all samples gradually increased during the 28 day period. Cell attachment on wet spun PHA-PLA scaffolds was low as was on PHBV wet spun scaffolds but, after application of osteogenic medium on Day 7, cell number increased for each scaffold. Also, cell attachment and proliferation on TCPS was significantly higher than other groups for all time points ($p < 0.001$). However, cell proliferation on TCPS decreased on Day 21 because they most probably reached confluency and cells either died or were washed away during the washing steps. After this, free space for cell growth might form and this might lead to more cell proliferation between Day 21 and Day 28. Figure 3.13 shows that Alamar blue

result of FDM PHA-PLA scaffolds for each type. Although cell numbers on scaffolds continuously increased at all time points, cell proliferation rate decreased when osteogenic differentiation medium was applied on Day 7. Also, cell proliferation of TCPS was significantly higher than other groups and decreased on Day 21 due to the reason mentioned above.

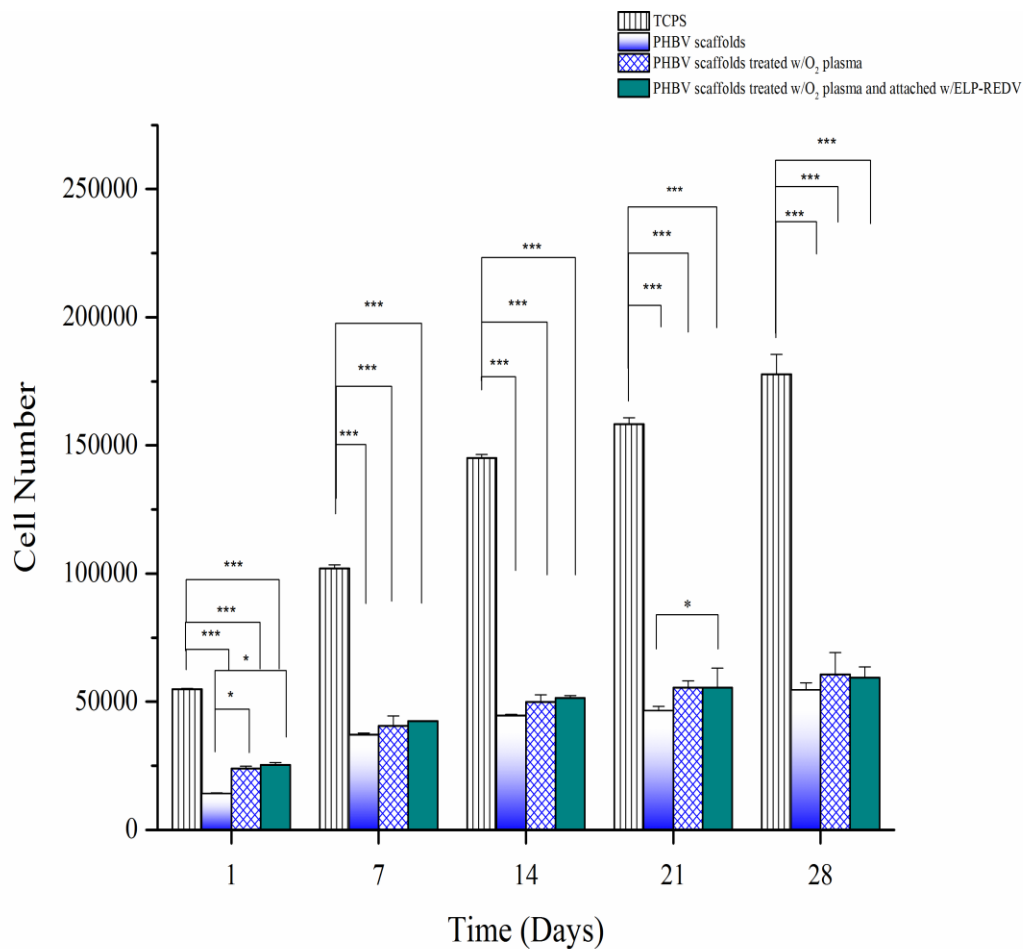


Figure 3.11: Rabbit BMSC proliferation on TCPS, and wet spun PHBV scaffolds. Statistical differences were determined between TCPS seeded and other groups by one way Anova (* $p < 0.05$, ** $p < 0.01$, *** $p < 0.001$).

When all types of scaffolds were compared, initial cell attachment on wet spun PHBV and PHA-PLA scaffolds were higher than FDM PHA-PLA scaffolds. This is related

with pore distribution within the scaffolds. While wet spun scaffolds have randomly distributed pores, regular pores are found in the FDM system because of their mesh like architecture. Thus, cell suspension leaked from the pores of FDM scaffolds into the well plates during cell seeding process. High cell proliferation on FDM scaffolds was observed large fibers for cells to spread and small pore sizes.

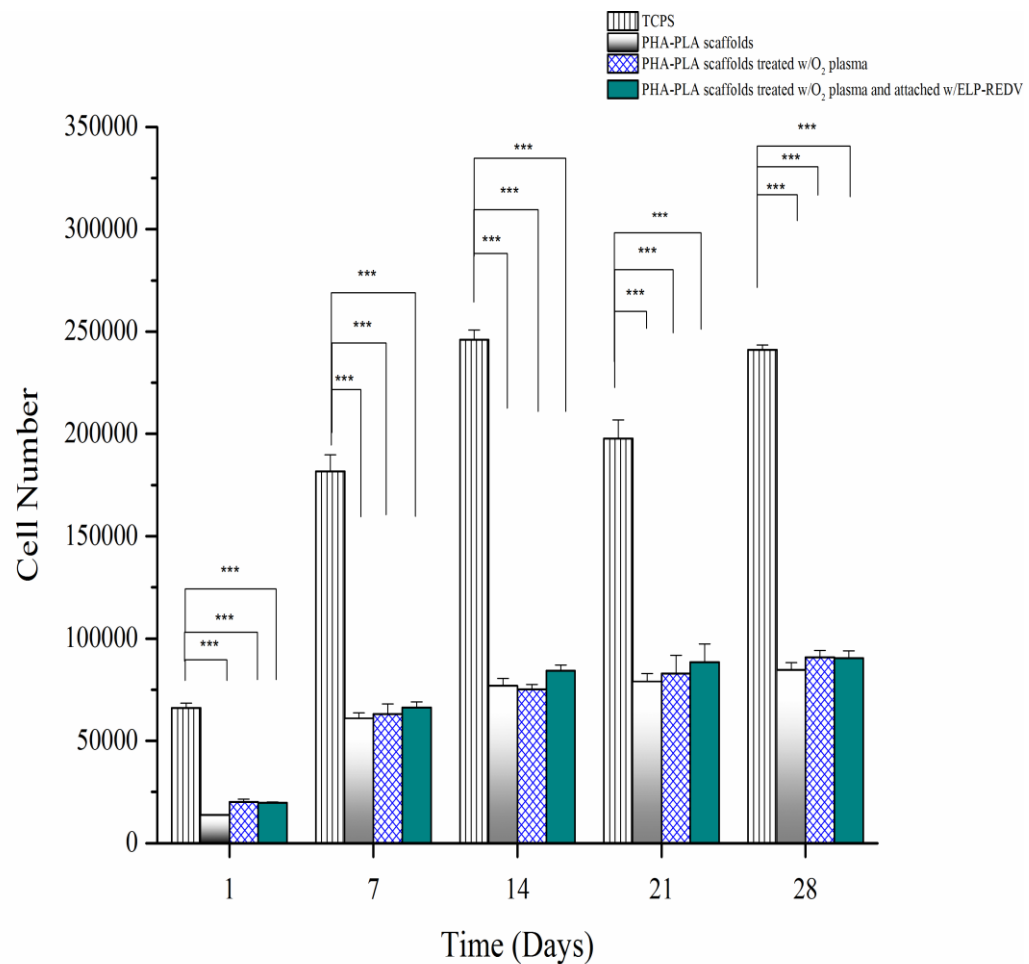


Figure 3.12: Rabbit BMSC proliferation on TCPS, wet spun PHA-PLA scaffolds. Statistical differences were determined between TCPS seeded and other groups by one way Anova (* $p < 0.05$, ** $p < 0.01$, *** $p < 0.001$).

This shows that FDM scaffolds provide a proper surface for cell proliferation. However, cell proliferation rate was decreased for all types of scaffolds when osteogenic medium was applied after 7 days. It was expected because low amount of cell proliferation was an indicator for MSC differentiation since cells stop proliferation and start secreting osteogenic markers like osteopontin and alkaline phosphatase during differentiation process (Arpornmaeklong et al., 2009). This result was also confirmed by ALP activity and microscopic analyses (SEM/EDX, Alizarin red and Osteopontin labeling).

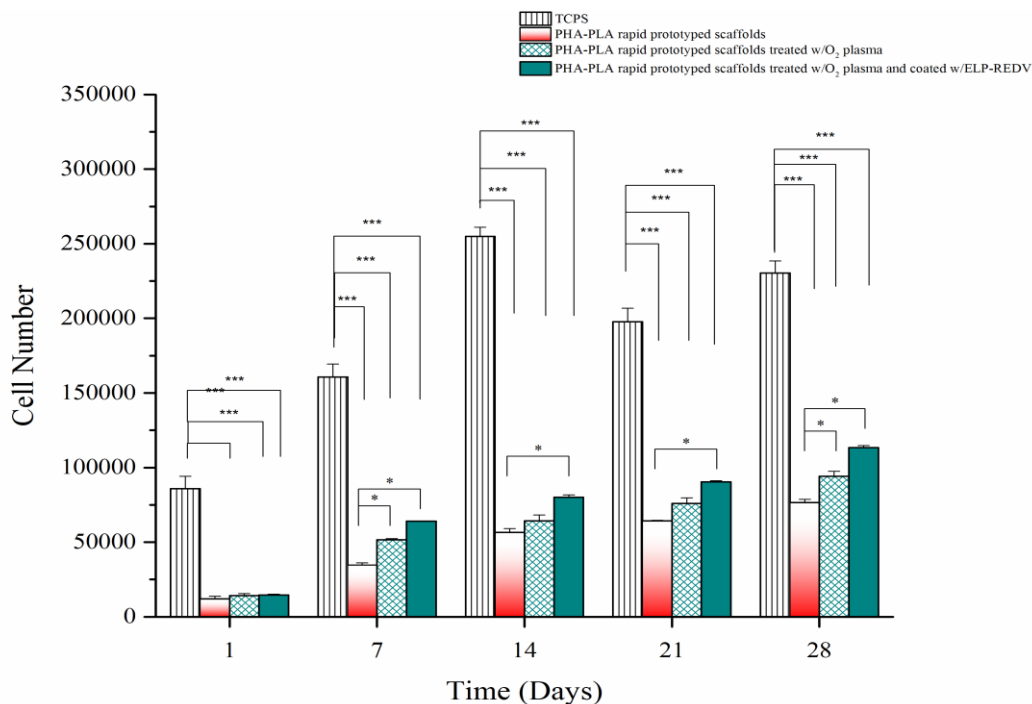


Figure 3.13: Rabbit BMSC proliferation on TCPS, FDM PHA-PLA scaffolds. Statistical differences were determined between TCPS seeded and other groups by one way Anova (* $p < 0.05$, ** $p < 0.01$, *** $p < 0.001$).

Moreover, all types of scaffolds treated with oxygen plasma treated and coated with ELP-REDV exhibited higher cell numbers than untreated scaffolds. In the literature, it was reported that cells attached and proliferated better on oxygen plasma treated PHBV

and poly (L-lactic acid) (PLA) surfaces because the surface became more hydrophilic and rough (Khorasani et al., 2008; Jacobs et al., 2012). In our case, contact angle values of PHBV and PHA-PLA films decreased from $83^{\circ} \pm 3.43$ to $59^{\circ} \pm 2.45$ and from $83^{\circ} \pm 0.50$ to $63^{\circ} \pm 0.44$ after oxygen plasma treatment and surface of scaffold become moderately hydrophilic (Section 3.1.5.1). AFM results also showed that surface roughness of films was increased or decreased after oxygen plasma treatment and ELP-REDV attachment (section 3.1.6). For these reasons, better cell attachment was observed. ELP-REDV sequences are specific sequences for endothelial cell attachment and proliferation (Kinikoglu et al., 2011). This sequence was also reported to enhance proliferation of other cell types like conjunctival epithelial cell line (Martínez-Osorio et al., 2009) and the increased numbers of rabbit BMSC on the ELP-REDV coated surfaces on Day 28 support this observation.

3.2.2 ALP analysis

Cells on the scaffolds were cultured in the nonosteogenic medium until Day 7 for cell attachment. After 7 day, cells osteogenic medium was introduced to differentiate cells towards osteogenic cells. ALP activity was analyzed to show osteoblastic differentiation of cells for all types of scaffolds.

3.2.2.1 ALP analysis of scaffolds

Fig 3.14 demonstrates that ALP activity of rabbit MSCs on PHBV scaffolds on Days 7, 14, 21, and 28. ALP activity was at a basal level from Day 0 to 7 because osteogenic medium was not introduced to differentiate the cells. After the osteogenic medium was introduced with cell seeded wet spun PHBV scaffolds, ALP activities were significantly increased and reached their highest level on Day 21 for each sample (Figure 3.14). This is an evidence of osteoblastic differentiation. Similar results were observed with wet spun and FDM PHA-PLA scaffolds (Figure 3.16, Figure 3.18). The ALP activities for

these scaffolds were significantly increased in the 2 weeks after osteogenic medium application. However, ALP production decreased after third week for all scaffolds. It is probably related with ALP being an early marker of osteogenic differentiation (Duan et al., 2010). When the ALP level was normalized to cell number, FDM PHA-PLA scaffolds exhibited highest osteogenic differentiation than wet spun PHBV and PHA-PLA scaffolds.

When the scaffolds were compared, ALP activities on all oxygen plasma treated and O₂ treated and REDV coated scaffolds were higher than untreated scaffolds on Days 14 and 21. This showed that more cells differentiated on the oxygen plasma treated and oxygen plasma treated and REDV coated scaffolds. It was an expected result because surface roughness of the structure can affect differentiation of cells. In our case, it was observed that oxygen plasma treatment change the surface roughness of scaffolds (RMS deviation) (Section 3.1.6). In the literature, Paletta et al. (2010) reported that ALP production of hMSC on PLLA nanofibers treated with oxygen plasma was higher than untreated scaffolds after 10 days. In another study, it was reported that ALP activity of osteoblast cells on PCL scaffolds treated with oxygen plasma was higher than untreated scaffolds cultured with osteogenic medium after 14 days. Also, surface of PCL scaffolds coated with fibronectin displayed lower ALP activity than scaffolds treated with oxygen plasma in this study (Yildirim et al., 2010). Kose et al. (2003) reported that ALP activity of osteoblast on PHBV foams treated with oxygen plasma was higher than untreated PHBV foams because oxygen plasma treatment can enhance the surface roughness of materials which can induce proliferation and differentiation. In our case, similar results were observed with literature.

3.2.3 Microscopy

3.2.3.1 SEM analysis

Rabbit mesenchymal stem cell attachment, proliferation, and growth were analyzed by scanning electron microscope (SEM) for wet spun PHBV, PHA-PLA, and FDM PHA-PLA scaffolds

3.2.3.1.1 SEM analysis of PHBV wet spun scaffolds

Figure 3.17 shows SEM micrographs of unseeded and rabbit mesenchymal stem cell seeded PHBV scaffolds on Day 1 and Day 28. Unseeded scaffolds were used as control groups. On Day 1, cells attached and formed clusters on the surface of all types of PHBV scaffolds. In 28 days, cells extensively covered the surface of the fibers where cells extended between fibers and migrated into scaffolds. More cell proliferation was observed on O₂ plasma treated and O₂ plasma treated and REDV coated scaffolds than untreated scaffolds.

3.2.3.1.2 SEM analysis of PHA-PLA wet spun scaffolds

SEM micrographs of wet spun PHA-PLA scaffolds are shown in Figure 3.18. Results revealed that cells attached and proliferated on the fibers of all types of scaffolds on Day 1. However, when scaffolds treated with oxygen plasma were compared with untreated and ELP-REDV coated scaffolds, less cells attached on scaffold treated with oxygen plasma. According to Alamar Blue results, more cell attachment was determined on oxygen plasma treated scaffolds (section 3.2.1).

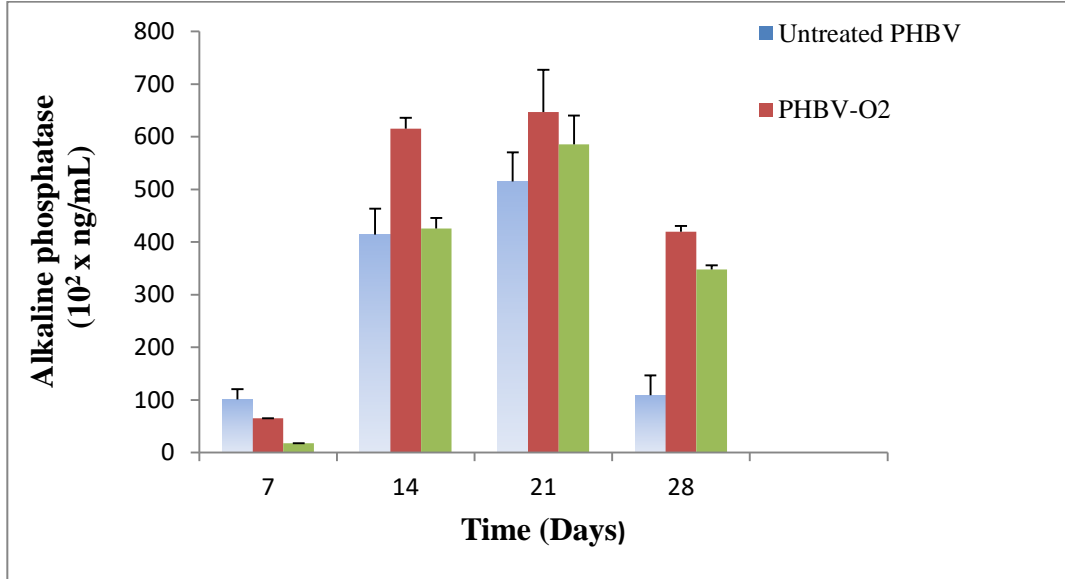


Figure 3.14: Alkaline phosphatase activity of RBMSC on wet spun PHBV scaffolds.

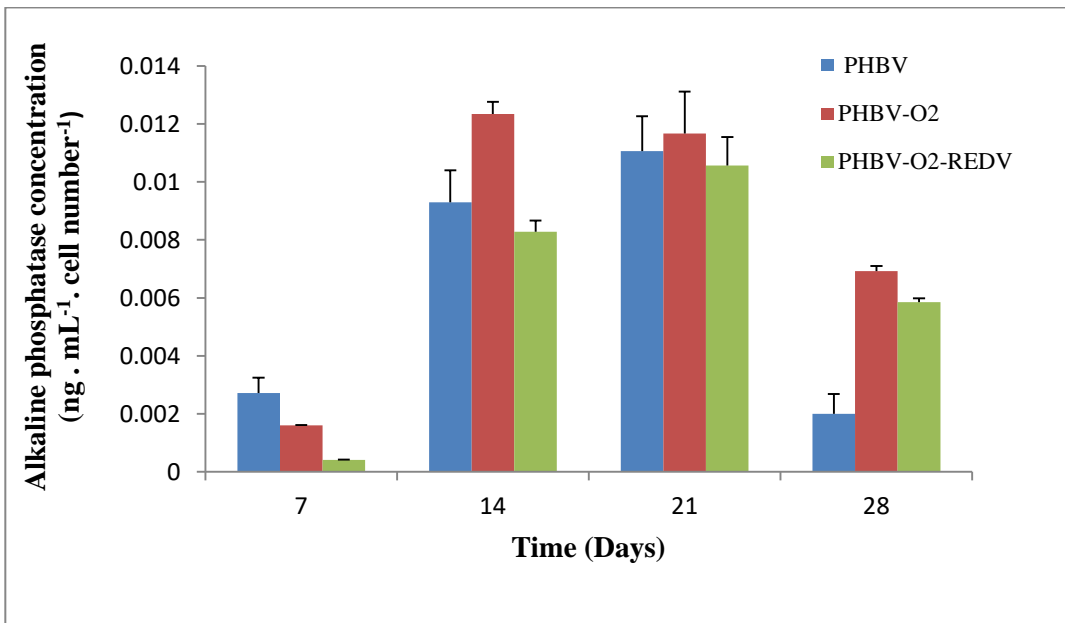


Figure 3.15: Alkaline phosphatase activity on wet spun PHBV is normalized to cell number.

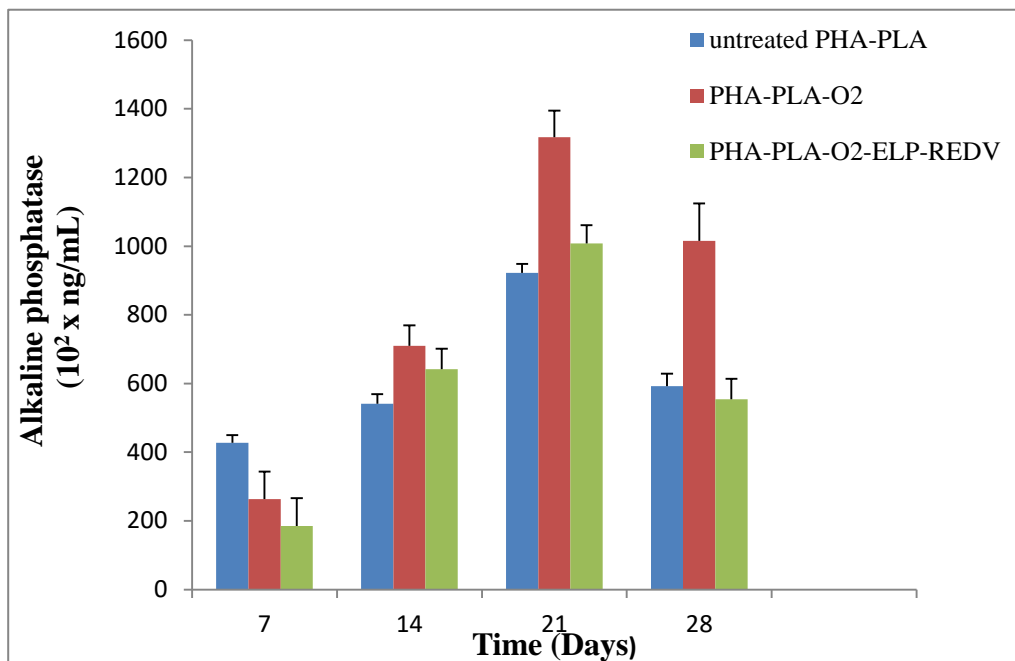


Figure 3.16: Alkaline phosphatase activity of RBMSC on wet spun PHA-PLA scaffolds.

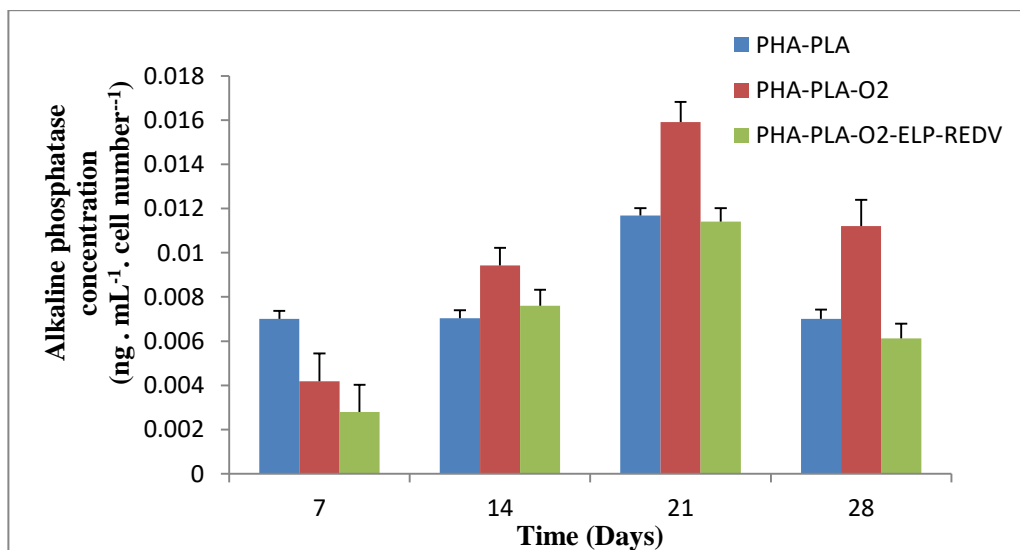


Figure 3.17: Alkaline phosphatase activity on wet spun PHA-PLA scaffold is normalized to cell number.

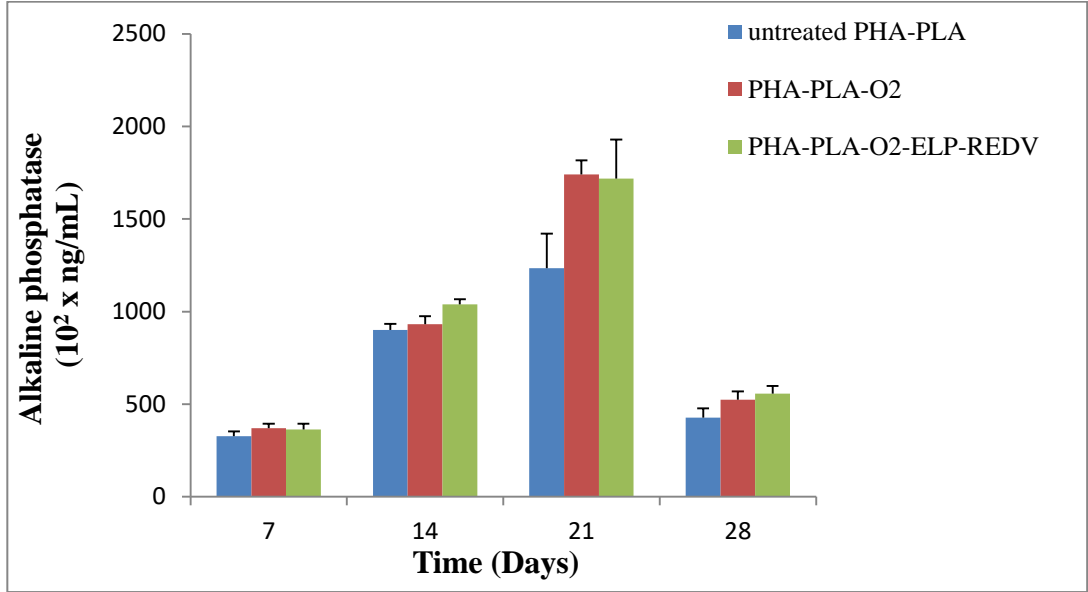


Figure 3.18: Alkaline phosphatase activity of RBMSC proliferation FDM PHA-PLA scaffolds.

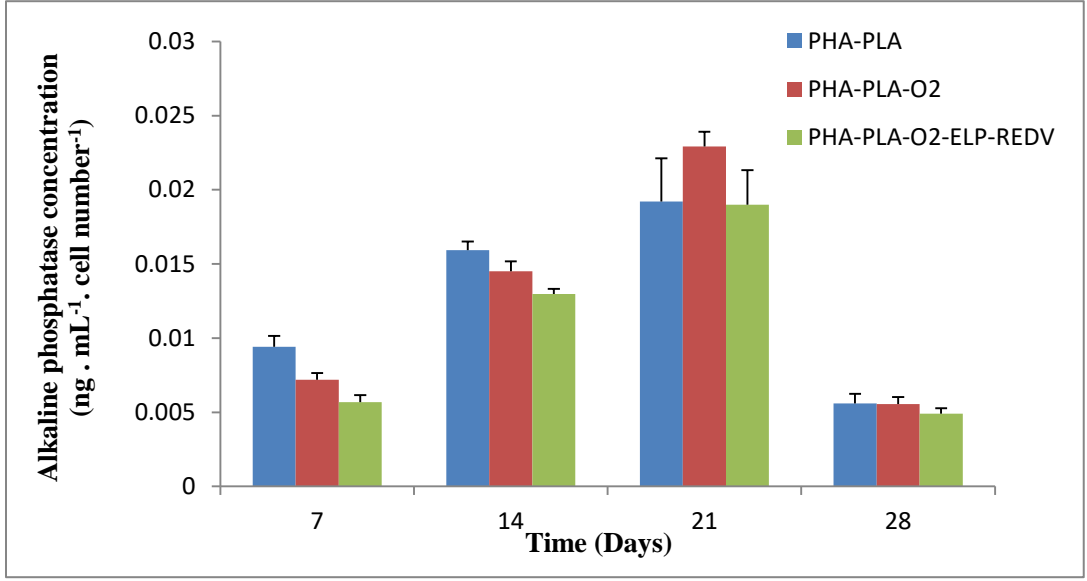


Figure 3. 19: Alkaline phosphatase activity on FDM PHA-PLA scaffolds is normalized to cell number.

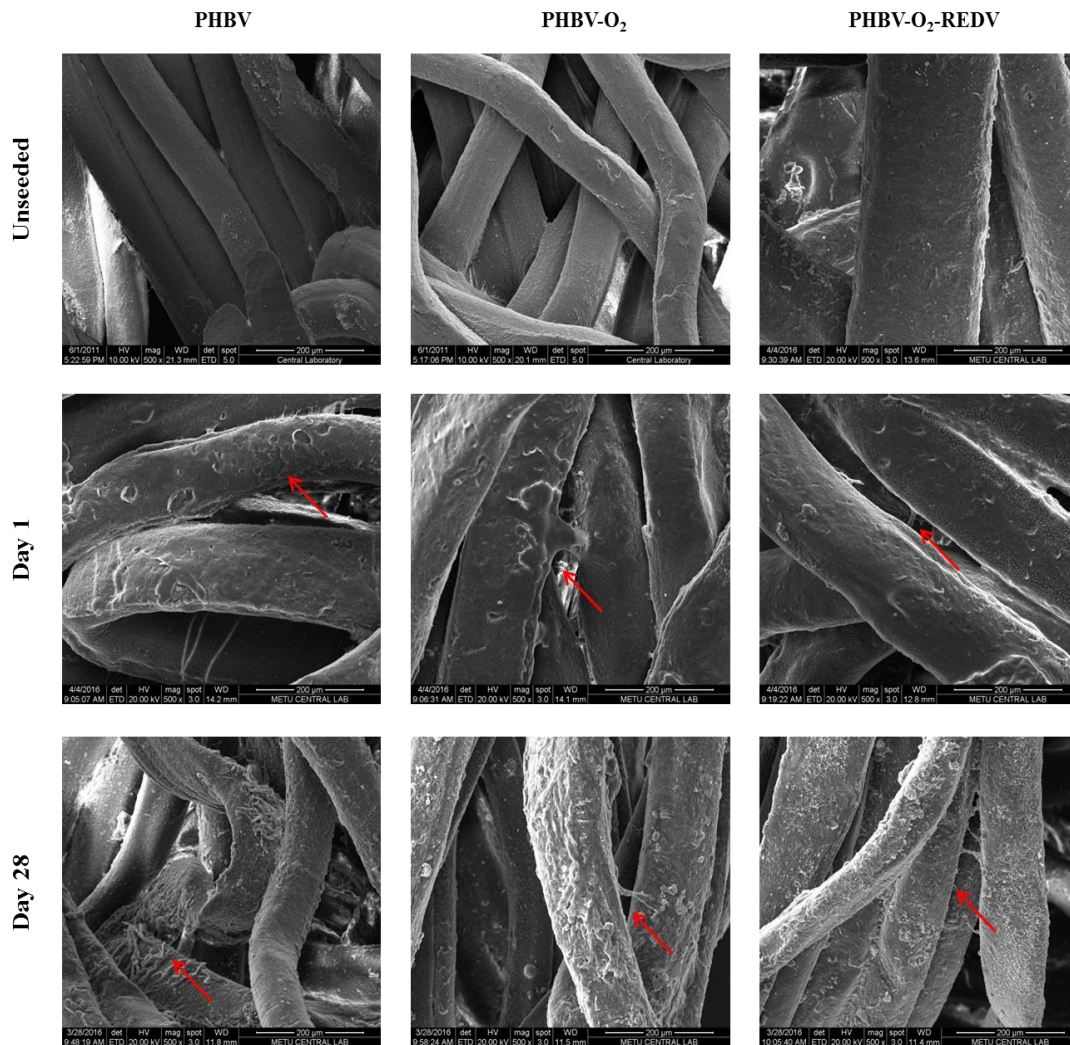


Figure 3.20: SEM micrographs of unseeded PHBV wet spun scaffolds and rabbit BMSCS on PHBV wet spun scaffolds (Arrow shows cells).

It may be related with hydrophilicity of the scaffold because some of the cells leaked from scaffolds to well plate during cell seeding process. Cells adhered and proliferated, and the surface of the most fibers was coated with cell sheet. When PHA-PLA wet spun scaffolds were compared to PHBV scaffolds, the similar results were observed on Day 28. It was expected because both types of scaffolds have similar morphological properties like fiber diameter, pore size, and porosity (section). Also, similar cell

proliferation results on both scaffolds were observed by Alamar Blue Assay which supported SEM micrographs results.

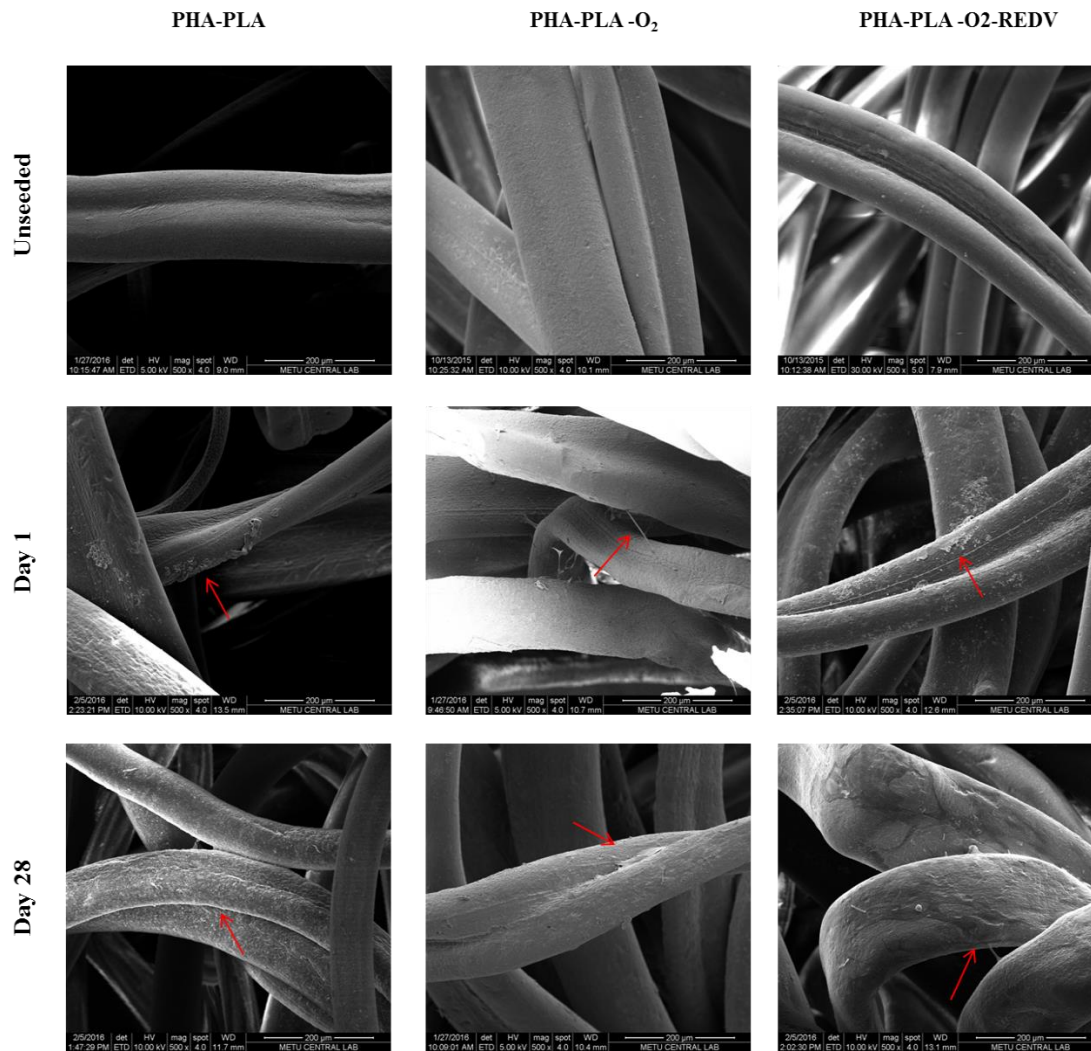


Figure 3.21: SEM micrographs of unseeded PHA-PLA wet spun scaffolds and rabbit BMSCS on wet spun PHA-PLA scaffolds (Arrow shows cells).

3.2.3.1.3 SEM analysis of FDM PHA-PLA scaffolds

Figure 3.19 shows SEM micrographs of the unseeded and seeded PHA-PLA FDM scaffolds which are untreated, oxygen plasma treated and oxygen plasma treated and then ELP-REDV coated. Cells attached and formed clusters at certain regions of the fibers on Day 1. They populated and completely covered the fiber surfaces and formed thick cell sheets and some of them were removed from the surface as layers on Day 28 because of more crowding. Also, cell bridges were not observed between fibers. When SEM micrographs were compared to all scaffolds on Day 28, more cells were observed for FDM scaffolds which were supported by cell proliferation results.

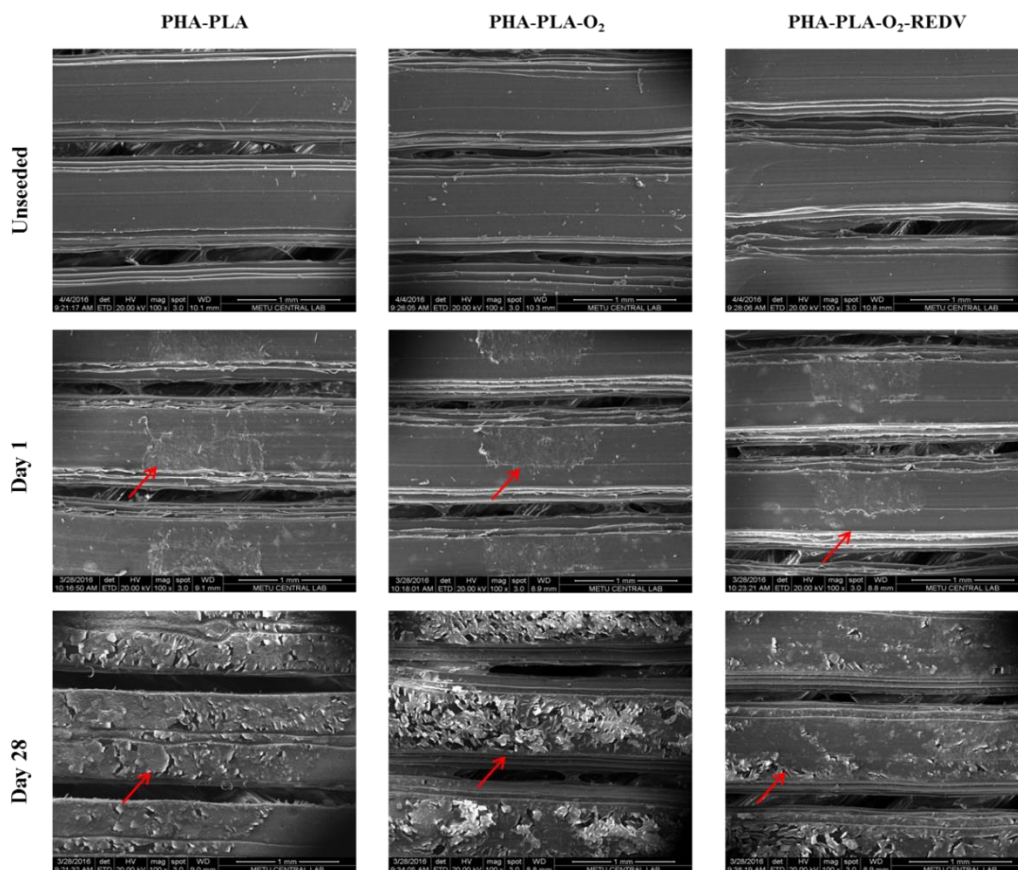


Figure 3.22: SEM micrographs of unseeded PHA-PLA FDM scaffolds and rabbit BMSCS on untreated FDM PHA-PLA scaffolds (Arrow shows cells).

3.2.4 Evaluation of Mineralization by Surface Analysis Using EDX Analysis

3.2.4.1 Energy dispersive X-ray (EDX) analysis

In this study, the osteogenic medium was applied on Day 7 to differentiate mesenchymal stem cells to osteogenic cells. SEM/EDX analysis was performed to quantitatively determine calcium phosphate amount produced by the cells after 4 weeks. Also, unseeded scaffolds were used as control groups. SEM micrographs at high magnification showed deposited crystals on the scaffolds.

3.2.4.1.1 Energy dispersive X-ray (EDX) analysis of scaffolds

Bone cells populated on all scaffolds, covered the surface of the fibers, and produced Ca-P elements as shown in the SEM images which were used to detect Ca-P deposition on the scaffolds via EDX analysis. Calcium phosphate crystals are known to function as nucleating agents for HA deposition for bone formation. In the literature, Ca/P molar ratios of hydroxyapatite (HA), tricalcium phosphate (TCP), octacalcium phosphate (OCP), amorphous calcium phosphate (ACP) and dicalcium phosphate dihydrate (DCPD) are reported as 1.67, 1.5, 1.33, 1.2-2.2 and 1.0, respectively (Francis et al., 1970). DCPD, ACP, and OCP are known as the precursors of HA. However, it is difficult to verify the presence of these precursors during biomineralization because they are unstable and can be converted to basic calcium phosphate via hydrolysis. Also, OCP and HA exhibit similar crystalline structures and resemble each other (Suzuki et al., 2006).

In this study, SEM/EDX analysis of PHBV scaffolds showed that Ca/P ratios for untreated, oxygen plasma treated and ELP-REDV coated PHBV wet spun scaffolds were 1.29, 1.34, 1.38, respectively (Figure 3.20) (Table 3.7). These values are close to the Ca/P molar ratio of octacalcium phosphate (OCP) (1.33 molar). OCP is produced at the early stages of mineralization during differentiation of MSCs and are involved in HA synthesis during bone formation (Hung et al., 2013). Thus, the formation of OCP is an

indication of osteogenic differentiation and mineralization. These results were also supported by ALP (Section 3.2.2.1).

SEM micrographs of wet spun PHA-PLA scaffolds are shown in Figure 3.21. Ca/P ratio of untreated, oxygen plasma treated and oxygen plasma treated and ELP-REDV coated scaffolds were found as 1.26, 1.28 and 1.34 molar by EDX analysis (Table 3.7). These results were to those wet spun PHBV scaffolds. These values are close to octacalcium phosphate (OCP) (1.33).

SEM micrographs of FDM PHA-PLA scaffolds at 4 weeks showed noticeable amounts of mineral nodules on the surface of scaffolds (Fig 3.22). The average Ca/P ratio of ELP-REDV coated scaffolds was 1.55 which was close to natural HAP component tricalcium phosphate (TCP) (1.5) while Ca/P ratio of untreated and oxygen plasma treated scaffolds were 1.39 and 1.25, respectively, which were close to octacalcium phosphate (OCP) (1.33) value (Table 3.7). This result was supported with cell proliferation and ALP results (section 3.2.2.1). More cell proliferation and ALP activity on FDM scaffolds coated with ELP-REDV were observed untreated and oxygen plasma treated scaffolds.

Table 3.7: Ca/P ratio on PHBV and PHA-PLA scaffolds at 4 week.

Samples	UT	O ₂ treated	O ₂ -REDV treated
Wet spun PHBV scaffolds	1.29 ± 0.11	1.34 ± 0.007	1.38 ± 0.05
Wet spun PHA-PLA scaffolds	1.26 ± 0.04	1.28 ± 0.05	1.34 ± 0.07
FDM PHA-PLA scaffolds	1.25 ± 0.10	1.39 ± 0.09	1.55 ± 0.04

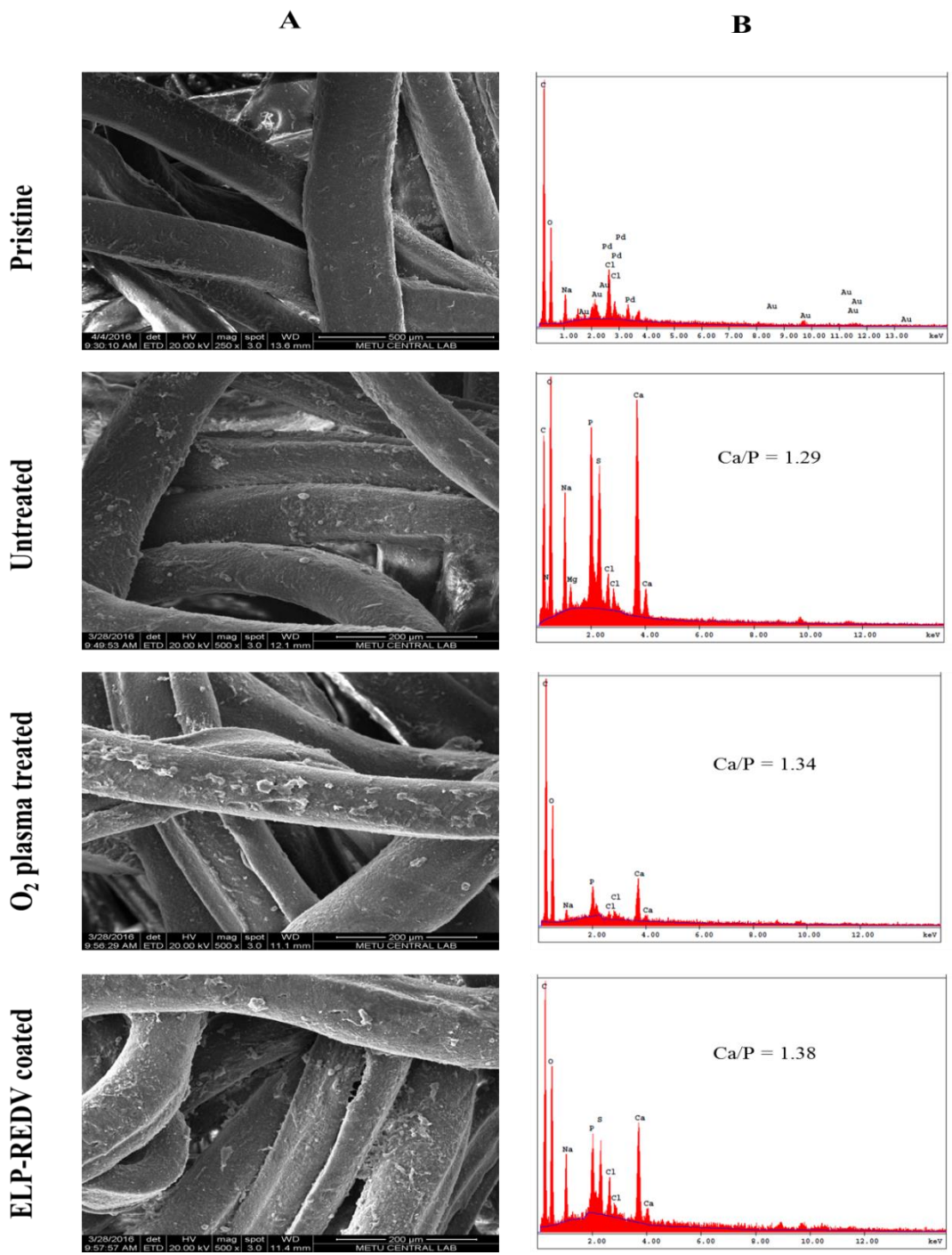


Figure 3.23: Elemental analysis of wet spun PHBV scaffold surfaces on Day 28. (A) SEM micrographs, and (B) EDX analysis.

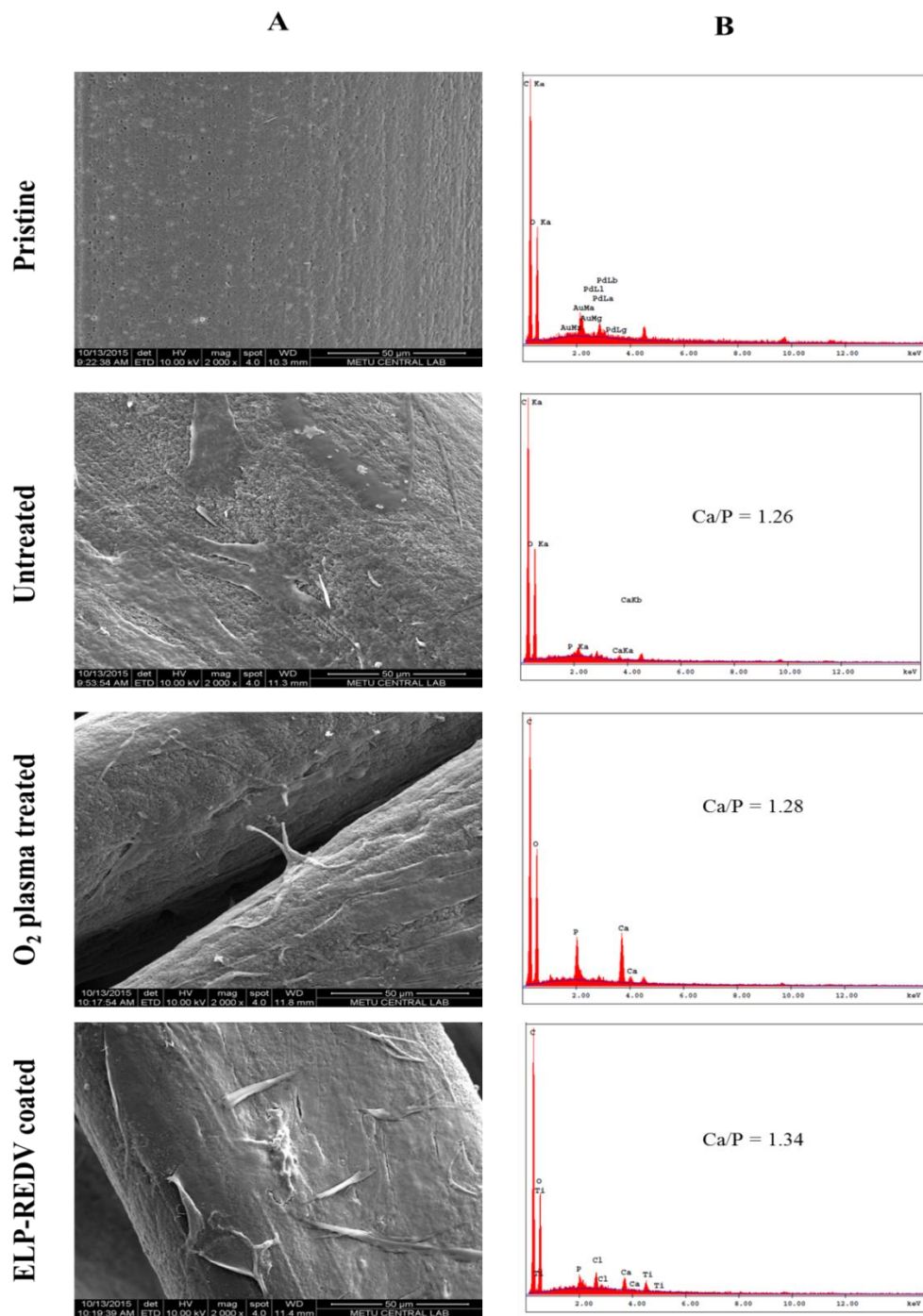


Figure 3.24: Elemental wet spun PHA-PLA scaffold surfaces on Day 28. (A) SEM micrographs, and (B) EDAX analysis.

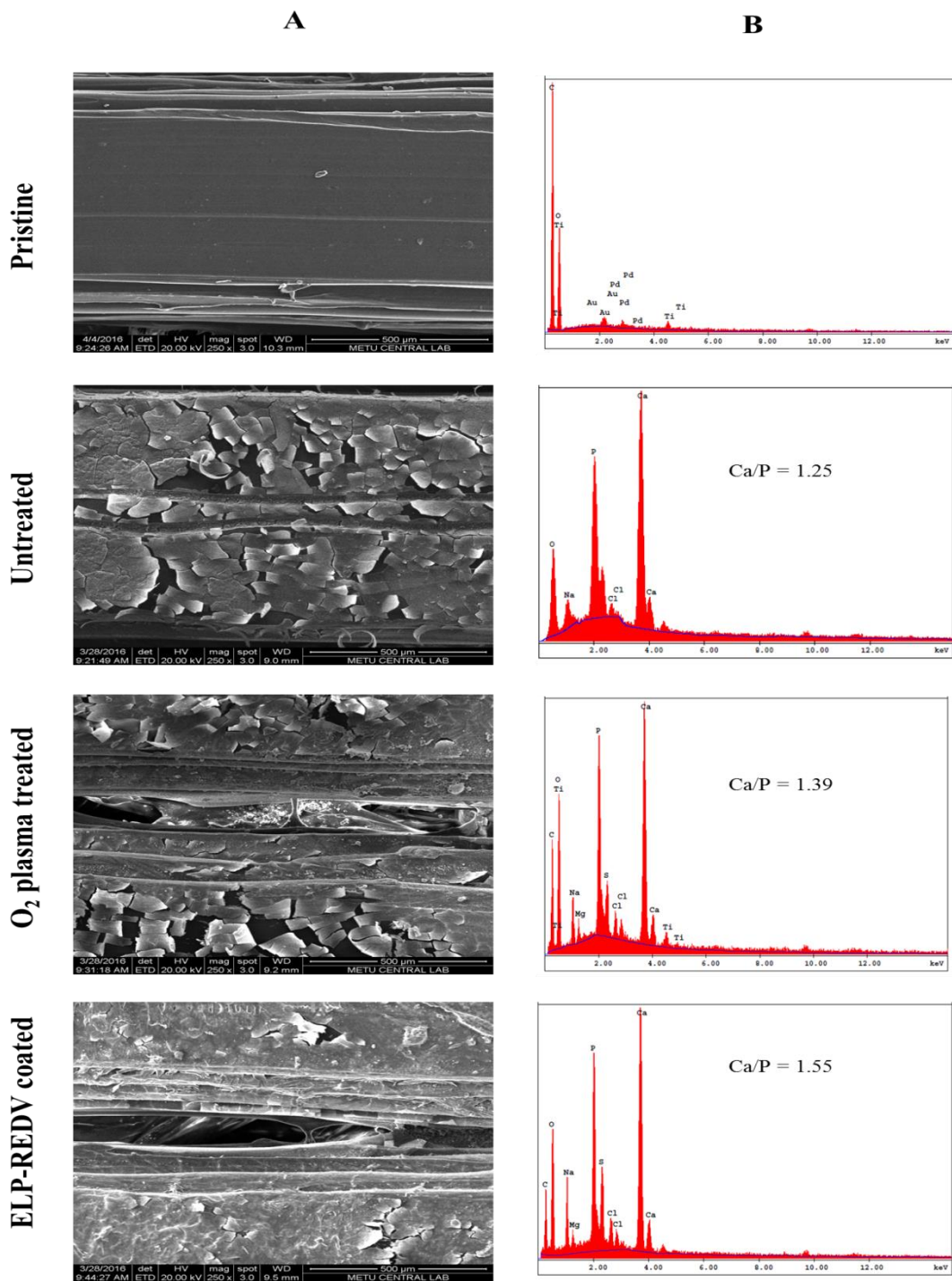


Figure 3.25: Elemental analysis of FDM PHA-PLA scaffold surfaces on Day 28. (A) SEM micrographs, and (B) EDAX analysis.

In this study, unseeded scaffolds used as control groups and Ca and P could not be detected on these structures. Instead, elements such as sulfur, sodium, titanium and chloride were observed in the EDX spectra of PHBV and PHA-PLA scaffolds. These elements may come from the materials used or from media used during culture.

3.2.5 Confocal microscopy

Cell morphology, proliferation, growth into the scaffolds and osteogenic differentiation were studied by using confocal laser scanning microscopy (CLSM) for the wet spun PHBV, PHA-PLA and FDM PHA-PLA scaffolds. Extracellular matrix of bone is composed of proteins such as osteopontin (OPN), osteonectin (ON), fibronectin (FN), vitronectin (VN), laminin (LM), collagen (CO) and other glycoproteins (El-Amin et al., 2003). In this study, staining for osteopontin was done to show osteogenic differentiation because this protein is secreted by mature osteoblasts at a late stage of osteoblastic differentiation and plays a role in the formation of mineralized bone matrix (Sodek et al., 2000; Limin et al., 2010). For this purpose, osteopontin stained with monoclonal antibody labelled with Alexa Fluor[®] 532 mouse against rabbit OPN (blue) , actin filaments of cytoskeletons were stained with Alexa Fluor[®] 488 Phalloidin (red), and nuclei of cell stained with DRAQ5 (green). Unseeded scaffolds were used as control groups.

3.2.5.1 Confocal microscopy of wet spun PHBV scaffolds

Figure 3.23 presents confocal micrographs of bone marrow mesenchymal stem cells on the all types of PHBV wet spun scaffolds on Day 28. No signal was observed in control groups. Surfaces of cell seeded scaffolds were completely covered by cells indicating normal cell growth. Also, cells penetrated and migrated into scaffolds. Osteogenic differentiation was shown by the expression of osteopontin which was positively stained.

3.2.5.2 Confocal microscopy of wet spun PHA-PLA scaffolds

Confocal micrographs of the rabbit mesenchymal stem cells seeded on PHA-PLA wet spun scaffolds are shown in Figure 3.24. Unseeded scaffolds were not auto-fluorescent under confocal microscope and they were not seen. Confocal micrographs revealed that cells attached and covered the surface of the fibers and ingrowth into wet spun scaffolds for each type after 28 days of culture. These results are supported by SEM micrographs and cell proliferation results. Also, cells on all types of scaffolds were positively stained with osteopontin which is an indication of bone matrix formation. This result was also supported by ALP and SEM/EDX analysis (Sections 3.2.2.1 and 3.2.4.1).

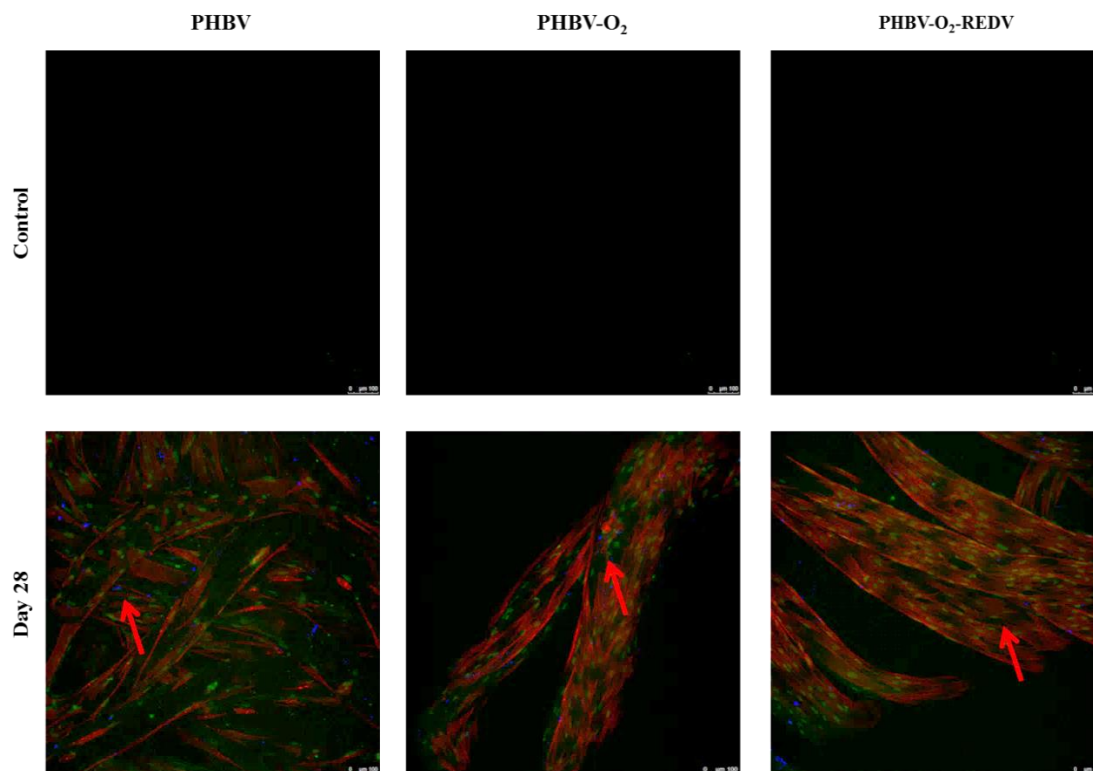


Figure 3.26: Osteopontin immunofluorescence of control (unseeded) and seeded wet spun PHBV scaffolds on Day 28. Stains: osteopontin: blue; DRUQ5: nuclei, green; FTIC: actin, red. Scale bars: 100 μ m. Arrows show osteopontin.

3.2.5.3 Confocal microscopy of PHA-PLA FDM scaffolds

Figure 3.25 showed confocal micrographs of the rabbit mesenchymal stem cells seeded on PHA-PLA FDM scaffolds for each type. Control groups were not auto-fluorescent and were not visible. Results demonstrated that cells attached and covered the fiber surfaces for each type. This result was paralleled with SEM results (Section 3.2.4.1). Also, cells were positively stained with osteopontin. It is an evidence of differentiation and supported results of ALP and SEM/EDX analysis.

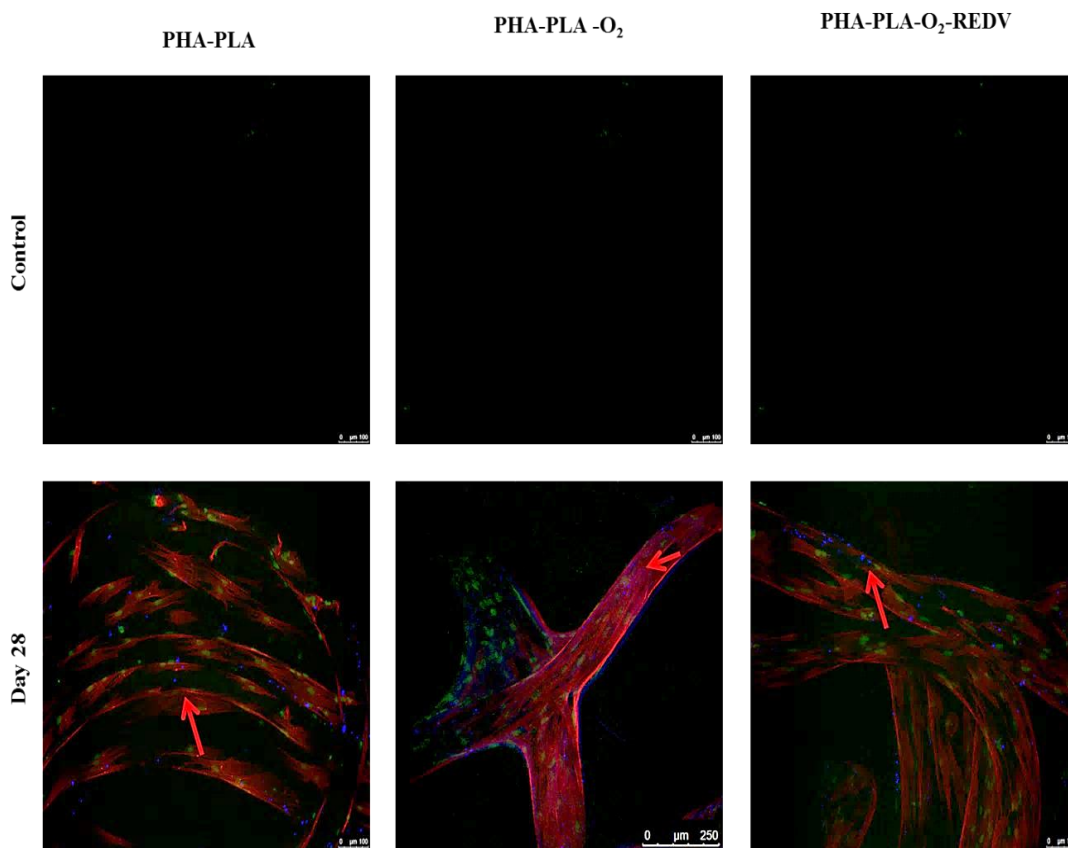


Figure 3.27: Osteopontin immunofluorescence of control (unseeded) and seeded wet spun PHA-PLA scaffolds on Day 28. Stains: osteopontin: blue; DRUQ5: nuclei, green; FTIC: actin, red. Scale bars: 100 μm. Arrows show osteopontin.

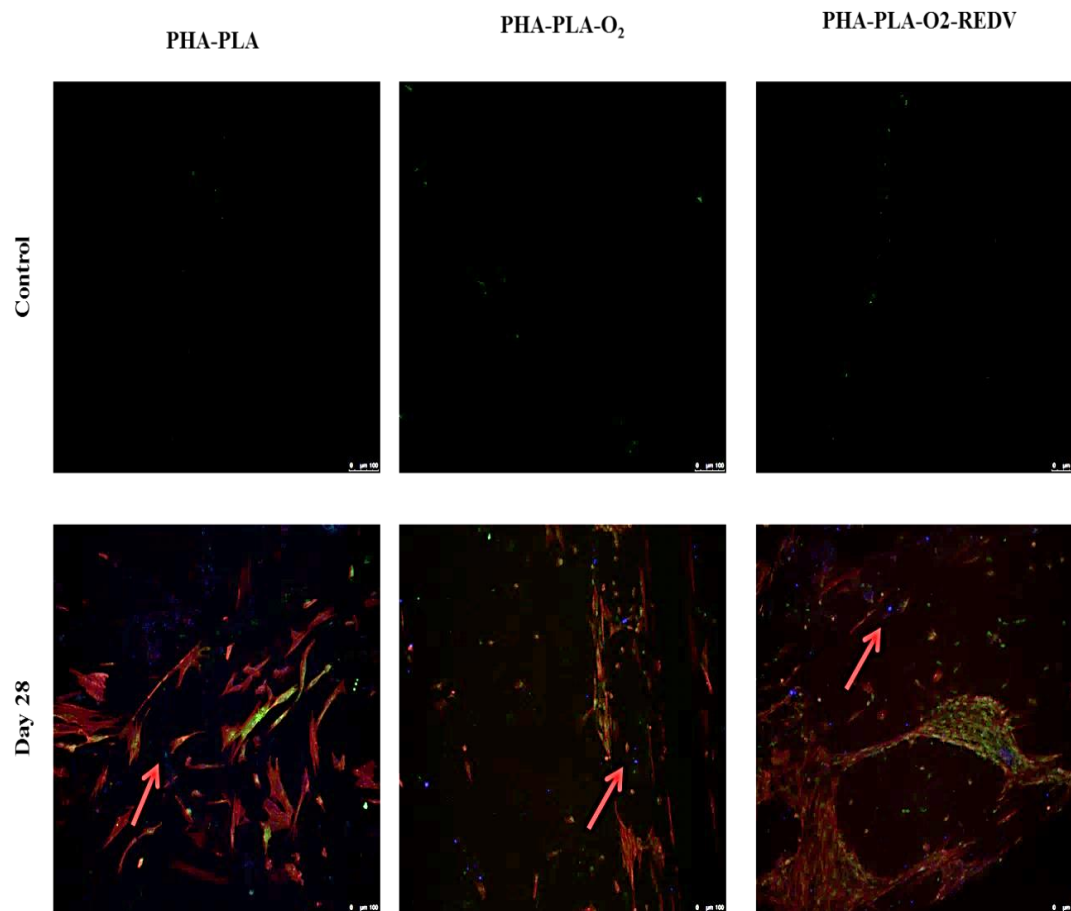


Figure 3.28: Osteopontin immunofluorescence of control (unseeded) and seeded FDM PHA-PLA scaffolds on Day 28. Stains: osteopontin: blue; DRUQ5: nuclei,green; FTIC: actin, red. Scale bars: 100 μm . Arrows show osteopontin.

3.2.6 Alizarin Red Staining

In the literature, different methods were used to determine mineralization on the scaffolds such as EDX analysis, haemotxylin- staining, von Kossa staining, Alizarin Red staining, and X-ray diffraction where Alizarin red staining has been a commonly used method to detect the Ca deposition on the cellular matrix because it is low cost and easy. In this study, as well as EDX analysis, Alizarin Red staining was used to qualitatively visualize calcium deposition on the scaffolds by using stereomicroscope and light

microscope after rabbit bone mesenchymal stem cells were cultured on PHBV, PHA-PLA wet spun and PHA-PLA FDM scaffolds on day 21 in osteogenic medium as previously described. Unseeded scaffolds were used as a control group.

3.2.6.1 Alizarin Red Staining of PHBV wet spun scaffolds

Cell seeded PHBV wet spun scaffolds were stained with Alizarin Red and then observed by phase contrast microscopy to detect Ca deposition on the scaffolds. All types of wet spun scaffolds were positively stained when compared to control groups which were unstained. Phase contrast microscope images showed small Ca nodules stained with Alizarin Red on the fibers whereas they were not present on control groups (Fig 3.26). These showed that mesenchymal stem cells differentiated osteogenic cells and produced mineralized tissue. It was also further confirmed by SEM/EDX analysis (Sections 3.2.4.1).

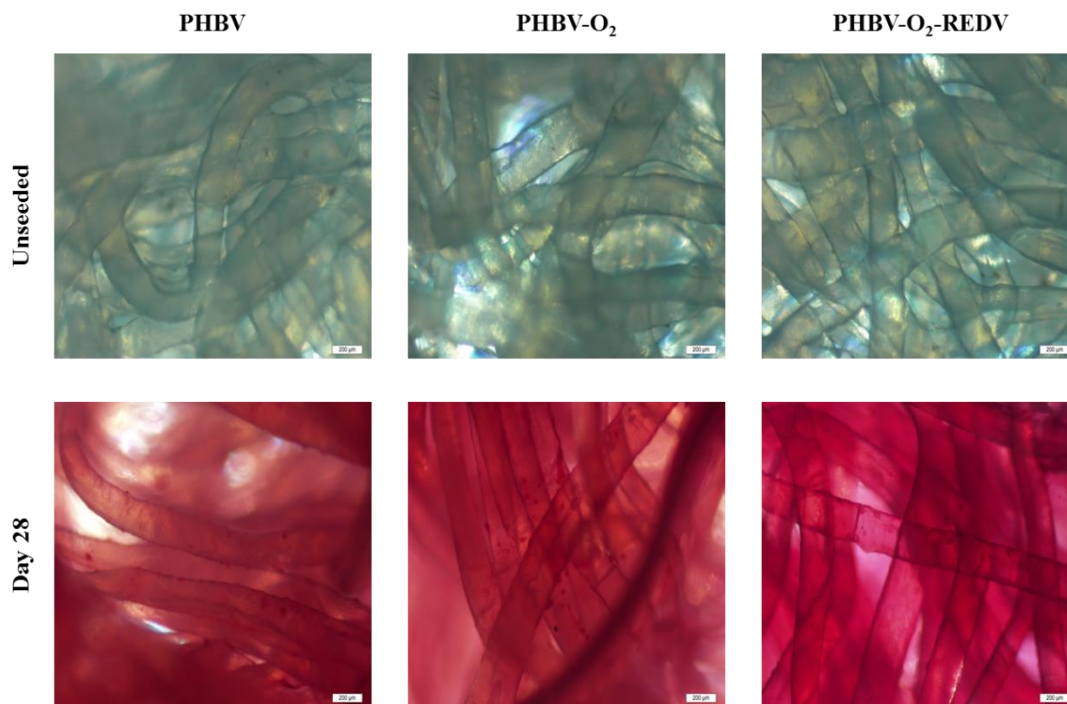


Figure 3.29: Alizarin Red staining of unseeded and seeded PHBV wet spun scaffolds on Day 28. Scale bars: 200 μ m.

3.2.6.2 Alizarin Red Staining of PHA-PLA wet spun scaffolds

PHA-PLA wet spun scaffolds with cells and cell free control groups were stained with Alizarin Red and then, examined with phase contrast microscope. Microscope images showed that calcium granules on the fiber were stained with dark red and formed close grained while control groups were not stained with Alizarin Red (Fig 3.27). This is an indication of bone formation.

3.2.6.3 Alizarin Red Staining of PHA-PLA FDM scaffolds

PHA-PLA FDM scaffolds for each type were stained with Alizarin Red and visualized calcium deposition on the scaffolds by stereomicroscope. As shown in Fig. 3.28, positive Alizarin Red staining on the cell seeded scaffolds were observed while control groups were negatively stained. Also, result revealed that Ca nodules with red patches were observed on the surface of fibers for oxygen plasma treated and ELP-REDV coated scaffolds while Ca nodules accumulated at side of fibers for untreated scaffolds.

Thus, stereomicroscope images showed that Ca accumulation was detected and bone mineralization was observed on the FDM scaffolds. This result was also supported by SEM/EDX analysis (Sections 3.2.4.1).



Figure 3.30: Alizarin Red staining of unseeded and seeded wet spun PHA-PLA scaffolds on Day 28. Scale bars: 200 μm .

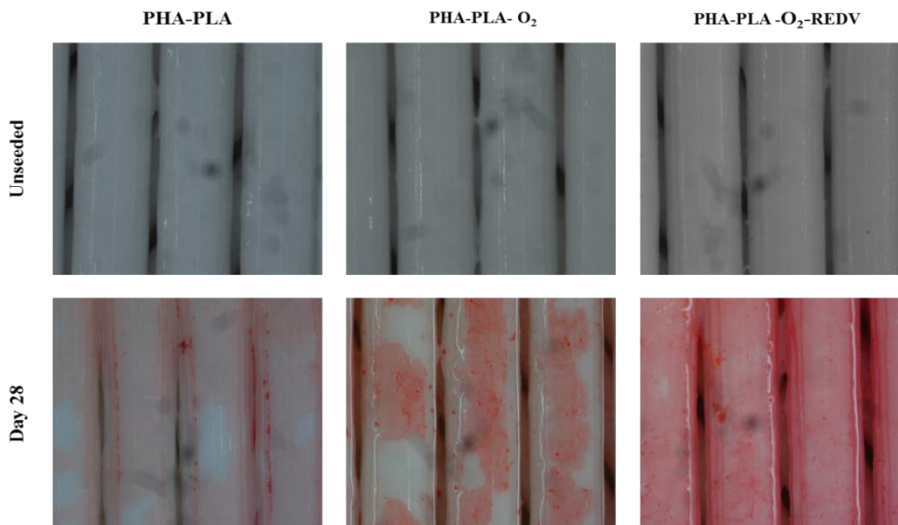


Figure 3.31: Alizarin Red staining of unseeded and seeded FDM PHA-PLA scaffolds on Day 28.

CHAPTER 4

CONCLUSION

Bone plays an important role in movement, support and protection of other organs and in production of blood and bone marrow stromal stem cells. Bone defects related with trauma, aging, diseases, tumors, and nonunion fractures increasingly create health problems. Although bone tissue has self regeneration capability, this ability is limited to a few millimeters in healthy bone. Thus, the regeneration process of bone is inadequate for large bone defects created by bone tumor resection or comminuted fractures. Bone tissue engineering is an increasingly effective approach to the treatment of bone defects where cell carriers, scaffolds, are seeded with autologous cells before implantation at the defect site.

Rapid prototyping is a recently developing tool for the production of devices to be used in biomaterials and tissue engineering because it can make controlled products with pore size and porosity, homogenous pore size and distribution. It can be used to tailor make 3D implants. Wet spinning is a simpler approach for biomedical device production that does not require expensive equipment but its products do not have controlled porosity or pores. This present study aimed to construct 3D scaffolds suitable for bone tissue engineering using these two techniques and compared them in terms of product quality such as mechanical properties, cell-scaffold interactions. Thus, two different techniques were investigated to find desirable architecture for bone tissue engineering application.

Scaffolds were produced from PHBV and PHA-PLA blend that are biocompatible, slow degradation rate and biological origin. Proper polymer concentrations were found 8% and 13% to form wet spun PHBV and PHA-PLA scaffolds respectively. Porosity of both wet spun scaffolds have similar and higher than FDM scaffold scaffolds because wet spun scaffolds are composed of randomly distributed fibers. On the other hand, mechanical properties of FDM PHA-PLA scaffolds were higher than that of wet spun

PHA-PLA and PHBV scaffold because fibers have certain predetermine contact points. Young's modulus of FDM scaffold was higher than wet spun PHA-PLA and PHBV scaffolds (to around 363.00 MPa vs 1.25MPa and 4.65 MPa). These results revealed that PHBV and PHA-PLA wet spun scaffolds can be used as bone filler at non load bearing area such as skull. On the other hand, PHA-PLA FDM scaffolds possess similar mechanical properties with cortical bone. Thus, this scaffold can be a viable choice for *in vivo* study.

Oxygen plasma modification was applied in order to improve hydrophilicity of scaffolds and coated with ELP-REDV that stimulates endothelial cell adhesion and proliferation. While contact angle of PHBV film was decreased from 83° to 59° for 4 min at 50W, contact angle of PHA-PLA film was decreased from 79° to 56° for 2 min at 50W after plasma treatment. Results indicated that wettability of PHBV and PHA-PLA films improved and proper surface was obtained for cell attachment and proliferation. After oxygen plasma treatment, scaffolds were directly dipped into ELP-REDV solution to coat surface of scaffolds. FTIR-ATR confirmed that surface coated with ELP-REDV to form amide I and amide II bands which are not found in chemical structures of PHBV and PHA-PLA blend. Also, Toluidine Blue staining showed that more blue dots were observed on ELP-REDV coating films when compared untreated and oxygen plasma treated PHBV and PHA-PLA films. Additionally, AFM analysis showed that surface roughness of films changed after oxygen plasma treatment and ELP-REDV coating. RMS (Root Mean Square) deviation value of PHBV film decreased after oxygen plasma treatment (303.4 nm vs 112.2 nm) and then increased after surface coated with ELP-REDV (112.2 nm vs 391.5 nm). On the other hand, RMS deviation value of PHA-PLA films increased after oxygen plasma treatment (243.0 nm vs 342.8 nm) and then decreased ELP-REDV coating (342.8 nm vs 153.5 nm).

All scaffolds were seeded with stem cells isolated from rabbit bone marrow and cell behavior for bone tissue was studied *in vitro*. Higher cell proliferation was observed on FDM scaffolds that with wet spun scaffolds because they have larger fibers for cells to attach and spread on. Additionally, while oxygen plasma modification made scaffolds

more suitable for cell growth than untreated scaffolds, ELP coated scaffolds exhibited higher cell proliferation than untreated or oxygen plasma treated scaffolds. This indicated that ELP-REDV improves cell proliferation. After application of osteogenic medium on 7 day, alkaline phosphatase activity was observed for all scaffolds. It is an evidence of osteoblastic differentiation. Confocal micrographs revealed that cells attached and covered well on the surface of fibers and ingrowth into scaffolds for each type. Also, osteopontin labelling of 3 week culture in the differentiation medium exhibited expression of osteopontin supporting the osteogenic differentiation of the rabbit bone marrow cells. Besides, calcium and phosphate mineralization was detected on all scaffolds by EDX analysis and higher Ca/P ratios was observed FDM PHA-PLA scaffolds coated with ELP-REDV which was close natural HAP component tricalcium phosphate (TCP) value. Also, Ca containing nodules were formed on the fibers. These results showed that mesenchymal stem cells differentiated osteogenic cells and produced mineralized tissue.

As a result, all scaffolds, especially FDM scaffolds have a great potential for cell attachment, proliferation and differentiation of bone marrow mesenchymal stem cells. While wet spun PHBV and PHA-PLA scaffolds are promising for non-load bearing region, FDM PHA-PLA scaffolds can be for used load bearing applications. Oxygen plasma modification increased the hydrophilicity of scaffolds and made them more suitable for cell growth and surfaces with ELP-REDV coating promotes cell attachment and proliferation. The future studies should consider *in vivo* and histological examination.

REFERENCES

- Andric, T., Sampson, A. C., & Freeman, J. W. (2011). Fabrication and characterization of electrospun osteon mimicking scaffolds for bone tissue engineering. *Materials Science and Engineering C*, *31*(1), 2–8. <http://doi.org/10.1016/j.msec.2010.10.001>
- Antoniali, A. Í. S., & Bolfarini, C. (2011). Numerical evaluation of reduction of stress shielding in laser coated hip prostheses. *Materials Research*, *14*(3), 331–334. <http://doi.org/10.1590/S1516-14392011005000043>
- Aravamudhan, A., Ramos, D. M., Nip, J., Harmon, M. D., James, R., Deng, M., Kumbar, S. G. (2013). Cellulose and collagen derived micro-nano structured scaffolds for bone tissue engineering. *Journal of Biomedical Nanotechnology*, *9*(4), 719–731. <http://doi.org/10.1166/jbn.2013.1574>
- Arpornmaeklong, P., Brown, S. E., Wang, Z., & Krebsbach, P. H. (2009). Phenotypic Characterization, Osteoblastic Differentiation, and Bone Regeneration Capacity of Human Embryonic Stem Cell–Derived Mesenchymal Stem Cells. *Stem Cells and Development*, *18*(7), 955–968. <http://doi.org/10.1089/scd.2008.0310>
- Asghari, F., Samiei, M., Adibkia, K., Akbarzadeh, A., & Davaran, S. (n.d.). Biodegradable and biocompatible polymers for tissue engineering application: a review. *Artificial Cells, Nanomedicine, and Biotechnology*, *0*(0), 1–8. <http://doi.org/10.3109/21691401.2016.1146731>
- Augst, A. D., Kong, H. J., & Mooney, D. J. (2006). Alginate hydrogels as biomaterials. *Macromolecular Bioscience*, *6*(8), 623–633. <http://doi.org/10.1002/mabi.200600069>
- Badylak, S. F., Taylor, D., & Uygun, K. (2010). Whole Organ Tissue Engineering: Decellularization and Recellularization of Three-Dimensional Matrix Scaffolds. *Annual Review of Biomedical Engineering*, *13*, 110301095218061. <http://doi.org/10.1146/annurev-bioeng-071910-124743>
- Baek, J.-Y., Xing, Z.-C., Kwak, G., Yoon, K.-B., Park, S.-Y., Park, L. S., & Kang, I.-K. (2012). Fabrication and Characterization of Collagen-immobilized Porous

- PHBV/HA Nanocomposite Scaffolds for Bone Tissue Engineering. *J. Nanomaterials*, 2012, 1:1–1:1. <http://doi.org/10.1155/2012/171804>
- Biazar, E., Ai, J., Heidari, S., & Asefnejad, a. (2011). Fabrication of Collagen-Coated Poly (beta-hydroxy by Chemical and Physical Methods, 27(2).
- Bohner, M. (2010). Resorbable biomaterials as bone graft substitutes. *Materials Today*. [http://doi.org/10.1016/S1369-7021\(10\)70014-6](http://doi.org/10.1016/S1369-7021(10)70014-6)
- Bose, S., Roy, M., & Bandyopadhyay, A. (2012). Recent advances in bone tissue engineering scaffolds. *Trends in Biotechnology*, 30(10), 546–54. <http://doi.org/10.1016/j.tibtech.2012.07.005>
- Bose, S., Vahabzadeh, S., & Bandyopadhyay, A. (2013). Bone tissue engineering using 3D printing. *Materials Today*, 16(12), 496–504. <http://doi.org/10.1016/j.mattod.2013.11.017>
- Boughton, P., Ferris, D., & Ruys, D. A. J. (2008). A Ceramic-Polymer Functionally Graded Material: A Novel Disk Prosthesis. In *25th Annual Conference on Composites, Advanced Ceramics, Materials, and Structures: B: Ceramic Engineering and Science Proceedings* (pp. 593–600). John Wiley & Sons, Inc. <http://doi.org/10.1002/9780470294703.ch67>
- Butscher, A., Bohner, M., Hofmann, S., Gauckler, L., & Miller, R. (2011). Structural and material approaches to bone tissue engineering in powder-based three-dimensional printing. *Acta Biomaterialia*, 7(3), 907–920. <http://doi.org/10.1016/j.actbio.2010.09.039>
- Caplan, A. I. (2007). Adult mesenchymal stem cells for tissue engineering versus regenerative medicine. *Journal of Cellular Physiology*. <http://doi.org/10.1002/jcp.21200>
- Castellanos, M. I., Zenses, A.-S., Grau, A., Rodríguez-Cabello, J. C., Gil, F. J., Manero, J. M., & Pegueroles, M. (2015). Biofunctionalization of REDV elastin-like recombinamers improves endothelialization on CoCr alloy surfaces for cardiovascular applications. *Colloids and Surfaces. B, Biointerfaces*, 127, 22–32. <http://doi.org/10.1016/j.colsurfb.2014.12.056>

- Castillo-Dalí, G., Castillo-Oyagüe, R., Terriza, A., Saffar, J. L., Batista, A., Barranco, A., Torres-Lagares, D. (2014). In vivo comparative model of oxygen plasma and nanocomposite particles on PLGA membranes for guided bone regeneration processes to be applied in pre-prosthetic surgery: a pilot study. *Journal of Dentistry*, 42(11), 1446–57. <http://doi.org/10.1016/j.jdent.2014.04.015>
- Chen, G., Deng, C., & Li, Y.-P. (2012). TGF- β and BMP signaling in osteoblast differentiation and bone formation. *International Journal of Biological Sciences*, 8(2), 272–88. <http://doi.org/10.7150/ijbs.2929>
- Chen, J., Chu, B., & Hsiao, B. S. (2006). Mineralization of hydroxyapatite in electrospun nanofibrous poly(L-lactic acid) scaffolds. *Journal of Biomedical Materials Research Part A*, 79A(2), 307–317. <http://doi.org/10.1002/jbm.a.30799>
- Chen, J.-P., & Su, C.-H. (2011). Surface modification of electrospun PLLA nanofibers by plasma treatment and cationized gelatin immobilization for cartilage tissue engineering. *Acta Biomaterialia*, 7(1), 234–43. <http://doi.org/10.1016/j.actbio.2010.08.015>
- Cornell, C. N., Lane, J. M., Chapman, M., Merkow, R., Seligson, D., Henry, S., Vincent, K. (1991). Multicenter trial of Collagraft as bone graft substitute. *Journal of Orthopaedic Trauma*, 5(1), 1–8. Retrieved from <http://www.ncbi.nlm.nih.gov/pubmed/2023034>
- Correia, C., Bhumiratana, S., Yan, L.-P., Oliveira, A. L., Gimble, J. M., Rockwood, D., Vunjak-Novakovic, G. (2012). Development of silk-based scaffolds for tissue engineering of bone from human adipose-derived stem cells. *Acta Biomaterialia*, 8(7), 2483–92. <http://doi.org/10.1016/j.actbio.2012.03.019>
- Correia, D. M., Ribeiro, C., Botelho, G., Borges, J., Lopes, C., Vaz, F., Lanceros-Méndez, S. (2016). Superhydrophilic poly(l-lactic acid) electrospun membranes for biomedical applications obtained by argon and oxygen plasma treatment. *Applied Surface Science*, 371, 74–82. <http://doi.org/10.1016/j.apsusc.2016.02.121>
- Costa-Pinto, A. R., Reis, R. L., & Neves, N. M. (2011). Scaffolds Based Bone Tissue Engineering: The Role of Chitosan. *Tissue Engineering Part B: Reviews*, 17(5),

331–347. <http://doi.org/10.1089/ten.teb.2010.0704>

Davies, J. E., Matta, R., Mendes, V. C., & de Carvalho, P. S. P. (2010). Development, characterization and clinical use of a biodegradable composite scaffold for bone engineering in oro-maxillo-facial surgery. *Organogenesis*, 6(3), 161–166. <http://doi.org/10.4161/org.6.3.12392>

Declercq, H. A., Desmet, T., Berneel, E. E. M., Dubruel, P., & Cornelissen, M. J. (2013). Synergistic effect of surface modification and scaffold design of bioploted 3-D poly- ϵ -caprolactone scaffolds in osteogenic tissue engineering. *Acta Biomaterialia*, 9(8), 7699–708. <http://doi.org/10.1016/j.actbio.2013.05.003>

Dehghani, F., & Annabi, N. (2011). Engineering porous scaffolds using gas-based techniques. *Current Opinion in Biotechnology*. <http://doi.org/10.1016/j.copbio.2011.04.005>

Deie, M., Ochi, M., Adachi, N., Nishimori, M., & Yokota, K. (2008). Artificial bone grafting [calcium hydroxyapatite ceramic with an interconnected porous structure (IP-CHA)] and core decompression for spontaneous osteonecrosis of the femoral condyle in the knee. *Knee Surgery, Sports Traumatology, Arthroscopy*, 16(8), 753–758. <http://doi.org/10.1007/s00167-008-0558-2>

Desmet, T., Morent, R., De Geyter, N., Leys, C., Schacht, E., & Dubruel, P. (2009). Nonthermal plasma technology as a versatile strategy for polymeric biomaterials surface modification: A review. *Biomacromolecules*. <http://doi.org/10.1021/bm900186s>

Dhandayuthapani, B., Yoshida, Y., Maekawa, T., & Kumar, D. S. (2011). Polymeric scaffolds in tissue engineering application: A review. *International Journal of Polymer Science*. <http://doi.org/10.1155/2011/290602>

Dorozhkin, S. (2010). Bioceramics of calcium orthophosphates. *Biomaterials*, 31(7), 1465–85. <http://doi.org/10.1016/j.biomaterials.2009.11.050>

Duan, B., Wang, M., Zhou, W. Y., Cheung, W. L., Li, Z. Y., & Lu, W. W. (2010). Three-dimensional nanocomposite scaffolds fabricated via selective laser sintering for bone tissue engineering. *Acta Biomaterialia*, 6(12), 4495–505.

<http://doi.org/10.1016/j.actbio.2010.06.024>

- El-Amin, S. F., Lu, H. H., Khan, Y., Burems, J., Mitchell, J., Tuan, R. S., & Laurencin, C. T. (2003). Extracellular matrix production by human osteoblasts cultured on biodegradable polymers applicable for tissue engineering. *Biomaterials*, *24*(7), 1213–1221. [http://doi.org/10.1016/S0142-9612\(02\)00451-9](http://doi.org/10.1016/S0142-9612(02)00451-9)
- Faucheux, N., Schweiss, R., Lützow, K., Werner, C., & Groth, T. (2004). Self-assembled monolayers with different terminating groups as model substrates for cell adhesion studies. *Biomaterials*, *25*(14), 2721–2730. <http://doi.org/10.1016/j.biomaterials.2003.09.069>
- Ferreira, A. M., Gentile, P., Chiono, V., & Ciardelli, G. (2012a). Collagen for bone tissue regeneration. *Acta Biomaterialia*. <http://doi.org/10.1016/j.actbio.2012.06.014>
- Ferreira, A. M., Gentile, P., Chiono, V., & Ciardelli, G. (2012b). Collagen for bone tissue regeneration. *Acta Biomaterialia*, *8*(9), 3191–3200. <http://doi.org/10.1016/j.actbio.2012.06.014>
- Ferreira, B. M. P., Pinheiro, L. M. P., Nascente, P. A. P., Ferreira, M. J., & Duek, E. A. R. (2009). Plasma surface treatments of poly(l-lactic acid) (PLLA) and poly(hydroxybutyrate-co-hydroxyvalerate) (PHBV). *Materials Science and Engineering C*, *29*(3), 806–813. <http://doi.org/10.1016/j.msec.2008.07.026>
- Francis, M. D., & Webb, N. C. (1970). Hydroxyapatite formation from a hydrated calcium monohydrogen phosphate precursor. *Calcified Tissue Research*, *6*(1), 335–342. <http://doi.org/10.1007/BF02196214>
- Fu, Q., Saiz, E., Rahaman, M. N., & Tomsia, A. P. (2011). Bioactive glass scaffolds for bone tissue engineering: state of the art and future perspectives. *Materials Science & Engineering. C, Materials for Biological Applications*, *31*(7), 1245–1256. <http://doi.org/10.1016/j.msec.2011.04.022>
- Gentile, P., Chiono, V., Carmagnola, I., & Hatton, P. V. (2014). An overview of poly(lactic-co-glycolic) acid (PLGA)-based biomaterials for bone tissue engineering. *International Journal of Molecular Sciences*, *15*(3), 3640–59. <http://doi.org/10.3390/ijms15033640>

- Gerhardt, L.-C., & Boccaccini, A. R. (2010). Bioactive Glass and Glass-Ceramic Scaffolds for Bone Tissue Engineering. *Materials*, 3(7), 3867–3910. <http://doi.org/10.3390/ma3073867>
- Girotti, A., Reguera, J., Rodriguez-Cabello, J. C., Arias, F. J., Alonso, M., & Testera, A. M. (n.d.). Design and bioproduction of a recombinant multi(bio)functional elastin-like protein polymer containing cell adhesion sequences for tissue engineering purposes. *Journal of Materials Science: Materials in Medicine*, 15(4), 479–484. <http://doi.org/10.1023/B:JMSM.0000021124.58688.7a>
- Gloria, A., Ronca, D., Russo, T., D'Amora, U., Chierchia, M., De Santis, R., Ambrosio, L. (2011). Technical features and criteria in designing fiber-reinforced composite materials: from the aerospace and aeronautical field to biomedical applications. *Journal of Applied Biomaterials & Biomechanics: JABB*, 9(2), 151–63. <http://doi.org/10.5301/JABB.2011.8569>
- Gloria, A., Santis, R. De, & Ambrosio, L. (2010). Polymer-based composite scaffolds for tissue engineering. *J Appl Biomater Biomech*, 8(2), 57–67.
- Gomes, M. E., Azevedo, H. S., Moreira, A. R., Ellä, V., Kellomäki, M., & Reis, R. L. (2008). Starch-poly(ϵ -caprolactone) and starch-poly(lactic acid) fibre-mesh scaffolds for bone tissue engineering applications: Structure, mechanical properties and degradation behaviour. *Journal of Tissue Engineering and Regenerative Medicine*, 2(5), 243–252. <http://doi.org/10.1002/term.89>
- Gonzalez De Torre, I., Santos, M., Quintanilla, L., Testera, A., Alonso, M., & Rodriguez Cabello, J. C. (2014). Elastin-like recombinamer catalyst-free click gels: Characterization of poroelastic and intrinsic viscoelastic properties. *Acta Biomaterialia*, 10(6), 2495–2505. <http://doi.org/10.1016/j.actbio.2014.02.006>
- Goonoo, N., Bhaw-Luximon, A., Bowlin, G. L., & Jhurry, D. (2013). An assessment of biopolymer- and synthetic polymer-based scaffolds for bone and vascular tissue engineering. *Polymer International*. <http://doi.org/10.1002/pi.4474>
- Goyenvalle, E., Aguado, E., Pilet, P., & Daculsi, G. (2010). Biofunctionality of MBCP ceramic granules (TricOs[®]) plus fibrin sealant (Tisseel[®]) versus

- MBCP ceramic granules as a filler of large periprosthetic bone defects: an investigative ovine study. *Journal of Materials Science: Materials in Medicine*, 21(6), 1949–1958. <http://doi.org/10.1007/s10856-010-4043-3>
- Hasirci, N., Endogan, T., Vardar, E., Kiziltay, A., & Hasirci, V. (2010). Effect of oxygen plasma on surface properties and biocompatibility of PLGA films. *Surface and Interface Analysis*, 42(6-7), 486–491. <http://doi.org/10.1002/sia.3247>
- Hilfiker, A., Kasper, C., Hass, R., & Haverich, A. (2011). Mesenchymal stem cells and progenitor cells in connective tissue engineering and regenerative medicine: Is there a future for transplantation? In *Langenbeck's Archives of Surgery* (Vol. 396, pp. 489–497). <http://doi.org/10.1007/s00423-011-0762-2>
- Hing, K. A. (2004). Bone repair in the twenty-first century: biology, chemistry or engineering? *Philosophical Transactions of the Royal Society of London A: Mathematical, Physical and Engineering Sciences*, 362(1825), 2821–2850. <http://doi.org/10.1098/rsta.2004.1466>
- Hung, P. S., Kuo, Y. C., Chen, H. G., Chiang, H. H. K., & Lee, O. K. S. (2013). Detection of Osteogenic Differentiation by Differential Mineralized Matrix Production in Mesenchymal Stromal Cells by Raman Spectroscopy. *PLoS ONE*, 8(5). <http://doi.org/10.1371/journal.pone.0065438>
- Intranuovo, F., Gristina, R., Brun, F., Mohammadi, S., Ceccone, G., Sardella, E., Favia, P. (2014). Plasma Modification of PCL Porous Scaffolds Fabricated by Solvent-Casting/Particulate-Leaching for Tissue Engineering. *Plasma Processes and Polymers*, 11(2), 184–195. <http://doi.org/10.1002/ppap.201300149>
- Jacobs, T., Morent, R., De Geyter, N., Dubruel, P., & Leys, C. (2012). Plasma surface modification of biomedical polymers: Influence on cell-material interaction. *Plasma Chemistry and Plasma Processing*. <http://doi.org/10.1007/s11090-012-9394-8>
- Jayakumar, P., & Di Silvio, L. (2010). Osteoblasts in bone tissue engineering. *Proceedings of the Institution of Mechanical Engineers. Part H, Journal of Engineering in Medicine*, 224(12), 1415–1440.

<http://doi.org/10.1243/09544119JEIM821>

- Jayaswal, G. P., Dange, S. P., & Khalikar, A. N. (2010). Bioceramic in dental implants: A review. *Journal of Indian Prosthodontist Society*. <http://doi.org/10.1007/s13191-010-0002-4>
- Jiao, Y.-P., & Cui, F.-Z. (2007). Surface modification of polyester biomaterials for tissue engineering. *Biomedical Materials (Bristol, England)*, 2(4), R24–R37. <http://doi.org/10.1088/1748-6041/2/4/R02>
- Kose, G. T., Ber, S., Korkusuz, F., & Hasirci, V. (2003). Poly(3-hydroxybutyric acid-co-3-hydroxyvaleric acid) based tissue engineering matrices. In *Journal of Materials Science: Materials in Medicine* (Vol. 14, pp. 121–126). <http://doi.org/10.1023/A:1022063628099>
- Kose, G. T., Korkusuz, F., Ozkul, A., Soysal, Y., Ozdemir, T., Yildiz, C., & Hasirci, V. (2005). Tissue engineered cartilage on collagen and PHBV matrices. *Biomaterials*, 26(25), 5187–5197. <http://doi.org/10.1016/j.biomaterials.2005.01.037>
- Kaigler, D., Avila, G., Wisner-Lynch, L., Nevins, M. L., Nevins, M., Rasperini, G., Giannobile, W. V. (2011). Platelet-derived growth factor applications in periodontal and peri-implant bone regeneration. *Expert Opinion on Biological Therapy*, 11(3), 375–385. <http://doi.org/10.1517/14712598.2011.554814>
- Kara, F., Aksoy, E. A., Yuksekdog, Z., Hasirci, N., & Aksoy, S. (2014). Synthesis and surface modification of polyurethanes with chitosan for antibacterial properties. *Carbohydrate Polymers*, 112, 39–47. <http://doi.org/10.1016/j.carbpol.2014.05.019>
- Kasoju, N., & Bora, U. (2012). Silk Fibroin in Tissue Engineering. *Advanced Healthcare Materials*, 1(4), 393–412. <http://doi.org/10.1002/adhm.201200097>
- Keogh, M. B., O'Brien, F. J., & Daly, J. S. (2010). A novel collagen scaffold supports human osteogenesis - Applications for bone tissue engineering. *Cell and Tissue Research*, 340(1), 169–177. <http://doi.org/10.1007/s00441-010-0939-y>
- Khorasani, M. T., Mirzadeh, H., & Irani, S. (2008). Plasma surface modification of poly (l-lactic acid) and poly (lactic-co-glycolic acid) films for improvement of nerve cells adhesion. *Radiation Physics and Chemistry*, 77(3), 280–287.

<http://doi.org/10.1016/j.radphyschem.2007.05.013>

- Kinikoglu, B., Rodriguez-Cabello, J. C., Damour, O., & Hasirci, V. (2011). A smart bilayer scaffold of elastin-like recombinamer and collagen for soft tissue engineering. *Journal of Materials Science: Materials in Medicine*, 22(6), 1541–1554. <http://doi.org/10.1007/s10856-011-4315-6>
- Ko, H.-F., Sfeir, C., & Kumta, P. N. (2010). Novel synthesis strategies for natural polymer and composite biomaterials as potential scaffolds for tissue engineering. *Philosophical Transactions of the Royal Society of London A: Mathematical, Physical and Engineering Sciences*, 368(1917), 1981–1997. <http://doi.org/10.1098/rsta.2010.0009>
- Kretlow, J. D., & Mikos, A. G. (2007). Review: mineralization of synthetic polymer scaffolds for bone tissue engineering. *Tissue Engineering*, 13(5), 927–938. <http://doi.org/10.1089/ten.2006.0394>
- Langer, R., & Vacanti, J. P. (1993). Tissue engineering. *Science (New York, N.Y.)*, 260(5110), 920–6. <http://doi.org/10.1126/science.8493529>
- Lasprilla, A. J. R., Martinez, G. A. R., Lunelli, B. H., Jardini, A. L., & Filho, R. M. (2012). Poly-lactic acid synthesis for application in biomedical devices - A review. *Biotechnology Advances*. <http://doi.org/10.1016/j.biotechadv.2011.06.019>
- Laurencin, C., Khan, Y., & El-Amin, S. F. (2006). Bone graft substitutes. *Expert Review of Medical Devices*, 3(1), 49–57. <http://doi.org/10.1586/17434440.3.1.49>
- Lee, K., Silva, E. A., & Mooney, D. J. (2011). Growth factor delivery-based tissue engineering: general approaches and a review of recent developments. *Journal of the Royal Society, Interface / the Royal Society*, 8(55), 153–70. <http://doi.org/10.1098/rsif.2010.0223>
- Lei, C., Zhu, H., Li, J., Li, J., Feng, X., & Chen, J. (2015). Preparation and characterization of polyhydroxybutyrate-co-hydroxyvalerate/silk fibroin nanofibrous scaffolds for skin tissue engineering. *Polymer Engineering & Science*, 55(4), 907–916. <http://doi.org/10.1002/pen.23958>
- Liao, C.-J., Chen, C.-F., Chen, J.-H., Chiang, S.-F., Lin, Y.-J., & Chang, K.-Y. (2002).

- Fabrication of porous biodegradable polymer scaffolds using a solvent merging/particulate leaching method. *Journal of Biomedical Materials Research*, 59(4), 676–681. <http://doi.org/10.1002/jbm.10030>
- Liu, H., Zhang, D., Shen, F., Zhang, G., & Song, S. (2012). Corrosion and ion release behavior of Cu/Ti film prepared via physical vapor deposition in vitro as potential biomaterials for cardiovascular devices. *Applied Surface Science*, 258(19), 7286–7291. <http://doi.org/10.1016/j.apsusc.2012.03.106>
- Liu, X., & Ma, P. X. (2004). Polymeric scaffolds for bone tissue engineering. *Annals of Biomedical Engineering*, 32(3), 477–486. <http://doi.org/10.1023/B:ABME.0000017544.36001.8e>
- Liu, X., Won, Y., & Ma, P. X. (2006). Porogen-induced surface modification of nanofibrous poly(L-lactic acid) scaffolds for tissue engineering. *Biomaterials*, 27(21), 3980–7. <http://doi.org/10.1016/j.biomaterials.2006.03.008>
- Liu, Y. F., Dong, X. T., & Zhu, F. D. (2010). Overview of Rapid Prototyping for Fabrication of Bone Tissue Engineering Scaffold. *Advanced Materials Research*, 102-104, 550–554. <http://doi.org/10.4028/www.scientific.net/AMR.102-104.550>
- Luo, T., Zhang, W., Shi, B., Cheng, X., & Zhang, Y. (2012). Enhanced bone regeneration around dental implant with bone morphogenetic protein 2 gene and vascular endothelial growth factor protein delivery. *Clinical Oral Implants Research*, 23(4), 467–473. <http://doi.org/10.1111/j.1600-0501.2011.02164.x>
- Marolt, D., Knezevic, M., & Novakovic, G. V. (2010). Bone tissue engineering with human stem cells. *Stem Cell Research & Therapy*, 1(2), 10. <http://doi.org/10.1186/scrt10>
- Martínez-Osorio, H., Juárez-Campo, M., Diebold, Y., Girotti, A., Alonso, M., Arias, F. J., Juárez-Campo, O. (2009). Genetically Engineered Elastin-Like Polymer as a Substratum to Culture Cells from the Ocular Surface. *Current Eye Research*, 34, 48–56. <http://doi.org/10.1080/02713680802542053>
- Meinel, L., Zoidis, E., Zapf, J., Hassa, P., Hottiger, M. O., Auer, J. A., Von Rechenberg, B. (2003). Localized insulin-like growth factor I delivery to enhance new bone

- formation. *Bone*, 33(4), 660–672. [http://doi.org/10.1016/S8756-3282\(03\)00207-2](http://doi.org/10.1016/S8756-3282(03)00207-2)
- Meng, W., Xing, Z. C., Jung, K. H., Kim, S. Y., Yuan, J., Kang, I. K., Shin, H. I. (2008). Synthesis of gelatin-containing PHBV nanofiber mats for biomedical application. *Journal of Materials Science: Materials in Medicine*, 19(8), 2799–2807. <http://doi.org/10.1007/s10856-007-3356-3>
- Meng, Z. X., Wang, Y. S., Ma, C., Zheng, W., Li, L., & Zheng, Y. F. (2010). Electrospinning of PLGA/gelatin randomly-oriented and aligned nanofibers as potential scaffold in tissue engineering. *Materials Science and Engineering: C*, 30(8), 1204–1210. <http://doi.org/10.1016/j.msec.2010.06.018>
- Mijiritsky, E., & Karas, S. (2004). Removable partial denture design involving teeth and implants as an alternative to unsuccessful fixed implant therapy: a case report. *Implant Dentistry*, 13(3), 218–222. <http://doi.org/10.1097/01.id.0000136919.13387.94>
- Morent, R., De Geyter, N., Desmet, T., Dubruel, P., & Leys, C. (2011). Plasma surface modification of biodegradable polymers: A review. *Plasma Processes and Polymers*. <http://doi.org/10.1002/ppap.201000153>
- Mouriño, V., & Boccaccini, A. R. (2010). Bone tissue engineering therapeutics: controlled drug delivery in three-dimensional scaffolds. *Journal of the Royal Society, Interface / the Royal Society*, 7(43), 209–27. <http://doi.org/10.1098/rsif.2009.0379>
- Murphy, C. M., Haugh, M. G., & O'Brien, F. J. (2010). The effect of mean pore size on cell attachment, proliferation and migration in collagen-glycosaminoglycan scaffolds for bone tissue engineering. *Biomaterials*, 31(3), 461–466. <http://doi.org/10.1016/j.biomaterials.2009.09.063>
- Murphy, C. M., O'Brien, F. J., Little, D. G., & Schindeler, A. (2013). Cell-scaffold interactions in the bone tissue engineering triad. *European Cells and Materials*.
- Neuhaus, S., Padeste, C., Solak, H. H., & Spencer, N. D. (2010). Functionalization of fluoropolymer surfaces with nanopatterned polyelectrolyte brushes. *Polymer*, 51(18), 4037–4043. <http://doi.org/10.1016/j.polymer.2010.07.002>

- Nguyen, D. T., McCanless, J. D., Mecwan, M. M., Noblett, A. P., Haggard, W. O., Smith, R. A., & Bumgardner, J. D. (2013). Balancing mechanical strength with bioactivity in chitosan-calcium phosphate 3D microsphere scaffolds for bone tissue engineering: air- vs. freeze-drying processes. *J Biomater Sci Polym Ed*, *24*. <http://doi.org/10.1080/09205063.2012.735099>
- Nguyen, L. H., Annabi, N., Nikkhah, M., Bae, H., Binan, L., Park, S., Khademhosseini, A. (2012). Vascularized Bone Tissue Engineering: Approaches for Potential Improvement. *Tissue Engineering Part B: Reviews*, *18*(5), 363–382. <http://doi.org/10.1089/ten.teb.2012.0012>
- Nicol, A., Channe Gowda, D., & Urry, D. W. (1992). Cell adhesion and growth on synthetic elastomeric matrices containing ARG-GLY-ASP-SER-3. *Journal of Biomedical Materials Research*, *26*(3), 393–413. <http://doi.org/10.1002/jbm.820260309>
- Park, J.-E., & Todo, M. (2011). Development and characterization of reinforced poly(L-lactide) scaffolds for bone tissue engineering. *Journal of Materials Science. Materials in Medicine*, *22*(5), 1171–82. <http://doi.org/10.1007/s10856-011-4289-4>
- Peltola, S. M., Melchels, F. P. W., Grijpma, D. W., & Kellomäki, M. (2008). A review of rapid prototyping techniques for tissue engineering purposes. *Annals of Medicine*, *40*(4), 268–280. <http://doi.org/10.1080/07853890701881788>
- Polini, A., Pagliara, S., Stabile, R., Netti, G. S., Roca, L., Prattichizzo, C., Pisignano, D. (2010). Collagen-functionalised electrospun polymer fibers for bioengineering applications. *Soft Matter*, *6*(8), 1668. <http://doi.org/10.1039/b921932c>
- Prabhakaran, M. P., Venugopal, J., & Ramakrishna, S. (2009). Electrospun nanostructured scaffolds for bone tissue engineering. *Acta Biomaterialia*, *5*(8), 2884–2893. <http://doi.org/10.1016/j.actbio.2009.05.007>
- Puppi, D., Chiellini, F., Piras, A. M., & Chiellini, E. (2010). Polymeric materials for bone and cartilage repair. *Progress in Polymer Science*, *35*(4), 403–440. <http://doi.org/10.1016/j.progpolymsci.2010.01.006>
- Puppi, D., Mota, C., Gazzarri, M., Dinucci, D., Gloria, A., Myrzabekova, M., Chiellini,

- F. (2012). Additive manufacturing of wet-spun polymeric scaffolds for bone tissue engineering. *Biomedical Microdevices*, 14(6), 1115–1127. <http://doi.org/10.1007/s10544-012-9677-0>
- Qu, D., Li, J., Li, Y., Gao, Y., Zuo, Y., Hsu, Y., & Hu, J. (2011). Angiogenesis and osteogenesis enhanced by bFGF ex vivo gene therapy for bone tissue engineering in reconstruction of calvarial defects. *Journal of Biomedical Materials Research - Part A*, 96 A(3), 543–551. <http://doi.org/10.1002/jbm.a.33009>
- Ramay, H. R. R., & Zhang, M. (2004). Biphasic calcium phosphate nanocomposite porous scaffolds for load-bearing bone tissue engineering. *Biomaterials*, 25(21), 5171–5180. <http://doi.org/10.1016/j.biomaterials.2003.12.023>
- Rengier, F., Mehndiratta, A., Von Tengg-Kobligh, H., Zechmann, C. M., Unterhinninghofen, R., Kauczor, H. U., & Giesel, F. L. (2010). 3D printing based on imaging data: Review of medical applications. *International Journal of Computer Assisted Radiology and Surgery*. <http://doi.org/10.1007/s11548-010-0476-x>
- Rocca-Smith, J. R., Karbowski, T., Marcuzzo, E., Sensidoni, A., Piasente, F., Champion, D., Debeaufort, F. (2016). Impact of corona treatment on PLA film properties. *Polymer Degradation and Stability*. <http://doi.org/10.1016/j.polymdegradstab.2016.03.020>
- Roh, H.-S., Jung, S.-C., Kook, M.-S., & Kim, B.-H. (2016). In vitro study of 3D PLGA/n-HAp/ β -TCP composite scaffolds with etched oxygen plasma surface modification in bone tissue engineering. *Applied Surface Science*. <http://doi.org/10.1016/j.apsusc.2015.12.243>
- Sachs, E., Cima, M., Cornie, J., Brancazio, D., Brecht, J., Curodeau, A., Fan, T., Khanuja, S., Lauder, A., Lee, J., Michaels, S. (1993). Three-Dimensional Printing: The Physics and Implications of Additive Manufacturing. *CIRP Annuals-Manufacturing Technology*, 42(1), 257-260. [http://doi.org/10.1016/S0007-8506\(07\)62438-X](http://doi.org/10.1016/S0007-8506(07)62438-X)
- Sahebalzamani, M., Biazar, E., Shahrezaei, M., Hosseinkazemi, H., & Rahiminavaie, H. (2014). Surface Modification of PHBV Nanofibrous Mat by Laminin Protein and

- Its Cellular Study. *International Journal of Polymeric Materials and Polymeric Biomaterials*, 64(3), 149–154. <http://doi.org/10.1080/00914037.2014.911179>
- Salgado, A. J., Coutinho, O. P., & Reis, R. L. (2004). Bone tissue engineering: State of the art and future trends. *Macromolecular Bioscience*. <http://doi.org/10.1002/mabi.200400026>
- Santos, M. I., & Reis, R. L. (2010). Vascularization in bone tissue engineering: Physiology, current strategies, major hurdles and future challenges. *Macromolecular Bioscience*. <http://doi.org/10.1002/mabi.200900107>
- Scholz, M. S., Blanchfield, J. P., Bloom, L. D., Coburn, B. H., Elkington, M., Fuller, J. D., Bond, I. P. (2011). The use of composite materials in modern orthopaedic medicine and prosthetic devices: A review. *Composites Science and Technology*. <http://doi.org/10.1016/j.compscitech.2011.08.017>
- Scislowska-Czarnecka, A., Szmigiel, D., Genet, M., Dupont-Gillain, C., Pamula, E., & Kolaczowska, E. (2015). Oxygen plasma surface modification augments poly(L-lactide-co-glycolide) cytocompatibility toward osteoblasts and minimizes immune activation of macrophages. *Journal of Biomedical Materials Research Part A*, 103(12), 3965–3977. <http://doi.org/10.1002/jbm.a.35509>
- Sell, S. A., Wolfe, P. S., Garg, K., McCool, J. M., Rodriguez, I. A., & Bowlin, G. L. (2010). The Use of Natural Polymers in Tissue Engineering: A Focus on Electrospun Extracellular Matrix Analogues. *Polymers*, 2(4), 522–553. <http://doi.org/10.3390/polym2040522>
- Seol, Y. J., Park, D. Y., Park, J. Y., Kim, S. W., Park, S. J., & Cho, D. W. (2013). A new method of fabricating robust freeform 3D ceramic scaffolds for bone tissue regeneration. *Biotechnology and Bioengineering*, 110(5), 1444–1455. <http://doi.org/10.1002/bit.24794>
- Seong, J. M., Kim, B.-C., Park, J.-H., Kwon, I. K., Mantalaris, A., & Hwang, Y.-S. (2010). Stem cells in bone tissue engineering. *Biomedical Materials (Bristol, England)*, 5(6), 062001. <http://doi.org/10.1088/1748-6041/5/6/062001>
- Serrano, V., Liu, W., & Franzen, S. (2007). An infrared spectroscopic study of the

- conformational transition of elastin-like polypeptides. *Biophysical Journal*, 93(7), 2429–2435. <http://doi.org/10.1529/biophysj.106.100594>
- Shrivats, A. R., McDermott, M. C., & Hollinger, J. O. (2014). Bone tissue engineering: State of the union. *Drug Discovery Today*. <http://doi.org/10.1016/j.drudis.2014.04.010>
- Sjostrom, T., McNamara, L. E., Yang, L., Dalby, M. J., & Su, B. (2012). Novel anodization technique using a block copolymer template for nanopatterning of titanium implant surfaces. *ACS Applied Materials and Interfaces*, 4(11), 6354–6361. <http://doi.org/10.1021/am301987e>
- Smith, I. O., & Ma, P. X. (2010). Cell and biomolecule delivery for regenerative medicine. *Science and Technology of Advanced Materials*, 11(1), 14102. <http://doi.org/10.1088/1468-6996/11/1/014102>
- Sodek, J., Ganss, B., & McKee, M. D. (2000). Osteopontin. *Critical Reviews in Oral Biology & Medicine*, 11(3), 279–303. <http://doi.org/10.1177/10454411000110030101>
- Sougaijam Vijay Singh¹, Saurabh Gupta¹, Deepak Sharma², Nympha Pandit³, Aruna Nangom⁴, H. S. (2015). No Title. *Journal of Conservative Dentistry*, 18(3), 196–199.
- Sridharan, G., & Shankar, A. (2012). Toluidine blue: A review of its chemistry and clinical utility. *Journal of Oral and Maxillofacial Pathology*, 16(2), 251–255. <http://doi.org/10.4103/0973-029X.99081>
- Stevens, M. M. (2008). Biomaterials for bone tissue engineering. *Materials Today*. [http://doi.org/10.1016/S1369-7021\(08\)70086-5](http://doi.org/10.1016/S1369-7021(08)70086-5)
- Sultana, N., & Wang, M. (2012). PHBV/PLLA-based composite scaffolds fabricated using an emulsion freezing/freeze-drying technique for bone tissue engineering: surface modification and in vitro biological evaluation. *Biofabrication*, 4(1), 015003. <http://doi.org/10.1088/1758-5082/4/1/015003>
- Sun, W., Puzas, J. E., Sheu, T. J., Liu, X., & Fauchet, P. M. (2007). Nano- to microscale porous silicon as a cell interface for bone-tissue engineering. *Advanced Materials*,

19(7), 921–924. <http://doi.org/10.1002/adma.200600319>

- Suzuki, O., Kamakura, S., & Katagiri, T. (2006). Surface chemistry and biological responses to synthetic octacalcium phosphate. *Journal of Biomedical Materials Research - Part B Applied Biomaterials*, 77(1), 201–212. <http://doi.org/10.1002/jbm.b.30407>
- Tejeda-Montes, E., Klymov, A., Nejadnik, M. R., Alonso, M., Rodriguez-Cabello, J. C., Walboomers, X. F., & Mata, A. (2014). Mineralization and bone regeneration using a bioactive elastin-like recombinamer membrane. *Biomaterials*, 35(29), 8339–47. <http://doi.org/10.1016/j.biomaterials.2014.05.095>
- Tezcaner, A., Bugra, K., & Hasirci, V. (2003). Retinal pigment epithelium cell culture on surface modified poly(hydroxybutyrate-co-hydroxyvalerate) thin films. *Biomaterials*, 24(25), 4573–4583. [http://doi.org/10.1016/S0142-9612\(03\)00302-8](http://doi.org/10.1016/S0142-9612(03)00302-8)
- Thadavirul, N., Pavasant, P., & Supaphol, P. (2014). Development of polycaprolactone porous scaffolds by combining solvent casting, particulate leaching, and polymer leaching techniques for bone tissue engineering. *Journal of Biomedical Materials Research - Part A*, 102(10), 3379–3392. <http://doi.org/10.1002/jbm.a.35010>
- Thuaksuban, N., Nuntanarant, T., Pattanachot, W., Suttapreyasri, S., & Cheung, L. K. (2011). Biodegradable polycaprolactone-chitosan three-dimensional scaffolds fabricated by melt stretching and multilayer deposition for bone tissue engineering: assessment of the physical properties and cellular response. *Biomedical Materials (Bristol, England)*, 6(1), 015009. <http://doi.org/10.1088/1748-6041/6/1/015009>
- Tuzlakoglu, K., Pashkuleva, I., Rodrigues, M. T., Gomes, M. E., Van Lenthe, G. H., Miller, R., & Reis, R. L. (2010). A new route to produce starch-based fiber mesh scaffolds by wet spinning and subsequent surface modification as a way to improve cell attachment and proliferation. *Journal of Biomedical Materials Research - Part A*, 92(1), 369–377. <http://doi.org/10.1002/jbm.a.32358>
- Valente, J. F. A., Valente, T. A. M., Alves, P., Ferreira, P., Silva, A., & Correia, I. J. (2012). Alginate based scaffolds for bone tissue engineering. *Materials Science and Engineering: C*, 32(8), 2596–2603. <http://doi.org/10.1016/j.msec.2012.08.001>

- Venkatesan, J., & Kim, S.-K. (2010). Chitosan Composites for Bone Tissue Engineering—An Overview. *Marine Drugs*, 8(8), 2252–2266. <http://doi.org/10.3390/md8082252>
- Venkatesan, J., Ryu, B., Sudha, P. N., & Kim, S.-K. (2012). Preparation and characterization of chitosan-carbon nanotube scaffolds for bone tissue engineering. *International Journal of Biological Macromolecules*, 50(2), 393–402. <http://doi.org/10.1016/j.ijbiomac.2011.12.032>
- Wang, L., Dormer, N. H., Bonewald, L. F., & Detamore, M. S. (2010). Osteogenic differentiation of human umbilical cord mesenchymal stromal cells in polyglycolic acid scaffolds. *Tissue Engineering. Part A*, 16(6), 1937–48. <http://doi.org/10.1089/ten.TEA.2009.0706>
- Wang, L., Du, J., Cao, D., & Wang, Y. (2013). Recent Advances and the Application of Poly(3-hydroxybutyrate-co-3-hydroxyvalerate) as Tissue Engineering Materials. *Journal of Macromolecular Science, Part A*, 50(8), 885–893. <http://doi.org/10.1080/10601325.2013.802540>
- Wang, X., & Puram, S. (2004). The toughness of cortical bone and its relationship with age. *Annals of Biomedical Engineering*, 32(1), 123–135. <http://doi.org/10.1023/B:ABME.0000007797.92559.5e>
- Wang, Y., Ke, Y., Ren, L., Wu, G., Chen, X., & Zhao, Q. (2009). Surface engineering of PHBV by covalent collagen immobilization to improve cell compatibility. *Journal of Biomedical Materials Research - Part A*, 88(3), 616–627. <http://doi.org/10.1002/jbm.a.31858>
- Wang, Y., Lu, L., Zheng, Y., & Chen, X. (2006). Improvement in hydrophilicity of PHBV films by plasma treatment. *Journal of Biomedical Materials Research Part A*, 76A(3), 589–595. <http://doi.org/10.1002/jbm.a.30575>
- Wei, D., Zhou, Y., Wang, Y., & Jia, D. (2008). Chemical etching of micro-plasma oxidized titania film on titanium alloy and apatite deposited on the surface of modified titania film in vitro. *Thin Solid Films*, 516(8), 1818–1825. <http://doi.org/10.1016/j.tsf.2007.08.034>

- Wu, S., Liu, X., Chan, Y. L., Ho, J. P. Y., Chung, C. Y., Chu, P. K., Luk, K. D. K. (2007). Nickel release behavior, cytocompatibility, and superelasticity of oxidized porous single-phase NiTi. *Journal of Biomedical Materials Research - Part A*, 81(4), 948–955. <http://doi.org/10.1002/jbm.a.31115>
- Wu, S., Liu, X., Yeung, K. W. K., Liu, C., & Yang, X. (2014). Biomimetic porous scaffolds for bone tissue engineering. *Materials Science and Engineering: R: Reports*, 80, 1–36. <http://doi.org/10.1016/j.mser.2014.04.001>
- Yildirim, E. D., Besunder, R., Pappas, D., Allen, F., Güceri, S., & Sun, W. (2010). Accelerated differentiation of osteoblast cells on polycaprolactone scaffolds driven by a combined effect of protein coating and plasma modification. *Biofabrication*, 2(1), 014109. <http://doi.org/10.1088/1758-5082/2/1/014109>
- Yildirim, E. D., Pappas, D., Goeri, S., & Sun, W. (2011). Enhanced cellular functions on polycaprolactone tissue scaffolds by o 2 plasma surface modification. *Plasma Processes and Polymers*, 8(3), 256–267. <http://doi.org/10.1002/ppap.201000009>
- Yilgor, P., Tuzlakoglu, K., Reis, R. L., Hasirci, N., & Hasirci, V. (2009). Incorporation of a sequential BMP-2/BMP-7 delivery system into chitosan-based scaffolds for bone tissue engineering. *Biomaterials*, 30(21), 3551–9. <http://doi.org/10.1016/j.biomaterials.2009.03.024>
- Yilgor, P., Yilmaz, G., Onal, M. B., Solmaz, I., Gundogdu, S., Keskil, S., Hasirci, V. (2012). An in vivo study on the effect of scaffold geometry and growth factor release on the healing of bone defects. *Journal of Tissue Engineering and Regenerative Medicine*. <http://doi.org/10.1002/term.1456>
- Zhang, S., Prabhakaran, M. P., Qin, X., & Ramakrishna, S. (2015). Biocomposite scaffolds for bone regeneration: Role of chitosan and hydroxyapatite within poly-3-hydroxybutyrate-co-3-hydroxyvalerate on mechanical properties and in vitro evaluation. *Journal of The Mechanical Behaviour of Biomedical Materials*, 51, 88–98. <http://doi.org/10.1016/j.jmbbm.2015.06.032>
- Zhang, W., Wang, G., Liu, Y., Zhao, X., Zou, D., Zhu, C., Zreiqat, H. (2013). The synergistic effect of hierarchical micro/nano-topography and bioactive ions for

enhanced osseointegration. *Biomaterials*, 34(13), 3184–95.

<http://doi.org/10.1016/j.biomaterials.2013.01.008>

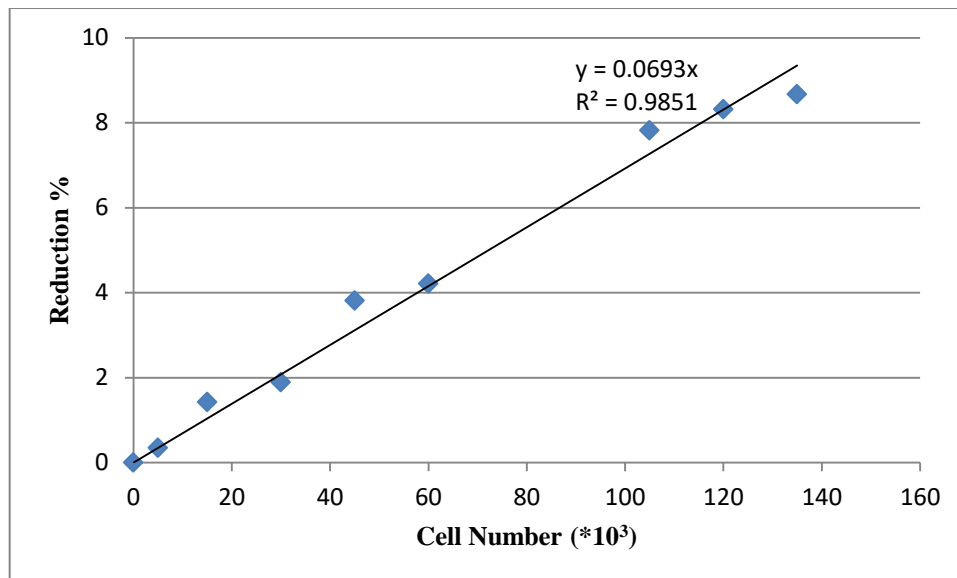
Zhang, Z.-Y., Teoh, S.-H., Hui, J. H. P., Fisk, N. M., Choolani, M., & Chan, J. K. Y. (2012). The potential of human fetal mesenchymal stem cells for off-the-shelf bone tissue engineering application. *Biomaterials*, 33(9), 2656–2672. <http://doi.org/10.1016/j.biomaterials.2011.12.025>

Zhou, C., Shi, Q., Guo, W., Terrell, L., Qureshi, A. T., Hayes, D. J., & Wu, Q. (2013). Electrospun bio-nanocomposite scaffolds for bone tissue engineering by cellulose nanocrystals reinforcing maleic anhydride grafted PLA. *ACS Applied Materials and Interfaces*, 5(9), 3847–3854. <http://doi.org/10.1021/am4005072>

Zonari, A., Cerqueira, M. T., Novikoff, S., Goes, A. M., Marques, A. P., Correlo, V. M., & Reis, R. L. (2014). Poly(hydroxybutyrate-co-hydroxyvalerate) bilayer skin tissue engineering constructs with improved epidermal rearrangement. *Macromolecular Bioscience*, 14(7), 977–990. <http://doi.org/10.1002/mabi.201400005>

APPENDICES

APPENDIX A



Appendix A: Calibration curve for the determination of rabbit bone marrow MSCs using Alamar Blue Test.

Alamar Blue Equation

$$\text{Reduction (\%)} = \frac{((\epsilon_{\text{ox}})_{\lambda_2} \times A_{\lambda_1}) - ((\epsilon_{\text{ox}})_{\lambda_1} \times A_{\lambda_2})}{((\epsilon_{\text{red}})_{\lambda_1} \times A'_{\lambda_2}) - ((\epsilon_{\text{red}})_{\lambda_2} \times A'_{\lambda_1})} \times 100 \quad (1)$$

where,

$$\lambda_1 = 570 \text{ nm} \quad \lambda_2 = 595 \text{ nm}$$

A_{λ_1} and A_{λ_2} = Absorbance of test well,

A'_{λ_1} and A'_{λ_2} = Absorbance of negative control well (blank)

Molar Extinction

$$(\epsilon_{\text{ox}})_{\lambda_2} = 117.216$$

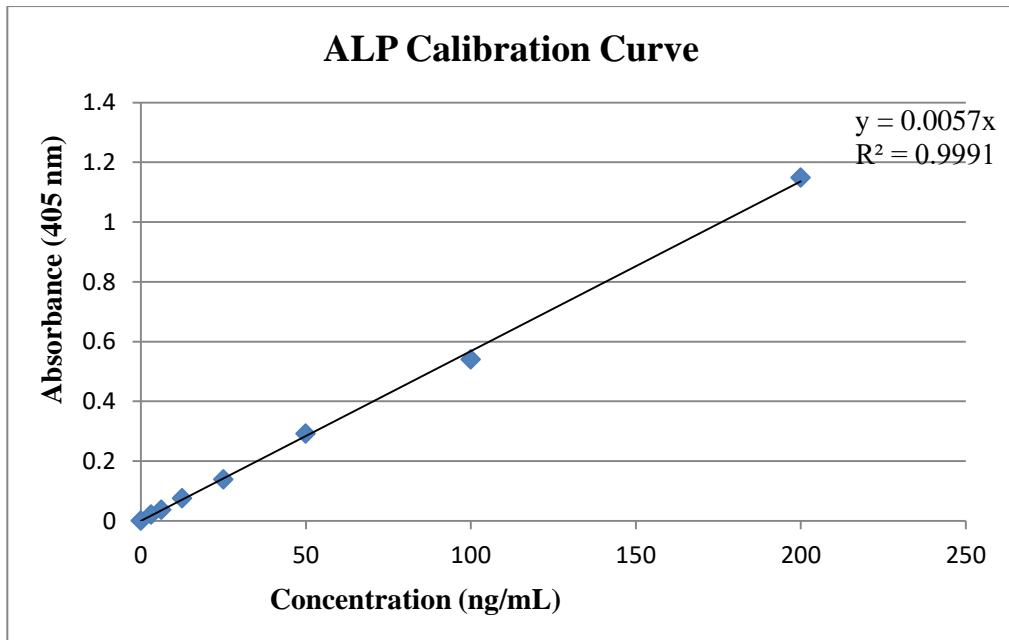
$$(\epsilon_{\text{ox}})_{\lambda_1} = 80.586$$

Coefficients

$$(\epsilon_{\text{red}})_{\lambda_1} = 155.677$$

$$(\epsilon_{\text{red}})_{\lambda_2} = 14.652$$

APPENDIX B



Appendix B: Calibration curve for the determination of ALP activity of rabbit bone marrow MSCs using Alkaline Phosphatase Assay.

CURRICULUM VITAE

PERSONAL INFORMATION

Surname, Name: Alagöz, Ayşe Selcen

Nationality: Turkish

Date and Place of Birth: 13 October 1982, Ankara

Marital Status: Single

Phone: +90 (537) 961 3161

Email: aysecelenalagoz@gmail.com, selcen.alagoz@metu.edu.tr

EDUCATION

Degree	Institution	Year of Graduation
M.Sc.	Selçuk Üniversitesi	2009
B.Sc.	Ankara Üniversitesi	2005

WORK EXPERIENCE

Year	Place	Enrollment
2014-	BIOMATEN CoE in Biomaterials and Tissue Engineering	Research Specialist

FOREIGN LANGUAGES

English: Advanced

HOBBIES

Reading, Music, Travelling.